From the Klinik für Anästhesiologie und Operative Intensivmedizin

(Academic Representative: Prof. Dr. med. Norbert Weiler)

at the University Medical Center Schleswig-Holstein, Campus Kiel

at Christian-Albrechts-Universität zu Kiel - Kiel University

Effects of the sodium-glucose cotransporter 2 inhibitors Canagliflozin, Dapagliflozin and Empagliflozin on endothelial barrier dysfunction: An in-vitro study

Dissertation

to acquire the doctoral degree (Dr. med.)

at the Faculty of Medicine

at Christian-Albrechts-Universität zu Kiel - Kiel University

presented by

Gregor Römer

from Köln

Kiel 2023

1st Reviewer: Prof. Dr. Martin Albrecht

2nd Reviewer: Priv.-Doz. Dr. med. Rouven Berndt

Date of oral examination: 09.10.2023

Approved for printing, Kiel, 16.06.2023

Signed:

Prof. Dr. Martin Albrecht

(Chairperson of the Examination Committee)

Contents

Abbrevations

AJs	Adherens junctions
BP	Bandpass filter
BSA	Bovine serum albumin
CANA	Canagliflozin
CMECs	Cardiac microvascular endothelial cells
CVDs	Cardiovascular diseases
CW	Center wavelength
DAPA	Dapagliflozin
DAPI	4',6-Diamidino-2-phenylindol
DM	Diabetes mellitus
DMSO	Dimethylsulfoxid
DTT	DL-dithiothreitol
EDTA	Ethylenediaminetetraacetic acid disodium salt dihydrate
Em	Emission
EMPA	Empagliflozin
Ex	Excitation
F-actin	Filamentous actin
FBS	Fetal bovine serum
Fl/cell	Fluorescence intensity/cell
GJs	Gap junctions
GLUT	Glucose transporter
h	Hour
HCAECs	Human coronary artery endothelial cells
HEPES	4-(2-Hydroxyethyl)-1-piperazineethanesulfonic acid
HF	Heart failure
HMVECs	Human microvascular endothelial cells
HPAECs	Human pulmonary arterial endothelial cells
HPB	Half power bandwith
HPP	Half power point
HUVECs	Human umbilical vein endothelial cells
IHD	Ischemic heart disease
kDA	Kilodalton
LPS	Lipopolysaccharide
mAB	Monoclonal antibody

min	Minute
MOPS	4-Morpholinepropanesulfonic acid
NAC	N-acety-l-cysteine
NAD(P)H	Nicotinamide adenine dinucleotide phosphate
nm	Nanometer
NOS	Nitric oxide synthase
NOX	NAD(P)H oxidase
PBS	Phosphate buffered saline
RMS	Repeated mechanical stress
ROS	Reactive oxygen species
RPM	Rounds per minute
RS	Repeated stretching
RT	Room temperature
s	Second
SD	Standard deviation
SDS	Sodium dodecyl sulfate
SGLT2	Sodium-glucose cotransporter 2
SGLT2i	Sodium-glucose cotransporter 2 inhibitor
TJs	Tight junctions
TNF-α	Tumor necrosis factor-α
V	Volt
VCBM	Vascular cell basal medium
VCGM	Vascular cell growth medium
VE-cadherin	Vascular endothelial cadherin
VEGF	Vascular endothelial growth factor
XOR	Xanthine oxidase

Directory of figures

Page

Directory of tables

Page

1 Introduction

1.1 Cardiovascular diseases (CVDs) and sodium-glucose cotransporter 2 inhibitors (SGLT2is)

Cardiovascular diseases (CVDs) are by far the leading cause of death around the world. In 2015 CVDs were responsible for 31% of all global deaths, representing a total of estimated 17.9 million deaths. Within this group the top two leading causes are ischemic heart disease (IHD) and stroke (Joseph et al., 2017; Wang et al., 2016). By pointing out and targeting risk factors such as overweight, obesity, physical inactivity, as well as harmful use of tobacco and alcohol, most CVDs could be prevented. As a result of CVDs being the leading cause of death, early detection, and management of people with high cardiovascular risk factors is crucial (Mendis et al., 2011; Piepoli et al., 2016, 2020).

Besides the above mentioned, another important risk factor for the development of CVDs is diabetes mellitus (DM). From 1980-2014 the number of patients with DM has risen from 108 million to 422 million, equating to a global prevalence of 8.5% among adults over 18 years of age (Zhou et al., 2016). Estimations by the international diabetes federation project predict, that by 2045 around 700 million people worldwide, representing one out of ten, will suffer from DM (Saeedi et al., 2019). The most prevalent cause of mortality and morbidity among patients with DM are CVDs. Adults within this population are two to four times more likely to die due to IHD and stroke compared to those without DM (Matheus et al., 2013). One CVD which is frequently associated with DM is heart failure (HF). DM increases the risk of developing HF by more than two-fold in men and five-fold in women, with an estimated 25% of people with DM suffering chronic HF (Williams & Evans, 2020).

Due to the tight interplay between DM and the development of CVDs, treating patients with DM is an important aspect in preventing cardiovascular morbidity and mortality. A notable and recently approved class of oral antidiabetic drugs are Sodium-glucose cotransporter 2 inhibitors (SGLT2is). SGLT2is can bind to the Sodium-glucose cotransporter 2 (SGLT2) located in the S1 segment of the proximal tubule of the kidney. This transporter is responsible for around 90% of glucose reabsorption. By blocking the SGLT2, SGLT2is increase glycosuria and consequently decrease blood glucose levels (Beitelshees et al., 2019; Fonseca-Correa & Correa-Rotter, 2021) (**Figure 1**).

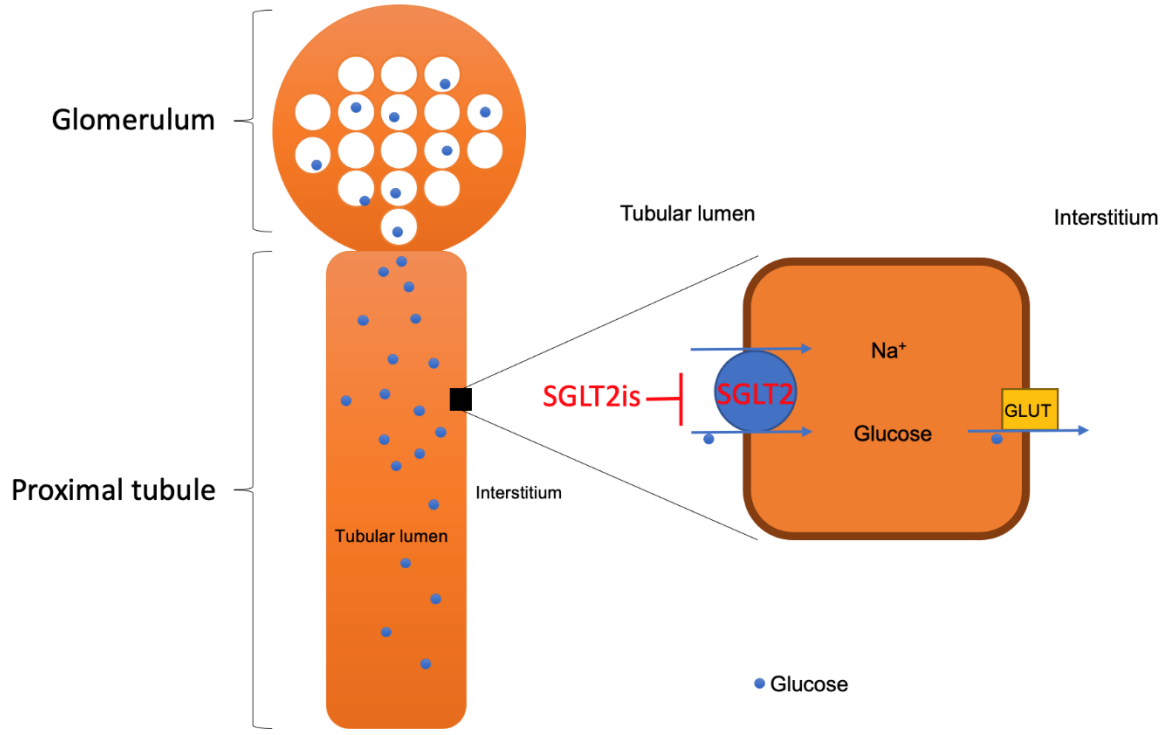

Figure 1. Schematic outline of the cellular mechanism of SGLT2is

By blocking the SGLT2 transporter in the proximal tubule SGLT2is prevent the glucose and sodium reabsorption, leading to lower blood glucose levels. GLUT, glucose transporter; SGLT2, sodium-glucose cotransporter 2; SGLT2is, sodium-glucose cotransporter inhibitors. Based on E. M. Wright et al., 2011.

Interestingly, SGLT2is have shown beneficial effects beyond decreasing blood glucose levels. In several large randomized cardiovascular outcome trials (EMPA-REG Outcome 2015, CANVAS 2017, DAPA-HF 2019, EMPEROR-Reduced 2020, DAPA-CKD 2020, EMPEROR-Preserved 2021) it has been shown that all studied drugs of the SGLT2is family decrease the risk of major adverse cardiovascular events and slow progression of diabetic kidney disease in patients with as well as without DM (Anker et al., 2021; Heerspink et al., 2020; McMurray et al., 2019; Neal et al., 2017; Packer et al., 2020; Zinman et al., 2015). Due to the positive and protective outcomes of these trials and the lack of knowledge about the mechanisms behind these effects, the SGLT2is have received special scientific attention.

At present, the exact mechanisms behind the cardiovascular- and renoprotective effects of the SGLT2is are still unclear. As SGLT2 expression in human endothelial- and cardiac cells is highly questionable (Chen et al., 2010; Mancini et al., 2018; Uthman et al., 2019), it is unlikely that direct interactions between the drug and the transporter explain the cardiovascular protective effects of SGLT2is. On the other hand, it is very improbable that the fast-occurring

cardiovascular benefits are solely related to the improvement in glycemic control. There are several other hypotheses that try to explain the mechanisms by which SGLT2is can improve the cardiovascular outcome. Reduction of plasma volume (Lambers Heerspink et al., 2013), natriuresis (Karg et al., 2018), improved vascular resistance, reduced blood pressure (Chilton et al., 2015; Scheen, 2019), suppression of damage mediated by advanced glycation end-products (Ojima et al., 2015), decreased oxidative stress (Ishibashi et al., 2015), and a shift towards ketone body metabolism (Ferrannini, Baldi, et al., 2016; Ferrannini, Mark, et al., 2016) are just a few of the hypotheses proposed by researchers (Cowie & Fisher, 2020) (**Figure 2**).

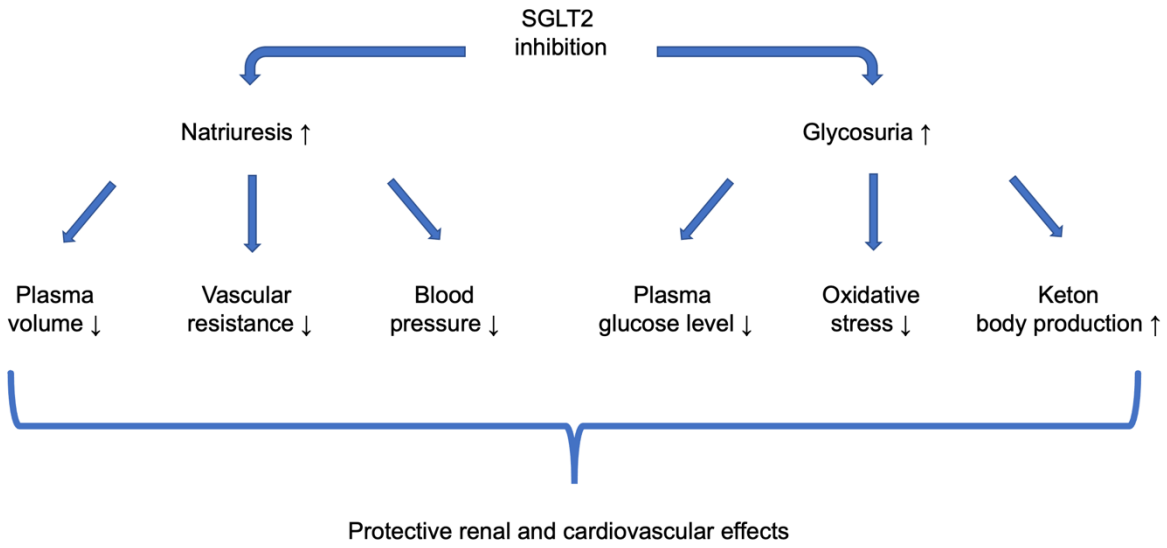

Figure 2. Proposed mechanisms responsible for the protective renal and cardiovascular effects of SGLT2is

SGLT2, sodium-glucose cotransporter 2. Based on Cowie & Fisher, 2020.

1.2 Endothelial barrier function and vascular permeability

The endothelium, a monolayer of endothelial cells building the inner cellular lining of blood vessels, is in direct and constant contact with the circulating blood, the circulating cells, and the tissue around the blood vessels (Félétou, 2011; Haybar et al., 2019). In an average adult human, the endothelial cell surface covers approximately 1 to 7m^2 and comprises 1 to 6 x 10^{13} cells (Cines et al., 1998; Yau et al., 2015). Among other mechanisms, the endothelium is responsible for the maintenance of vascular tone, the participation in inflammatory responses, and the regulation of vascular permeability (Galley & Webster, 2004; Marchio et al., 2019). Hence, a dysregulated vascular endothelium could also play a major role in the development of CVDs (Sun et al., 2020).

For normal and physiological blood vessel function an intact monolayer of endothelial cells is crucial. Endothelial cells are connected laterally by cell-cell junctions, while the basolateral part is connected via integrins to the basement membrane composed of collagen, fibronectin, laminin, and glycosaminoglycans. The most important barrier-forming adhesive structures responsible for barrier integrity are adherens junctions (AJs). AJs are largely assembled from vascular endothelial cadherin (VE-cadherin), a protein which is primarily in charge of sealing the paracellular space. Other important barrier-forming adhesive structures are gap junctions (GJs), which are essential for cell-cell communication, and tight junctions (TJs), which, in addition to AJs, further close the paracellular space (Rodrigues & Granger, 2015) (**Figure 3**).

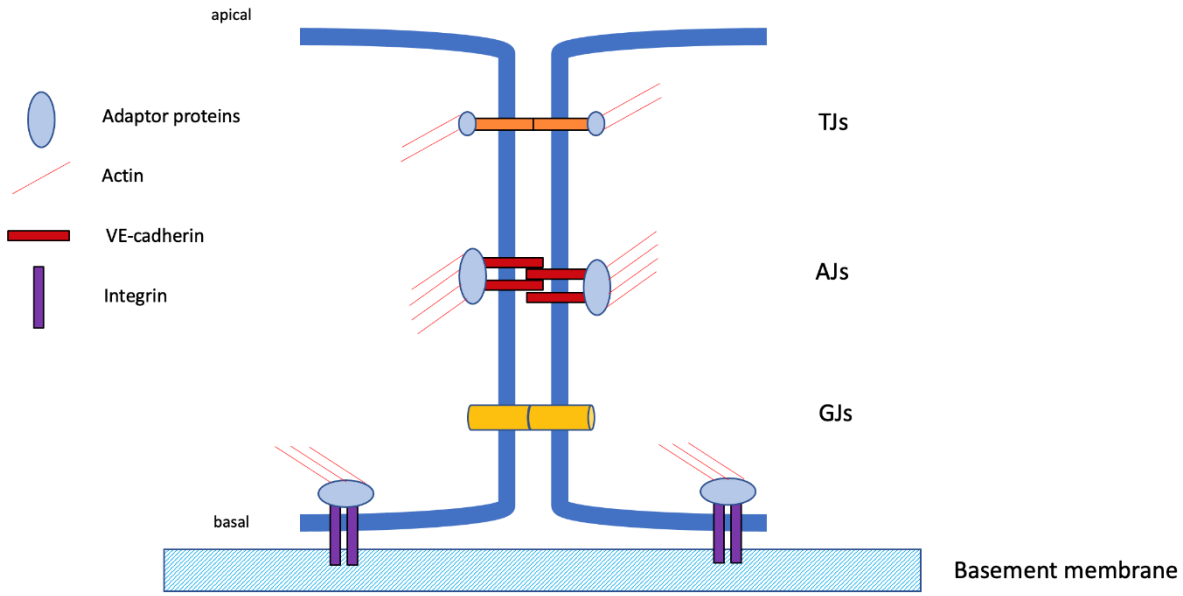

Figure 3. Overview of barrier-forming adhesive structures

AJs, adherens junctions; GJs, gap junctions; TJs, tight junctions; VE-cadherin, vascular endothelial cadherin. Based on Lüllmann-Rauch & Asan, 2019.

Various stimuli, including histamine (Shasby et al., 2002), tumor necrosis factor-α (TNF-α) (Angelini et al., 2006), vascular endothelial growth factor (VEGF) (Esser et al., 1998), and repeated mechanical stress (RMS) (Tian et al., 2016) have shown to increase endothelial permeability. The underlying mechanisms seem to be associated with impaired AJs. Since VE-cadherin is the major component of AJs, endothelial permeability has been postulated to be closely linked to this barrier-forming protein (Dejana et al., 2008; Rodrigues & Granger, 2015).

One cell type which expresses numerous cell junction proteins and is frequently used to investigate the effects of different stress stimuli on endothelial permeability and barrier function are human coronary artery endothelial cells (HCAECs) (Jamaluddin et al., 2009, 2013; Skaria et al., 2016; Wu et al., 2004). HCAECs are primary endothelial cells derived from human coronary arteries which are cultured in-vitro. Thus, in-vitro experiments on HCAECs are a suitable model to closely imitate physiological as well as pathophysiological situations occurring in coronary arteries (Lakota et al., 2018). In addition, HCAECs have previously shown to be more susceptible to inflammatory stimuli, as compared to other endothelial cells such as human umbilical vein endothelial cells (HUVECs) or human microvascular endothelial cells (HMVECs) (Lakota et al., 2007, 2009). Therefore, many studies on endothelial dysfunction and vascular inflammation have been performed using HCAECs (Krogmann et al., 2011; Ren et al., 2017; Wang et al., 2008).

1.3 Non-detrimental and detrimental repeated mechanical stress (RMS)

Endothelial cells are permanently exposed to hemodynamic forces. These hemodynamic forces either appear in the form of shear stress, caused by blood flow and acting parallel to the endothelial monolayer, or in the form of RMS, generated by pulsatile vessel deformation following blood pressure profile (Birukov, 2009; Chien, 2007; Fernandes et al., 2018; Zhuang et al., 2020) (**Figure 4**).

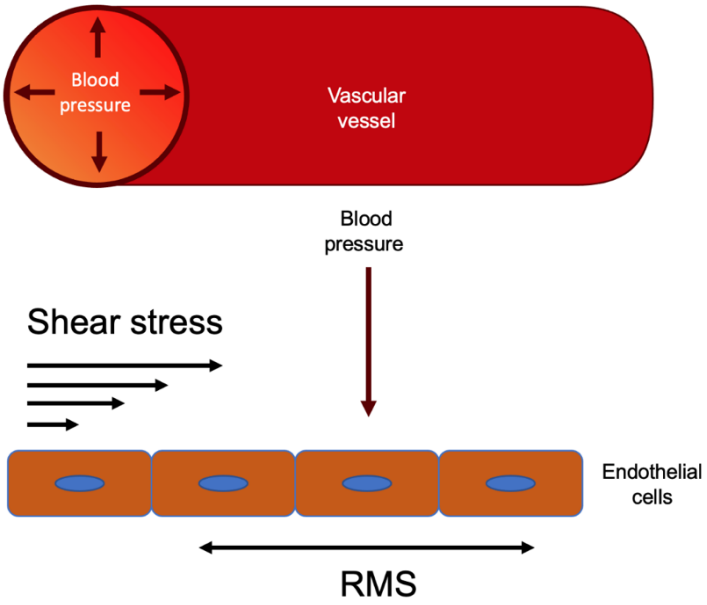

Figure 4. Hemodynamic forces acting on endothelial cells

RMS, repeated mechanical stress. Based on Fernandes et al., 2018.

It is well established, that non-detrimental RMS and intraluminal pressure are crucial for the maintenance of a healthy endothelial function (Fang et al., 2019). Several different studies have reported protective effects of non-detrimental RMS on endothelial permeability (Birukova et al., 2008; Collins et al., 2006). In addition, Birukova et al. reported beneficial effects of non-detrimental RMS on the recovery of endothelial monolayer integrity after thrombin induction (Birukova et al., 2006). In all these studies 5% repeated stretching (RS) of an endothelial cell monolayer in-vitro are regarded as a non-detrimental RMS.

In contrast, exposing endothelial cells to detrimental levels of RMS leads to an increase in inflammatory cytokines, enhanced expression of the proinflammatory surface molecule P-selectin, increased reactive oxygen species (ROS) production, disassembly of AJs, and endothelial barrier dysfunction (Kou et al., 2009; Moldobaeva et al., 2008; Yan et al., 2018). Furthermore, detrimental RMS enhances the thrombin induced endothelial gap formation and delays endothelial monolayer recovery (Birukova et al., 2006). Various studies have reported 10% RS to represent a detrimental RMS: in human aortic endothelial cells 10% RS leads to markedly enhanced monocyte binding to the endothelial monolayer. Additionally, monocytes cultured with endothelial cells exposed to 10% RS show an increased expression of inflammatory cytokines, including Interleukin (IL)-6 and TNF-α (Loperena et al., 2018). Moreover, 24h of 10% RS significantly reduces the overall adhesion of HUVECs to collagen substrate (Omidvar et al., 2018) and exposure to 10% RS increases ROS production in vascular cells as well as in whole vessels. However, exposure to 5% or 6% RS fails to induce a significant increase of ROS production (Hishikawa et al., 1997; Hishikawa & Lüscher, 1997; Lehoux et al., 2000). Therefore, it has been proposed that ROS production is only increased in cells exposed to a specific threshold of RMS (Lehoux, 2006).

1.4 Reactive oxygen species (ROS)

Under physiological conditions, cells remain in a well-balanced state between ROS production and antioxidant clearance. If this homeostatic state is disrupted, ROS production outweighs the antioxidant clearance, resulting in oxidative stress which can cause severe endothelial dysfunction (Pignatelli et al., 2018). Many CVDs develop from a wide range of different atherosclerotic risk factors, which include, but are not limited to, arterial hypertension, DM, hypercholesterolemia, and obesity. All these cardiovascular risk factors have one common feature, namely an increased ROS production (Pastori et al., 2014). Therefore, by minimizing the production of ROS, the onset of vascular injury and hypertensive end organ damage could be delayed or even prevented (Touyz & Schiffrin, 2004).

The main source of ROS production in endothelial cells, like in all vascular cell types, is the cell membrane-associated nicotinamide adenine dinucleotide phosphate (NAD(P)H) oxidase (NOX). NOXs have been described to be regulated by humoral factors, such as cytokines and growth factors, as well as by physical factors including RMS and shear stress. For vascular cells less important sources of ROS are the xanthine oxidase (XOR), the mitochondrial respiratory chain, and an uncoupled nitric oxide synthase (NOS) (Birukov, 2009) (**Figure 5**).

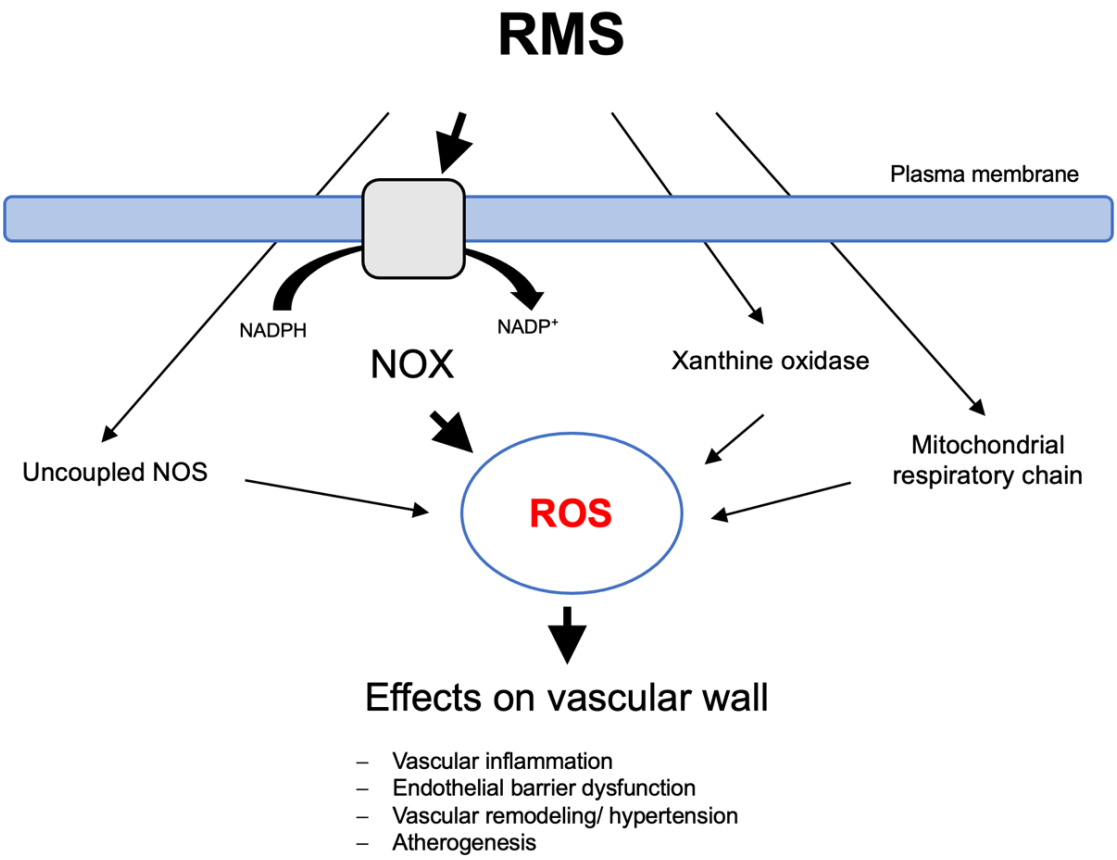

Figure 5. ROS induction via RMS

Upon RMS ROS production is upregulated via several different mechanisms. The most important ROS source in vascular cells is represented by the active NOX. Elevated ROS levels can have various harmful effects. Vascular inflammation, endothelial barrier dysfunction, hypertension, atherogenesis are just a few of these effects. NOS, nitric oxide synthase; NOX, NAD(P)H oxidase; RMS, repeated mechanical stress; ROS, reactive oxygen species. Based on Birukov, 2009.

In HUVECs exposure to RMS results in a significant increase of ROS levels, predominantly produced by NOX. Pre-incubation with either a ROS scavenger or a NOXs inhibitor significantly reduces this increase of ROS levels (Matsushita et al., 2001).

It is well known that increased ROS levels are a crucial promotor of endothelial barrier dysfunction and permeability (He et al., 2020; Pignatelli et al., 2018; Tseng et al., 2017; Zhou et al., 2013). In HUVECs stimulation with TNF-α leads to an increase of ROS levels and VE-cadherin phosphorylation, subsequently resulting in separation of lateral cell-cell junctions, internalization of VE-cadherin, and endothelial gap formation. Interestingly, blocking the increase of ROS levels via applying the ROS scavenger N-acetyl-l-cysteine (NAC) prevents VE-cadherin phosphorylation, intercellular gap formation and redistribution of VE-cadherin from cell-cell junctions. Thus, it has been suggested that the TNF-α induced endothelial barrier dysfunction is mediated through intracellular oxidants (Nwariaku et al., 2004). Correspondingly, in aging rat arteries increased ROS production causes an internalization and degradation of VE-cadherin and its loss from AJs, ultimately resulting in the disruption of these junctions. Blocking ROS not only reverts the degradation of VE-cadherin but also decreases the disruption of endothelial AJs (Chang et al., 2018).

Stimulating resting HCAECs with TNF-α also leads to a significant increase of intracellular ROS levels. Preincubation with the SGLT2is Empagliflozin (EMPA) and Dapagliflozin (DAPA) completely abolishes this increase of ROS levels, suggesting the reduction of ROS levels as one possible mechanism of how SGLT2is exert their cardioprotective effects (Uthman et al., 2019).

1.5 Aim of the study

This research project deals with the effects of three common SGLT2is (EMPA, DAPA and Canagliflozin [CANA]) on HCAECs exposed to non-detrimental and detrimental RMS. In particular, the following questions are evaluated:

1. Do SGLT2is, namely EMPA, DAPA and CANA, ameliorate the endothelial barrier dysfunction in HCAECs exposed to a detrimental RMS?
2. Is the endothelial protective feature of SGLT2is due to a decrease of ROS levels ?

To answer these questions the following readout parameters are investigated in HCAECs exposed to a non-detrimental and detrimental RMS:

1. Endothelial permeability
2. VE-cadherin expression
3. ROS levels

The findings of the study provide insights into the mechanisms of SGLT2is mediated protective effects on the endothelial barrier function and could be of relevance for a deeper understanding of the cellular mechanisms associated with CVDs.

2 Materials and Methods

2.1 Materials

2.1.1 Devices

Product name	Manufacturer
Accu-jet® pro pipette controller	Brand
Acculab ALC 2100.1	Sartorius
AR 4-8 exhaust filter with lubricant feedback	Leybold GmbH
Bench-top pH meter pH 209-209R	Hanna Instruments
Centrifuge 5430 R	Eppendorf
Centrifuge 5810 R	Eppendorf
Clean Air, biological safety cabinet, class II	Telstar
Cooler (4°C)	Bosch, Liebherr
Corning® Costar® serological pipettes (5ml, 10ml, 25ml)	Corning®
CP225D-0CE precision scale	Sartorius
Criterion™ blotter 560 BR	Bio-Rad-Laboratories
Criterion™ foam pads	Bio-Rad-Laboratories
Digital Sonifier® SLPe/Low power ultrasonic systems 2000 Lpt/LPe	Branson
Digital triple heat block	VWR International
DM6 B wide field microscope	Leica
DMi8 Advanced Light live cell microscope	Leica
Electronic benchtop laboratory autoclave 3150EL	Tuttnauer
Electrophoresis chamber Criterion™ cell 135 BR	Bio-Rad-Laboratories
Flexcell® Fx 5000™ tension system - Computer-controlled vacuum unit - Baseplate to hold flexible silicon rubber-bottomed culture dish	Flexcell® International Cooperation
Flexcell® water trap + drying filter	Flexcell® International Cooperation
Freezer (-20°C)	Liebherr
Gasprofi 1 SCS	WLD-TEC
Heracell™ 150i CO_2 incubator	Thermo

	Fisher Scientific®
Ice maker	Hoshizaki
K-Series cryostorage freezer (-180°C)	Worthington Industries
Lab microscope 090-135-001	Leica
MacBook Pro (Retina 13inch, 2015)	Apple
MDF-DU700VH-PE VIP freezer	Panasonic
MDF-DU702VH-PE VIP freezer	Panasonic
MDF-U73V VIP freezer	Panasonic
Microfuge PCV-2400	Grant Instruments
Microscope camera (EC4)	Leica
MilliQ synthesis ultrapure water system	Merck
Mr. Frosty™ freezing container	Thermo Fisher Scientific®
MTS 2/4 digital microtiter shaker	IKA
Odyssey® CLx	LI-COR Biosciences
Pipetboy/Pipetgirl	Integra
PMR-30 compact fixed- angle plaftorm rocker	Grant Instruments
PowerPac™ basic power supply	Bio-Rad-Laboratories
Research® plus single channel variable volume pipettors (0.1-2.5µl, 0.5-10µl, 2-20µl, 10-100µl, 20-200µl, 100-1000µl, 500-5000µl)	Eppendorf
See-saw rocker SSL4	Stuart™
SpectraMax M2e microplate reader	Molecular Devices
TCM20™ automated cell counter	Bio-Rad-Laboratories
Transferpette®-8 multichannel (10-100µl, 5-50µl, 20-200µl)	Brand
Trivac® B D8B ATEX rotary vane vacuum pump	Leybold GmbH
Julabo TW8 water bath	VWR International
Variomag® mono komet	H + P Labortechnik
Variomag® monotherm grau	H + P Labortechnik
Vortex-Genie™ 2	Scientific Industries
Vortex mixer	VWR International

Table 1. Devices

2.1.2 Disposables

Product name	Manufacturer
Aluminium foil	ITS
BD Plastipak™ sterile syringe (20ml)	BD Diagnostic System
Bioflex® 6 well plates collagen I coated	Flexcell® International Cooperation
Blotting paper	VWR
Cell counting slides for TC10™/TC20™ cell counter	Bio-Rad-Laboratories
CELLSTAR® cell culture T25 + T75 flask	Greiner Bio One
CELLSTAR® multi well culture plates (polystyrene, sterile, with lid) [6 + 12 well plate]	Greiner Bio One
Corning® Costar® serological pipettes (5ml, 10ml, 25ml)	Corning®
Criterion™ XT Bis-Tris precast gels	Bio-Rad-Laboratories
Disposable pipette tips (5000µl)	Eppendorf
Disposable pipette tips (graduated, refill, PP, natural, non-sterile) [10µl, 200µl, 1250µl]	Greiner Bio One
Falcon tube Cesllstar® tubes (15ml, 50ml)	Greiner Bio One
Falcon® cell scrapers	VWR International
Glas pasteur pipettes	Brand
Immobilion®-FL PVDF-membrane	Merck
Kartell™ 96-well microtitration plates	Thermo Fisher Scientific®
Low temperature freezing vials (2ml)	VWR International
Microcentrifuge tubes (0.5ml)	Brand
Microplate, 96-well, high binding	Greiner Bio One
Non-coded push cap tubes (1.4ml)	Micronic
Reaction tubes (graduated, PP, natural, attached cap) [1.5ml]	Greiner Bio One
Safe-lock tubes (2ml)	Eppendorf
Soft nitrile examination gloves	Klinion
Sterile disposable scalpels	Swann-Morton®
Sterile syringe filter (0.22µm, 0.45µm)	VWR International
Superfrost plus TM adhesion microscope slides	Thermo Fisher Scientific®

Table 2. Disposables

2.1.3 Antibodies

Primary antibodies						
Antigen	**Clone**	**Isotype**	**Reactivitiy**	**Application**	**Dilution**	**Manufacturer**
VE-cadherin	D87F2	Rabbit IgG	Human, Bovine, Pig	WB (molecular weight in kilodalton (kDA) 130)	1:1000	Cell Signaling Technology
VE-cadherin	16B1	Mouse IgG	Human	Immuno-staining	1:60	Thermo Fisher Scientific®
α-tubulin	T9026	Mouse IgG	Human, Bovine, Rat, Yeast, Mouse, Chicken, Fungi, Amphibian	WB (molecular weight in kDA 55)	1:20000	Sigma-Aldrich®

Table 3. Primary antibodies for western blot (WB) and immunostaining

Secondary Antibodies						
Antigen	**Clone**	**Isotype**	**Reactivitiy**	**Application**	**Dilution**	**Manufacturer**
AlexaFluor™ 488		Goat anti-Mouse IgG	Mouse	Immuno-staining	1:400	Thermo Fisher Scientific®
IRDye®680RD	926-68071	Goat anti-Rabbit IgG	Rabbit	WB	1:5000	LI-COR
IRDye®800CW	926-32210	Goat anti-Mouse IgG	Mouse	WB	1:5000	LI-COR

Table 4. Secondary antibodies for WB and immunostaining

2.1.4 Other reagents and chemicals

Product name	Manufacturer
4-(2-Hydroxyethyl)-1-piperazineethanesulfonic acid (HEPES) [$C_8H_{18}N_2O_4S$]	Sigma-Aldrich®
Alcohol ketonatus 70%	Denteck
Avidin, FITC conjugate	Thermo Fisher Scientific®
Bovine serum albumin (BSA)	Sigma-Aldrich®
Bromophenol blue sodium salt	Merck
Calcium chloride dihydrate ($CaCl_2 \cdot 2H_2O$)	Merck
Canagliflozin (CANA)	MedChemExpress
CellROX™ deep red reagent	Thermo Fisher Scientific®
Copper (II) sulphate ($CuSO_4 \cdot H_2O$)	Merck
Dapagliflozin (DAPA)	MedChemExpress
Dimethylsulfoxid (DMSO)	Merck
Disodium phosphate (Na_2HPO_4)	Sigma-Aldrich®
DL-dithiothreitol (DTT)	Sigma-Aldrich®
Empagliflozin (EMPA)	MedChemExpress
Ethylenediaminetetraacetic acid disodium salt dihydrate (EDTA)	Sigma-Aldrich®
EZ-Link™ NHS-LC-LC-biotin	Thermo Fisher Scientific®
Folin & Ciocalteu's phenol reagent	Sigma-Aldrich®
Formaldhyde 37%	Merck
Gelatin	BD Diagnostic System
Glycerol	Sigma-Aldrich®
Glycine	AppliChem GmbH
Halt™ protease and phosphatase inhibitor cocktail	VWR International
Intercept™ blocking buffer	LI-COR
Isopropanol	Merck
Magnesium chloride hexahydrate ($MgCl_2 \cdot 6H_2O$)	Merck
Mercaptoethanol (C_2H_6OS)	Sigma-Aldrich®
Methanol	Merck
4-Morpholinepropanesulfonic acid (MOPS)	Sigma-Aldrich®
N-acetyl-l-cysteine (NAC)	Merck

Potassium chloride (KCl)	Merck
Potassium dihydrogen phosphate (KH_2PO_4)	Merck
Potassium sodium tartrate (KNa-tartrate [$KNaC_4H_4O_6 \cdot 4H_2O$])	Merck
Precision plus Protein™ all-blue prestained standards	Bio-Rad
ProLong™ gold antifade mountant with 4',6-Diamidino-2-phenylindol (DAPI)	Thermo Fisher Scientific®
Rhodamine/Phalloidin	Thermo Fisher Scientific®
Sodium bicarbonate ($NaHCO_3$)	Merck
Sodium carbonate (Na_2CO_3)	Merck
Sodium chloride (NaCl)	Merck
Sodium dihydrogen phosphate dihydrate ($Na_2HPO_4 \cdot 2H_2O$)	Merck
Sodium dodecyl sulfate (SDS)	Sigma-Aldrich®
Sodium hydroxide (NaOH)	Merck
Triton™ X-100	Merck
Trizma® base	Sigma-Aldrich®
Tween® 20	Sigma-Aldrich®

Table 5. Other reagents and chemicals

2.1.5 Cell media and additives

Product name	**Manufacturer**
Endothelial cell growth kit-VEGF (ATCC® PCS-100-041™)	ATCC®
Fetal bovine serum (FBS)	TICO Europe
Gibco™ amphotericin B	Thermo Fisher Scientific®
Gibco™ L-glutamine	Thermo Fisher Scientific®
Gibco™ trypsin-EDTA	Thermo Fisher Scientific®
M199 medium	PAN Biotech GmbH
Penicillin/Streptomycin	Sigma-Aldrich®
Vascular cell basal medium PCS-100-030™ (VCBM)	ATCC®

Table 6. Cell media and additives

Media	Composition
Medium for adherent human coronary artery endothelial cells, vascular cell growth medium (10% VCGM)	411.5ml VCBM, + 50ml FBS, + 28.5ml endothelial growth kit-VEGF, + 5ml amphotericin B, + 5ml penicillin/streptomycin, store at 4°C
Medium for adherent human coronary artery endothelial cells, experimental medium (2% VCGM)	451.5ml VCBM, + 10ml FBS, + 28.5ml endothelial growth kit-VEGF, + 5ml amphotericin B, + 5ml penicillin/streptomycin, store at 4°C
Stop medium M199	435ml M199 medium, + 50ml FBS, + 5ml amphotericin B, + 5ml L-glutamine, + 5ml penicillin/streptomycin, store at 4°C
Freezing medium	15ml PBS (1x), + 4ml FBS, + 1ml DMSO

Table 7. Composition of cell culture media

2.1.6 Buffers and gels

Name	Composition
1% BSA/PBS	1g BSA dissolved in 100ml PBS (1x)
Cell lysis buffer	2.5ml homogenization buffer, 0.025ml DTT 100mM, 0.125ml Triton-100X 10%, 0.025ml Halt™ protease & phosphatase inhibitor single-use cocktail
DTT 100mM	0.015 g DTT, dissolved in 1ml milliQ water
Formalin 4%	108.1ml formaldhyde 37% + 891.9ml PBS
Gelatin coating solution	375mg gelatin dissolved in 50ml milliQ water
Homogenization buffer	0.25M sucrose + 0.02M $C_8H_{18}N_2O_4S$, pH adjusted to 7.4
Lowry A	10g Na_2CO_3, 500ml 0.1M NaOH

Lowry B	2g $KNaC_4H_4O_6 \cdot 4H_2O$, 100ml milliQ water
Lowry C	1g $CuSO_4 \cdot H_2O$, 100ml milliQ water
Lowry solution 1	20ml Lowry A, 200µl Lowry B, 200µl Lowry C
Lowry solution 2	Folin & Ciocalteu's phenol reagent, dilute 1/1 in milliQ water
$NaHCO_3$ 0.1M	4.2g $NaHCO_3$ dissolved in 500ml milliQ water
PBS (10x)	400g NaCl, 10g KCl, 72g Na_2HPO_4, 12g KH_2PO_4, 5000ml milliQ water, pH 7.4
PBS (1x)	100ml PBS (10x), 900ml milliQ water, adjusted to pH 7.4
PBS-Tween	1000ml PBS (1x), 1ml Tween® 20
PBS+ (1x)	1l PBS (1x), 0.1g $MgCl_2 \cdot 6H_2O$, 0.1g $CaCl_2 \cdot 2H_2O$
Primary antibody solution (WB)	5ml Intercept™ blocking buffer, 5ml PBS (1x), 100µl Tween® 20, desired dilution of the primary antibody - VE-cadherin dilution 1/1000 - α-tubulin dilution 1/20000
SDS page electrophoresis running buffer, (MOPS running buffer, 10X)	60.6g Trizma® base, 104.6g MOPS, 10.0g SDS, 3.0g EDTA, 1000ml milliQ water
SDS page electrophoresis running buffer, (MOPS running buffer, 1x)	100ml MOPS running buffer (10x), 900ml milliQ water
SDS page sample buffer (5x)	1.0g SDS, 0.025g bromophenol blue, 0.150g Trizma® base, 4ml milliQ water, 5ml glycerol, 1ml C_2H_6OS
Secondary antibody solution (WB)	5ml Intercept™ blocking buffer, 5ml PBS(1x), 100µl Tween® 20 (10%), 2µl of the desired secondary antibody (dilution 1/5000) - IRDye®680RD 926-68071 Goat anti-Rabbit IgG for VE-cadherin - IRDye®800CW 926-32210 Goat anti-Mouse IgG for α-tubulin
Transfer buffer (10x)	30.0g Trizma® base, 144.0g glycine, 900ml milliQ water
Transfer buffer (1x)	100ml transfer buffer (10x), 200ml methanol, 700ml milliQ water
Triton-100X 0.01%	0.1ml Triton-100X 10% + 100ml milliQ water
Triton-100X 10%	5ml Triton-100X dissolved in 45ml milliQ water
Tween® 20 (10%)	9ml milliQ water, 1ml Tween® 20

Table 8. Composition of buffers and gels

2.1.7 Endothelial cells

Product code	Description	Source
PCS-100-020	Human coronary artery endothelial cells (HCAECs)	ATCC®, USA
C-12221	Human coronary artery endothelial cells (HCAECs)	PromoCell, Germany

Table 9. Endothelial cells

2.1.8 Fluorescence filters

Fluorescence filters for Leica DM6 B wide field microscope			
Name	**Excitation (Ex) filter** in nanometer (nm)	**Emission (Em) filter** in nm	**Use**
DAPI	Bandpass filter (BP), center wavelength (CW) 350/half power bandwith (HPB) 50	BP, CW 460/HPB 50	Nuclei staining (ProLong™ gold antifade mountant with DAPI: Ex-/Em peak 360/460nm)
L5	BP, CW 480/HPB 40	BP, CW 527/HPB 30	VE-cadherin staining (AlexaFluor™ 488 secondary antibody: Ex-/Em peak 490/525nm)
Y3	BP, CW 546/HPB 10	BP, CW 585/HPB 40	F-actin staining (Rhodamine/Phalloidin: Ex-/Em peak 540/565nm)
Y5	BP, CW 620/HPB 60	BP, CW 700/HPB 75	ROS detection (CellROX™ deep red reagent: Ex-/Em peak 644/665nm)

Table 10. Fluorescence filters for Leica DM6 B wide field microscope

Fluorescence filters for Leica DMi8 Advanced Light live cell microscope			
Name	**Excitation (Ex) filter** in nanometer (nm)	**Emission (Em) filter** in nm	**Use**
A	BP, short-wave half power point (HPP)	Longpass filter, cut-on wavelength 425	Nuclei staining

	340/long-wave HPP 380		(ProLong™ gold antifade mountant with DAPI: Ex-/Em peak 360/460nm)
C1	BP, short-wave HPP 450/long-wave HPP 490	BP, short-wave HPP 500/long-wave HPP 550	Cell permeability detection (Avidin, FITC conjugate: Ex-/Em peak 494/518nm)

Table 11. Fluorescence filters for Leica DMi8 Advanced Light live cell microscope

2.1.9 Software

Name	**Company**
Image Studio™ Ver. 5.2.5	LI-COR Biosciences
Image J 1.52e	Research Services Branch (imageJ.nih.gov)
LAS EZ 3.4.0	Leica
M2e SoftMaxPro 6.5.1	Molecular device
Microsoft Office for Mac	Microsoft Corporation
GraphPad Prism 9.3.1	Graph Pad Software
FlexSoft ® FX5000™ software	Flexcell® International Corporation

Table 12. Software

2.2 Methods

2.2.1 Human coronary artery endothelial cells (HCAECs) cultivation

For all experiments commercially available HCAECs (PCS-100-020 from ATCC, Manassas, VA, USA; C-12221 from PromoCell, Heidelberg, Germany) at passage 7 were used. Cells were cultured in 10% VCGM including additives (for details please refer to 2.1.5). During cell culture, cells were constantly incubated within a humidified atmosphere of 5% carbon dioxide/95% air at 37°C (CO_2 Incubator Heracell 150i).

Passaging was performed by trypsinization using 0.05% trypsin-EDTA for 1 minute (min) after reaching approximately 80% confluence. Stop medium M199 was used to wash off the cells and stop the trypsin reaction. The cell suspension was collected in a 50ml falcon tube and centrifuged at 234g for 10min at 4°C (Centrifuge 5810 R, Eppendorf). Subsequently, the supernatant was removed, the cell pellet resuspended in VCGM and reseeded in the desired density.

2.2.2 Cell counting

To assess the number of viable cells, 10µl of cell suspension were pipetted into each of the two counting chambers of the cell counting slides for the TC20™ automated cell counter. Following, the TCM20™ automated cell counter calculated the number of cells/ml for each chamber. The mean of the two results was taken as the actual cell number.

2.2.3 Freezing and thawing of cells

For freezing cells, trypsin dissociated cells were counted (for details see 2.2.2), centrifuged to form cell pellets and resuspended with freezing media, at a concentration of 500.000 cells/ml. The cell suspension was transferred into CryoS freezing tubes (1ml/tube), put into an isopropanol filled Mr. Frosty™ freezing container and transferred to a -80°C freezer. After 24h, the freezing tubes were transferred to liquid nitrogen tanks for long-term storage.

Thawing was performed using a 37°C water bath. Freezing tubes were left in the water bath until only small amounts of cell suspension were still frozen. Thereafter, the cell suspension of each freezing tube was resuspended with 1ml pre-heated 10% VCGM and subsequently pipetted into cell culture flasks/plates. 24h later the medium was replaced by new 10% VCGM.

2.2.4 Preparation for RMS experiments

Before seeding HCAECs on collagen I pre-coated Bioflex® 6 well plates, these plates were coated overnight with either biotinylated gelatin or gelatin + DMSO. To prepare biotinylated gelatin, gelatin was dissolved in bicarbonate buffer (0.1mol/l $NaHCO_3$, pH 8.3) to a final concentration of 10mg/ml at room temperature (RT) with constant stirring. EZ-Link NHS-LC-LC-biotin dissolved in DMSO (5.7mg/ml) was added to 10mg/ml gelatin solution to generate a solution of 0.57mg/ml biotin and 9mg/ml gelatin. The biotin conjugation to gelatin was performed for 1h at RT with constant stirring. Thereafter 1.7ml aliquots of biotinylated gelatin were frozen in -20°C. Additionally, a solution of gelatin + DMSO, but without biotin, was prepared the same way. The same amount of DMSO, which was used to generate a solution of 0.57mg/ml biotin, was added without biotin to 10mg/ml gelatin solution. Again 1.7ml aliquots of gelatin + DMSO were frozen in -20°C.

One day prior seeding stretch plates with HCAECs, an aliquot of biotinylated gelatin or gelatin + DMSO was thawed in a 37°C water bath for 10min, diluted with 0.1mol/l bicarbonate buffer (pH 8.3) to a final gelatin concentration of 0.25mg/ml, sterilized by filtering through a 0.22µm filter and added to 6-well stretch plates (3ml/well). Absorption of the biotinylated gelatin or gelatin + DMSO was performed at 4°C in the dark overnight. After protein absorption, plates were washed twice with PBS (pH 7.4, 1ml/well) and seeded with 100.000 cells/well. Plates used for cell permeability detection were coated with biotinylated gelatin, while plates for all other experiments were coated with gelatin + DMSO.

2.2.5 Experimental setup

Exposure to RMS was performed with the Flexcell® Fx 5000™ tension system for 24h at a frequency of 1 hertz. 5% RS was used as a non-detrimental RMS, while 10% RS was used as a detrimental RMS (for reasoning of these values refer to 1.3). A schematic outline of the Flexcell® Fx 5000™ tension system and the corresponding baseplate can be seen in **Figure 6**.

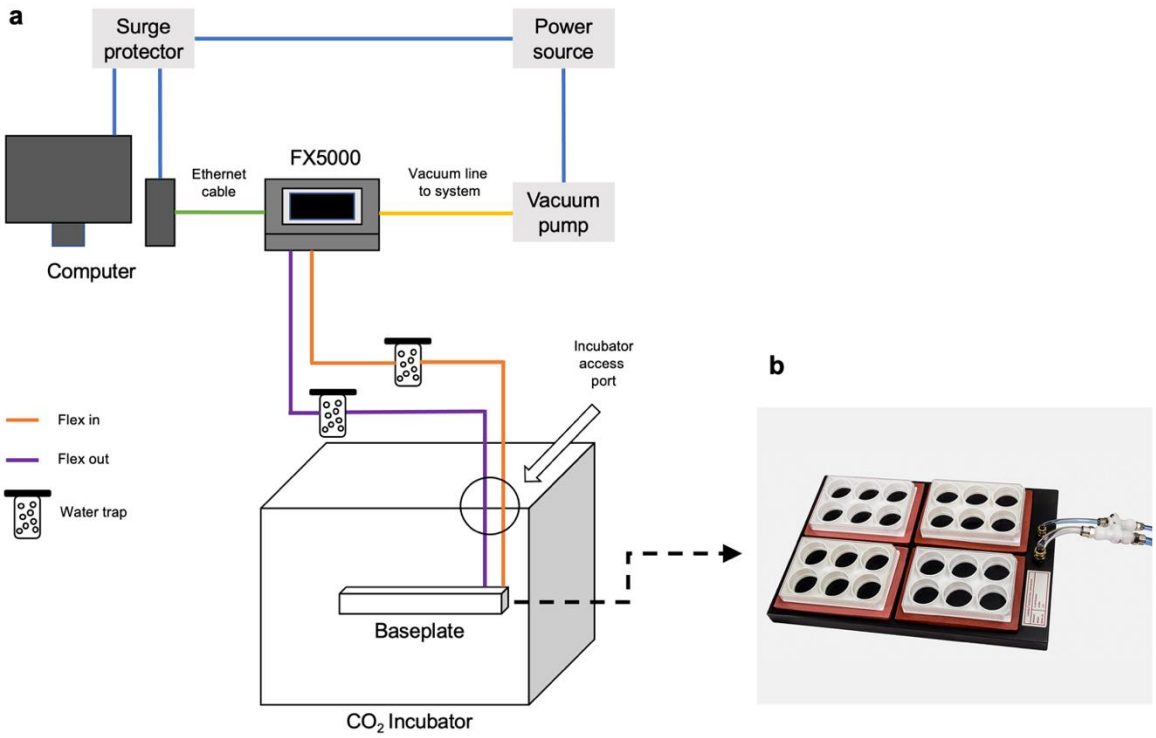

Figure 6. Flexcell® Fx 5000™ tension system

a Schematic outline of the Flexcell® Fx 5000™ tension system. **b** Baseplate kit for the Flexcell® Fx 5000™ tension system. Based on User manual Flexcell® Fx 5000™ tension system, 2009.

18h before exposure to RMS, cells were starved by changing the medium to 2% VCGM. 2h prior to exposure to RMS, cells were incubated with 0.06% DMSO (vehicle), 1µM EMPA, 1µM DAPA, 3µM CANA, or 5mM of the ROS scavenger NAC (Zafarullah et al., 2003).

After exposure to RMS for 24h, the readout parameters endothelial cell permeability, ROS levels, and VE-cadherin expression were determined. In addition, immunofluorescence images for VE-cadherin and filamentous actin (F-actin) were generated after exposure to RMS for 24h (**Figure 7**).

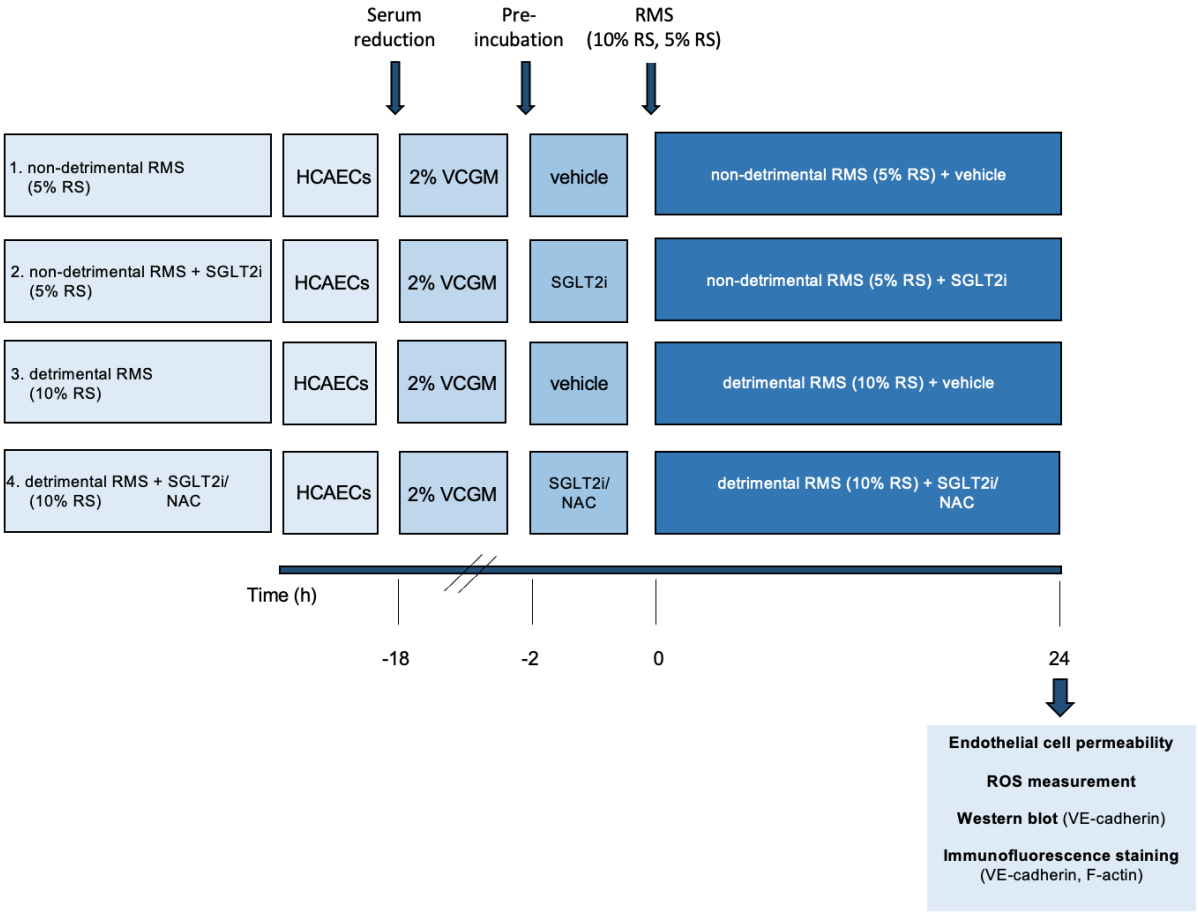

Figure 7. Experimental setup

F-actin, filamentous actin; HCAECs, human coronary artery endothelial cells; NAC, N-acetyl-l-cysteine; RMS, repeated mechanical stress; ROS, reactive oxygen species; RS, repeated stretching; SGLT2i, sodium-glucose cotransporter 2 inhibitor; VCGM, vascular cell growth medium; VE-cadherin, vascular endothelial cadherin.

2.2.6 Endothelial cell permeability

The cell permeability assessment of this study is based on a method described by Dubrovskyi et al., which makes it possible to visualize cell permeability via high affinity interactions between FITC-avidin and biotinylated gelatin (Dubrovskyi et al., 2013). A graphical layout of the assay principle can be seen in **Figure 8**.

After exposure to RMS for 24h, 10µl of FITC-avidin was added to the 2.5ml culture medium of each well, leading to a working concentration of 25µg/ml. Due to the light sensitivity of FITC-avidin the light of the flow cabinet was turned off and the plates were covered in aluminum foil,

before placing them in the incubator for an additional 3min. Thereafter, cells were washed three times with PBS+ to remove excessive FITC-avidin. Subsequently, cells were fixed with 4% formalin for 10min, washed three times with PBS+, permeabilized with 0.01% Triton-100X (2-3min), and washed again three times with PBS+. Next, membranes were cut out of the stretch plates. One drop of DAPI was added on clean microscope slides, and the membranes were transferred face down on the microscope slides.

Images were taken with the Leica DMi8 Advanced Light live cell microscope using two fluorescence filters, DAPI for picturing the nuclei, and A for picturing cell permeability. For each independent experiment six pictures per condition/well were taken (200x magnification). Quantification of these images was carried out in a blinded manner with ImageJ 1.8.0 by two different researchers. Fluorescence intensity per cell was calculated according to the following formula: Total fluorescence intensity/number of nuclei. In the following it is described as fluorescence intensity/cell (Fl/cell).

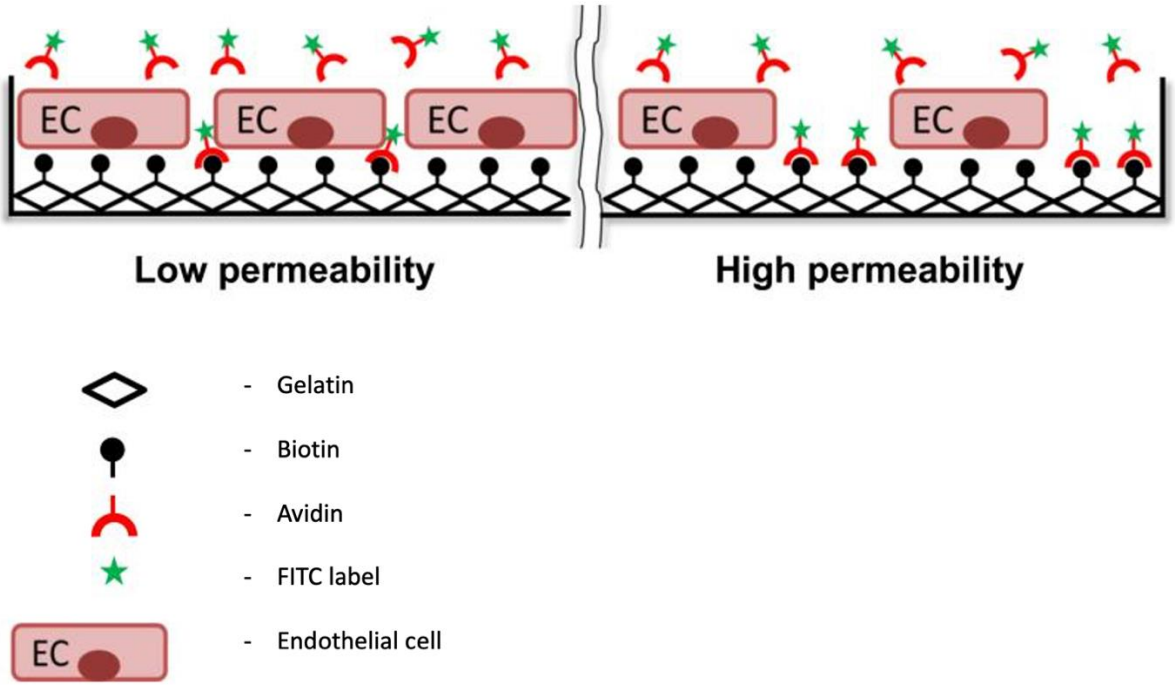

Figure 8. Cell permeability assay

Permeability is assayed via the high affinity binding between FITC-avidin and biotinylated gelatin. If the endothelial monolayer becomes disrupted, gaps between endothelial cells occur and FITC-avidin can freely bind to biotinylated gelatin. These bindings result in a fluorescence signal. The intensity of this fluorescence signal is determined by the number of bindings between FITC-avidin and biotinylated gelatin, which in turn represents the degree of permeability. Based on Dubrovskyi et al., 2013.

2.2.7 ROS measurement

After exposure to RMS for 24h, 4µl of the CellROX™ reagent for oxidative stress detection was added to each well and incubated for an additional 30min in the incubator. Subsequently, cells were washed one time with PBS+ and fixed with 4% formalin for 15min. Thereafter, cells were washed once again with PBS+, the membrane was cut out of the stretch plate, and transferred to microscope slides with one drop of DAPI solution.

Imaging was performed within 2h after fixation with a Leica DM6 B wide-field microscope. For ROS detection the fluorescence filter Y5 was used, while for nuclei staining the fluorescence filter DAPI was used. For each independent experiment six pictures per condition/well were taken (400x magnification). Quantification of these images was carried out in a blinded manner with ImageJ 1.8.0 by two different researchers. Fluorescence intensity was divided by the corresponding cell number, generating Fl/cell.

2.2.8 Immunofluorescence staining

After exposure to RMS for 24h, monolayers of HCAECs were fixed with 4% formalin for 10min. Cells were washed three times with PBS+ and non-specific bindings of the antibodies were blocked by incubation with 1% BSA/PBS. Next, cells were incubated with VE-cadherin monoclonal antibodies (1/60 dilution in 1% BSA/PBS) for 1h at RT. Unbound antibodies were removed by washing three times with PBS+. Afterwards, goat anti-mouse secondary antibodies (1/400 dilution in 1% BSA/PBS, AlexaFlour® 488) and Rhodamine/Phalloidin (1/40 dilution in 1% BSA/PBS) were added to each well for 30min, followed by three times washing with PBS+. Membranes were loaded on microscope slides with mounting fluid containing DAPI and imaged with Leica DM6 B wide field microscope at 1000x magnification. The fluorescence filter L5 was used for VE-cadherin staining, the fluorescence filter Y3 for F-actin staining and the fluorescence filter DAPI for nuclear staining.

2.2.9 Western blot

After exposure to RMS for 24h, cells were washed two times with ice-cold PBS, lysed with cell lysis buffer and scraped from the stretch plates. Cell lysates were sonicated on ice in repeated short cycles (5s, energy mode, 20joules, 70% amplitude, repeated 3x) using the Digital Sonifier® SLPe with microtip. After centrifugation at 20817g (Eppendorf centrifuge 5430 R) at 4°C for 10min, the supernatant was collected and stored at -80°C until use.

Prior to western blotting, protein contents of the samples were measured using the Lowry protein determination assay. BSA standards were prepared, samples were diluted 1/20 using milliQ water, and kept on ice. Next, 100µl of each of the diluted standards/samples was incubated with 500µl of Lowry solution 1 for 10min at RT. Then, 50µl of Lowry solution 2 was added to each standard/sample. After 30min incubation in the dark at RT, 200µl of each standard/sample was transferred to a 96-well plate. Subsequently, protein levels were determined using the SpectraMax M2e microplate reader with the software SoftMaxPro 6.5. Following, protein concentrations were adjusted to 1mg/ml per sample using homogenization buffer.

For electrophoresis the Criterion™ XT Bis-Tris precast gel was inserted into the electrophoresis chamber Criterion™ cell 135 BR. Next, the electrophoresis chamber was filled with MOPS running buffer (1x) to the filling lines. Subsequently, samples were diluted 4/1 with sample buffer and heated for 5min at 95°C. The gel was then loaded with 2µl precision plus Protein™ all-blue prestained standard and 15µl sample per following lane. To separate proteins a constant voltage of 120 Volt (V) was applied for 50-85min.

Following electrophoresis, the proteins were transferred to a Immobilion®-FL transfer membrane using the Bio-Rad PowerPac™. For protein transfer the gel was placed on the membrane in between blotting papers and Criterion™ foam pads in the Criterion™ blotter 560 BR. Thereafter, the transfer chamber was filled with 4°C cold transfer buffer, an ice pack was added, and the gel was blotted at 100V for 30min.

Next, the membrane was removed and blocked with 15ml Intercept™ blocking buffer at RT for 60min. For protein probing, the membrane was incubated with the desired primary antibody solution with gentle shaking at 4°C overnight. To detect VE-cadherin a monoclonal antibody (mAB) from rabbit in a dilution 1/1000 was used. For detection of α-tubulin a mAB from mouse in a dilution 1/20000 was used. After incubation with the primary antibody solution, membranes were washed three times for 5min with PBS-Tween and incubated with the corresponding infrared dye-labelled secondary antibody solutions (IRDye®680RD 926-68071 Goat anti-Rabbit IgG for VE-cadherin and IRDye®800CW 926-32210 Goat anti-Mouse IgG for α-tubulin, both 1/5000 dilution) at RT in the dark for 60min.

Thereafter, membranes were washed three times for 5min with PBS-Tween and scanned with the Odyssey CLx operator at auto-scan setting for dynamic range, 169µm resolution, and medium quality. Quantification of the bands was performed with Image Studio™ software

according to the manufacturer´s instruction. Each signal of the target protein was normalized to the reference protein α-tubulin.

2.2.10 Statistical analysis

Data are presented as the mean ± standard deviation (SD). The exact number of independent experiments is mentioned as “n” and is listed in the respective figure legend. All data were normalized to non-detrimental RMS (5% RS) + vehicle. Statistical analyses were performed using GraphPad Prism 9.3.1. for Mac. Data were analysed by one-way ANOVA with Bonferroni post hoc correction. P-values less than 0.05 were considered statistically significant.

3 Results

3.1 SGLT2is do not influence endothelial barrier function of HCAECs exposed to non-detrimental RMS

First, the influence of SGLT2is on endothelial permeability and VE-cadherin expression of HCAECs exposed to non-detrimental RMS was measured. Compared to vehicle alone, none of the SGLT2is affected endothelial permeability or VE-cadherin expression of HCAECs subjected to non-detrimental RMS (**Figure 9 a + b**). In the following experiments vehicle treated HCAECs exposed to non-detrimental RMS served as a baseline control group.

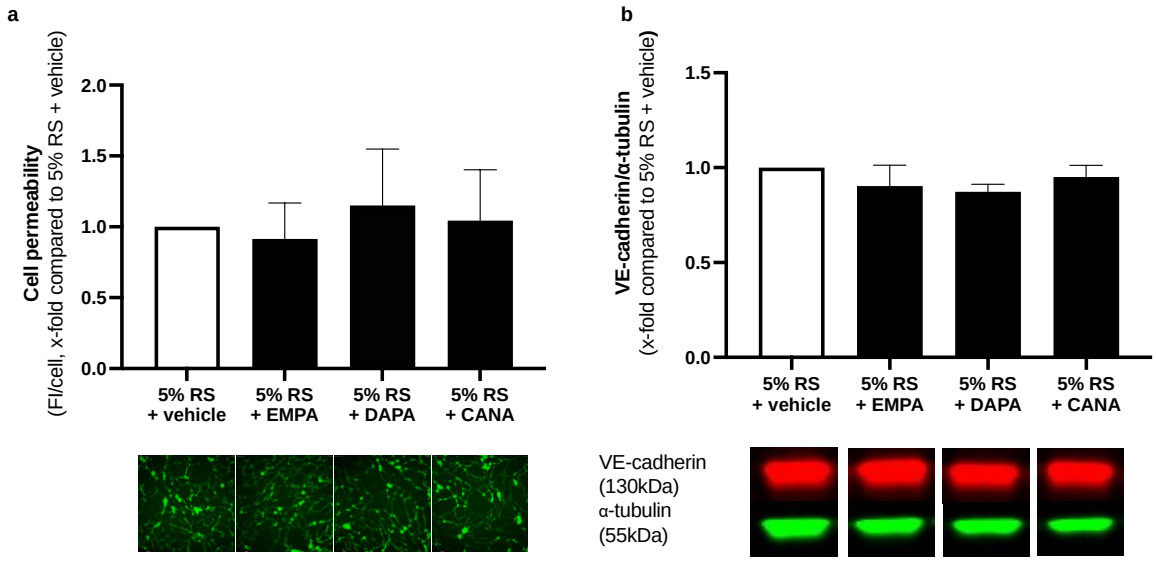

Figure 9. Cell permeability and VE-cadherin expression levels of HCAECs exposed to non-detrimental RMS with and without addition of SGLT2is

a Permeability of an endothelial cell layer exposed to non-detrimental RMS with and without addition of SGLT2is (n=5 individual experiments). Representative images are shown below the bar graph (200x magnification). **b** VE-cadherin expression of endothelial cells exposed to non-detrimental RMS with and without addition of SGLT2is. α-tubulin served as a loading control. Representative bands of VE-cadherin and α-tubulin are shown below the bar graph (n=4 individual experiments). Data are normalized to 5% RS + vehicle and presented as mean ± SD. CANA, Canagliflozin; DAPA, Dapagliflozin; EMPA, Empagliflozin; Fl/cell, fluorescence intensity/cell; kDa, kilodalton; RS, repeated stretching; VE-cadherin, vascular endothelial cadherin.

3.2 SGLT2is ameliorate endothelial barrier dysfunction caused by detrimental RMS

Next, HCAECs were exposed to detrimental RMS. Compared to non-detrimental RMS, detrimental RMS significantly increased cell permeability (1.614 ± 0.426-fold, p<0.001). 1µM EMPA, 1µM DAPA and 3µM CANA significantly attenuated the detrimental RMS induced hyper-permeability (detrimental RMS + vehicle vs. detrimental RMS + EMPA, DAPA or CANA: 1.614 ± 0.426-fold vs. 1.202 ± 0.456-fold, p<0.001; 1.055 ± 0.372-fold, p<0.001; 1.202 ± 0.386-fold, p<0.001) (**Figure 10**).

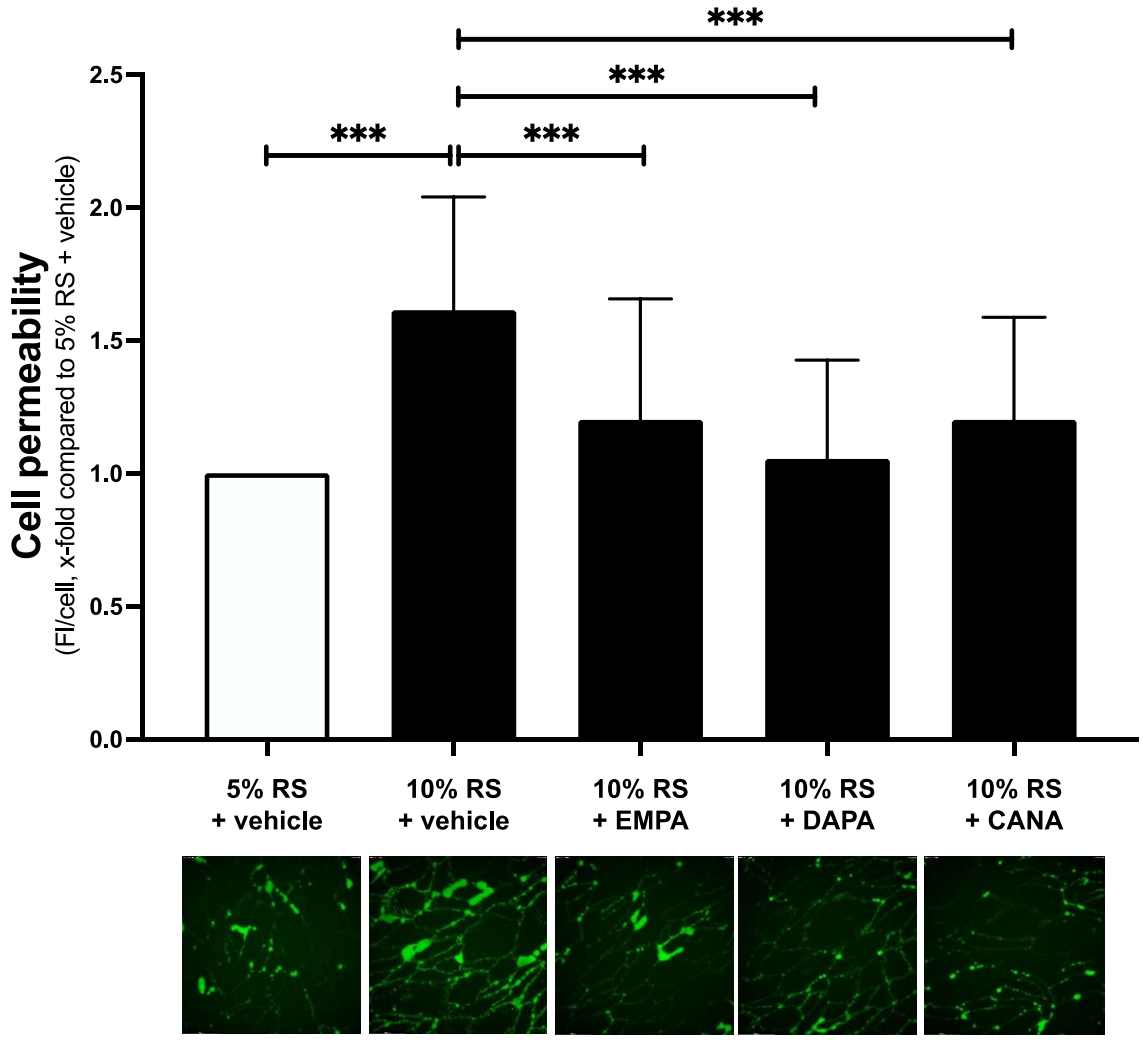

Figure 10. Cell permeability of HCAECs exposed to RMS with and without addition of SGLT2is

Permeability of an endothelial cell layer exposed to RMS with and without addition of SGLT2is (n= 5 individual experiments). Representative images are shown below the bar graph (200x magnification). Data are normalized to 5% RS + vehicle and presented as mean ± SD. ***p<0.001. CANA, Canagliflozin; DAPA, Dapagliflozin; EMPA, Empagliflozin; FI/cell, fluorescence intensity/cell; RS, repeated stretching.

Images of fluorescence stainings suggested lower VE-cadherin expression in HCAECs exposed to detrimental RMS (compared to non-detrimental RMS), especially in regions of cell-cell contacts. Addition of SGLT2is seemed to restore VE-cadherin expression (**Figure 11**).

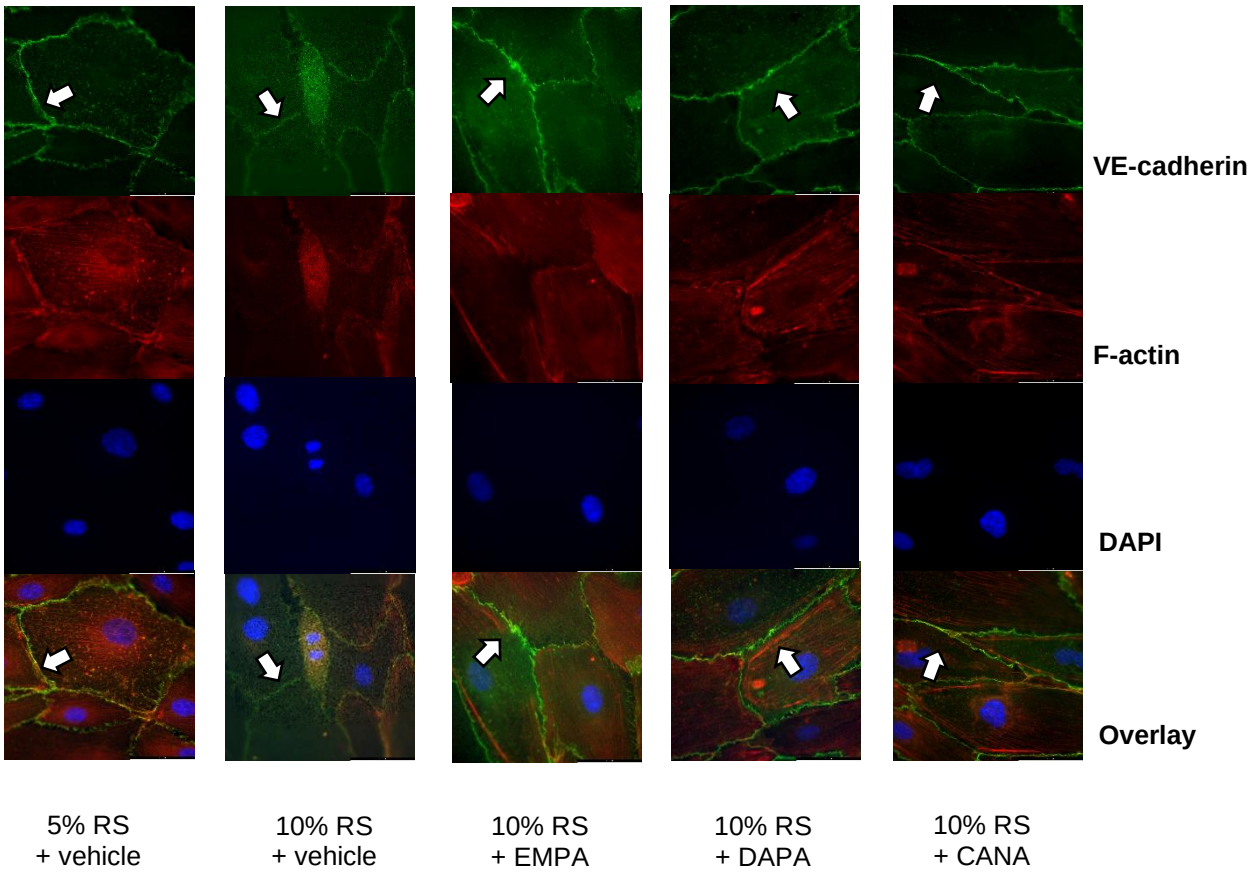

Figure 11. Fluorescence stainings of HCAECs exposed to RMS with and without addition of SGLT2is
Images of fluorescence stainings of HCAECs exposed to RMS with and without addition of SGLT2is (n= 3 individual experiments). Cells were stained for VE-cadherin, F-actin and DAPI. Representative images are shown (1000x magnification). Arrows indicate VE-cadherin expression in regions of cell-cell contacts. CANA, Canagliflozin; DAPA, Dapagliflozin; EMPA, Empagliflozin; F-actin, filamentous actin; RS, repeated stretching; VE-cadherin, vascular endothelial cadherin.

To quantify differences in VE-cadherin expression between the various conditions western blots were performed. Compared to non-detrimental RMS, detrimental RMS led to significant VE-cadherin loss (0.67 ± 0.15-fold, p<0.001, **Figure 12 a**; 0.69 ± 0.07-fold, p<0.001, **Figure 12 b**; 0.76 ± 0.11-fold, p<0.01, **Figure 12 c**). Incubation with EMPA, DAPA and CANA significantly reduced this loss in VE-cadherin expression (detrimental RMS + vehicle vs. detrimental RMS + EMPA, DAPA or CANA: 0.67 ± 0.15-fold vs. 0.90 ± 0.11-fold, p<0.01, **Figure 12 a**; 0.69 ± 0.07-fold vs 0.95 ± 0.09-fold, p<0.05, **Figure 12 b**; 0.76 ± 0.11-fold vs. 0.99 ± 0.12-fold, p<0.01, **Figure 12 c**).

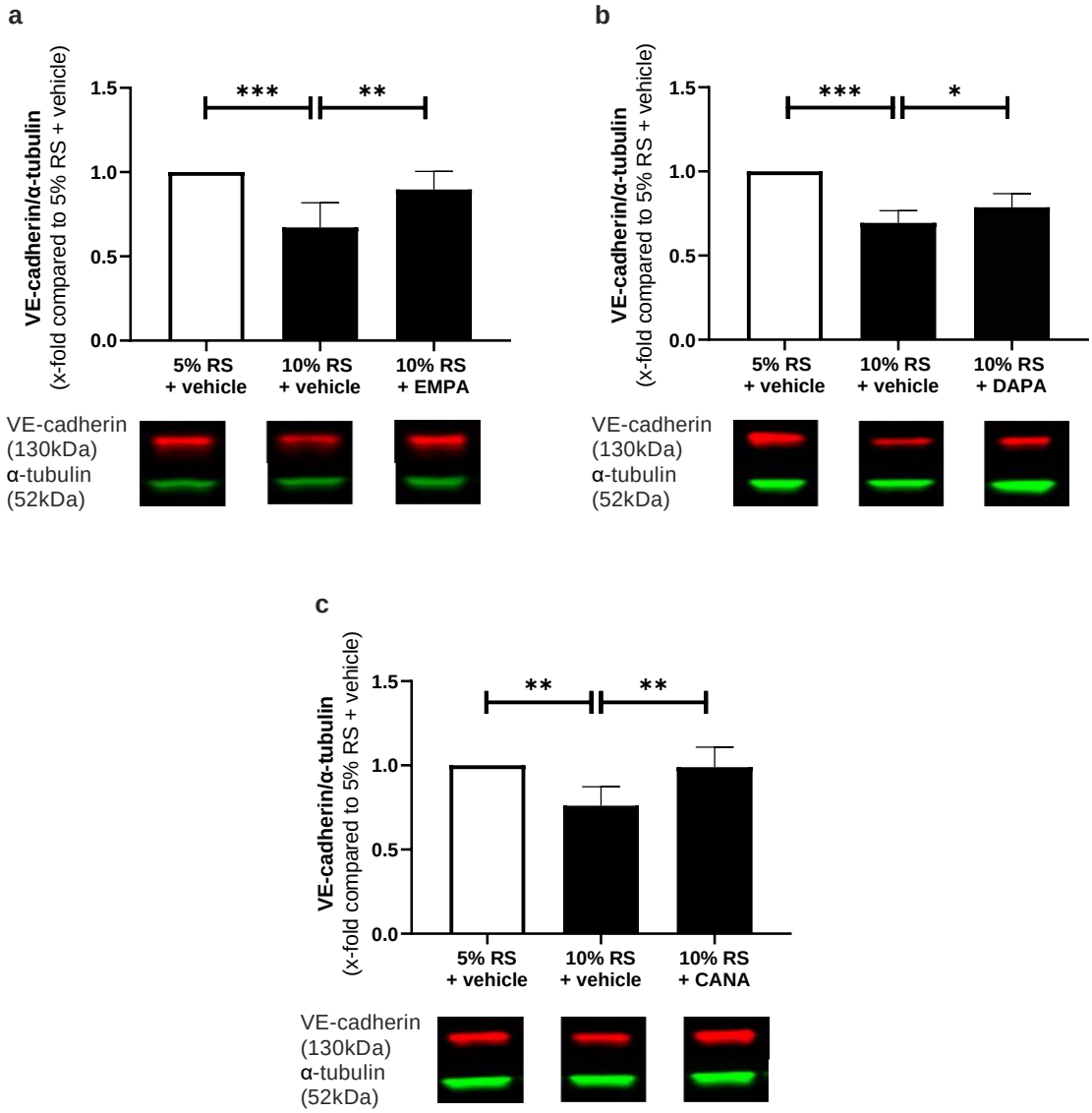

Figure 12. VE-cadherin expression levels of HCAECs exposed to RMS with and without addition of SGLT2is

a VE-cadherin expression levels of HCAECs exposed to RMS and incubated with EMPA (n= 6 individual experiments). **b** VE-cadherin expression levels of HCAECs exposed to RMS and incubated with DAPA (n= 6 individual experiments). **c** VE-cadherin expression levels of HCAECs exposed to RMS and incubated with CANA (n= 6 individual experiments). α-tubulin served as a loading control. Representative bands of VE-cadherin and α-tubulin are shown below the bar graphs. Data are normalized to 5% RS + vehicle and presented as mean ± SD. *p<0.05; **p<0.01; ***p<0.001. CANA, Canagliflozin; DAPA, Dapagliflozin; EMPA, Empagliflozin; kDa, kilodalton; RS, repeated stretching; VE-cadherin, vascular endothelial cadherin.

3.3 Detrimental RMS increases ROS levels in HCAECs

In a next step, the effect of detrimental RMS on ROS levels was measured. Compared to non-detrimental RMS, HCAECs exposed to detrimental RMS showed significantly higher ROS levels (2.475 ± 1.296-fold, p<0.001). Incubation with 5mM of the ROS scavenger NAC led to significantly lower ROS levels in HCAECs exposed detrimental RMS (detrimental RMS + vehicle vs. detrimental RMS + NAC: 2.475 ± 1.296-fold vs. 1.131 ± 0.585-fold, p<0.001) (**Figure 13**).

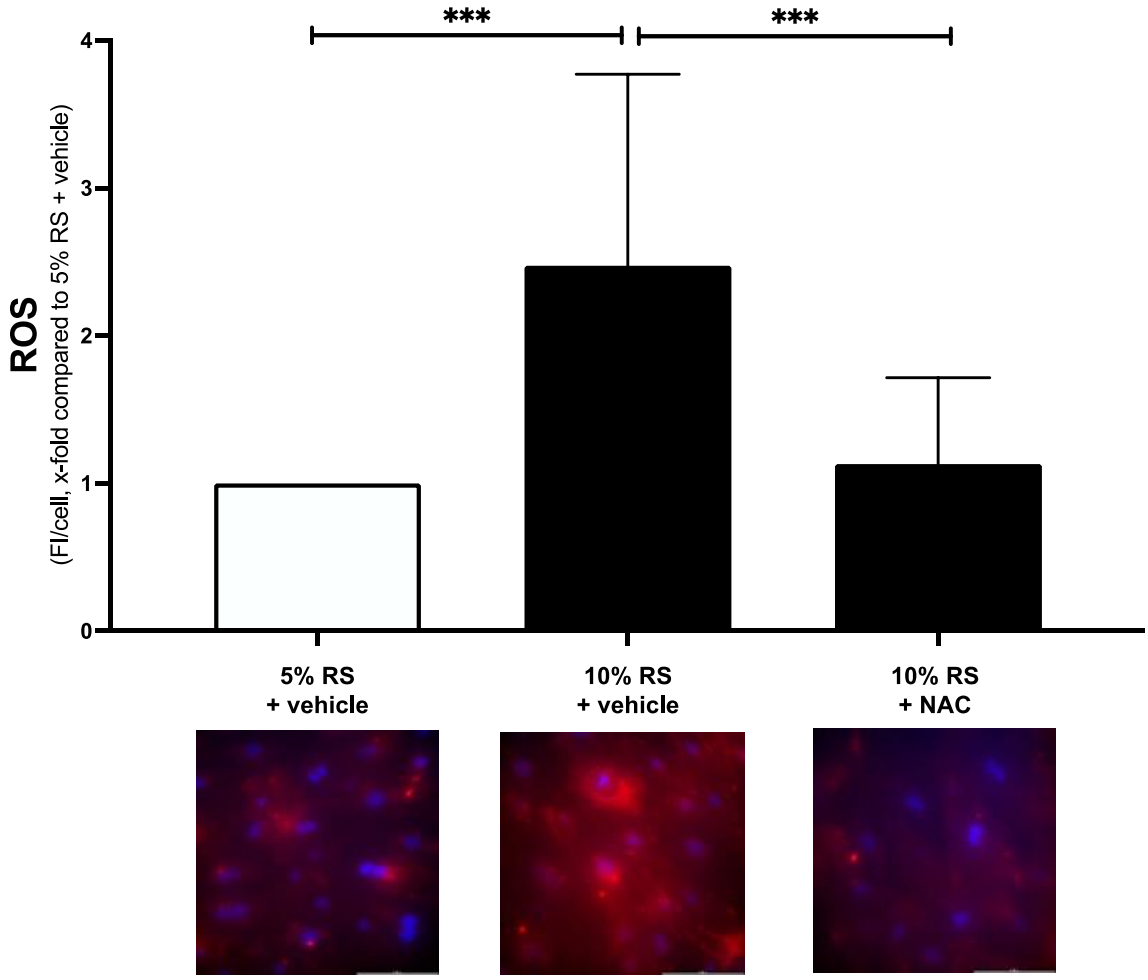

Figure 13. ROS levels of HCAECs exposed to RMS

ROS levels of HCAECs exposed to RMS with and without addition of NAC. Representative images are shown below the bar graph (400x magnification). Data are normalized to 5% RS + vehicle and presented as mean ± SD. ***p<0.001. FI/cell, fluorescence intensity/cell; NAC, N-acetyl-l-cysteine; ROS, reactive oxygen species; RS, repeated stretching.

3.4 SGLT2is reduce ROS levels in HCAECs exposed to detrimental RMS

Compared to vehicle treated HCAECs exposed to detrimental RMS, incubation with EMPA, DAPA and CANA also led to significantly lower ROS levels (detrimental RMS + vehicle vs. detrimental RMS + EMPA, DAPA or CANA: 2.392 ± 0.945-fold vs. 1.554 ± 0.978-fold, p<0.001; 1.406 ± 0.766-fold, p<0.001; 1.802 ± 0.867-fold, p<0.05) (**Figure 14**).

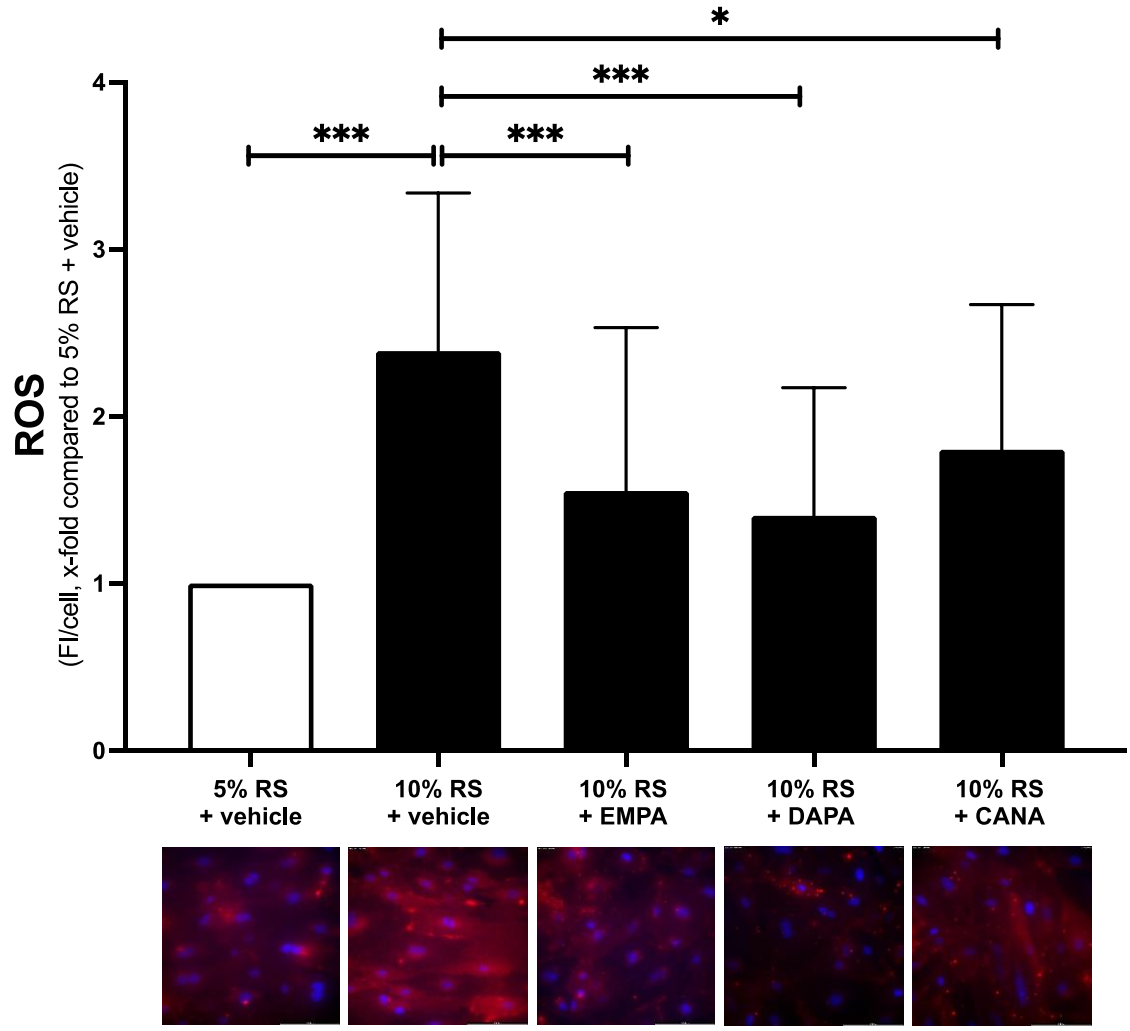

Figure 14. ROS levels of HCAECs exposed to RMS with and without addition of SGLT2is

ROS levels of HCAECs exposed to RMS with and without addition SGLT2is (n= 5 individual experiments). Representative images are shown below the bar graph (400x magnification). Data are normalized to 5% RS + vehicle and presented as mean ± SD. *p<0.05, ***p<0.001. CANA, Canagliflozin; DAPA, Dapagliflozin; EMPA, Empagliflozin; Fl/cell, fluorescence intensity/cell; ROS, reactive oxygen species; RS, repeated stretching.

3.5 NAC and EMPA attenuate the detrimental RMS induced increase in endothelial permeability

Incubation with 5mM of the ROS scavenger NAC significantly attenuated the detrimental RMS induced increase in endothelial permeability (detrimental RMS + vehicle vs detrimental RMS + NAC: 1.476 ± 0.534-fold vs. 1.044 ± 0.282-fold, p<0.001). This magnitude of reduction was similar to the reduction in cell permeability by EMPA (detrimental RMS + vehicle vs. detrimental RMS + EMPA: 1.476 ± 0.534-fold vs. 1.069 ± 0.360-fold, p<0.001). Furthermore, the combination of EMPA and NAC significantly reduced the detrimental RMS induced increase in cell permeability (detrimental RMS + vehicle vs. detrimental RMS + EMPA/NAC: 1.476 ± 0.534-fold vs. 0.961 ± 0.336-fold, p<0.001). However, no significant difference was found between EMPA and EMPA/NAC treated HCAECs exposed to detrimental RMS (detrimental RMS + EMPA vs. detrimental RMS + EMPA/NAC: 1.069 ± 0.360-fold vs. 0.961 ± 0.336-fold) (**Figure 15**).

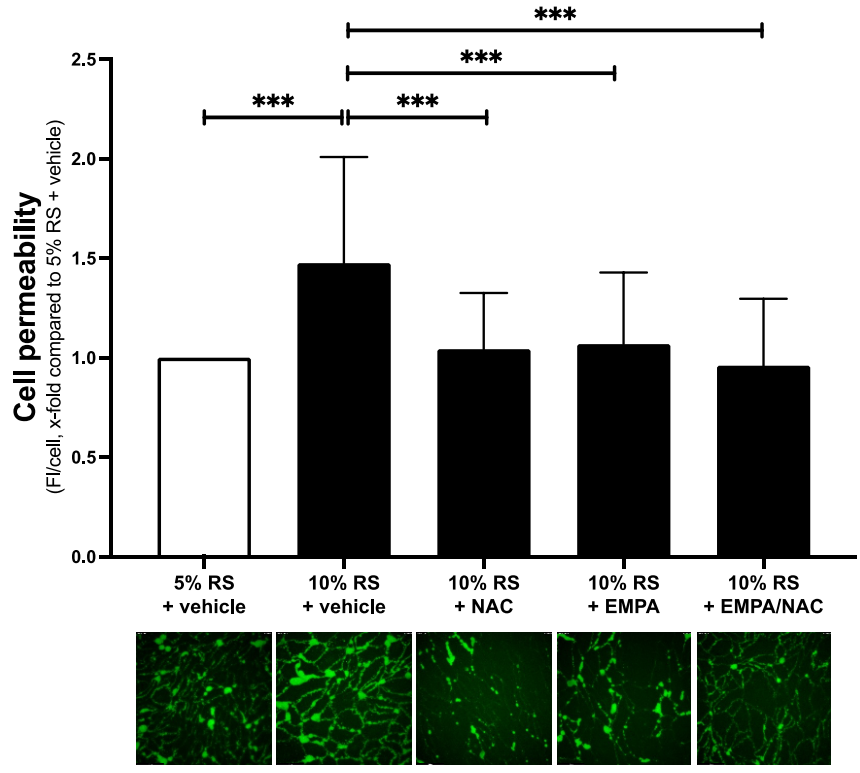

Figure 15. Cell permeability of HCAECs exposed to RMS with and without addition of EMPA and NAC
Permeability of an endothelial cell layer exposed to RMS with and without addition of NAC and EMPA (n= 5 individual experiments). Representative images of cell permeability are shown below the bar graph (200x magnification). Data are normalized to 5% RS + vehicle and presented as mean ± SD. ***p<0.001. EMPA, Empagliflozin; Fl/cell, fluorescence intensity/cell; NAC, N-acetyl-l-cysteine; RS, repeated stretching.

4 Discussion

The present study confirms that exposing HCAECs to detrimental RMS leads to endothelial barrier dysfunction, demonstrated by reduced VE-cadherin expression and increased endothelial permeability. With regards to the aims of this study, the key findings are: (1) SGLT2is, namely EMPA, DAPA and CANA, protect HCAECs against the detrimental RMS induced loss of VE-cadherin expression and rise in endothelial cell permeability; (2) detrimental RMS induces an increase of ROS levels; (3) the protective effects of SGLT2is on endothelial barrier dysfunction are likely mediated via a reduction of ROS levels.

4.1 Effects of SGLT2is on endothelial barrier function in HCAECs exposed to RMS

Endothelial cells are constantly exposed to hemodynamic forces. The two main hemodynamic forces acting on endothelial monolayers are shear stress, following blood flow, and RMS, caused by blood pressure profile. Due to the difficulty of conducting in-vivo experiments on the effects of these different hemodynamic forces on endothelial barrier function, many investigations focused on in-vitro models on either one of these two forces. Multiple studies which investigated the effects of RMS on endothelial barrier function have regarded 5% RS as a non-detrimental RMS and even reported protective effects of 5% RS on endothelial barrier function (Birukova et al., 2006, 2008; Collins et al., 2006). In turn, exposure to 10% RS or more has been regarded to represent detrimental RMS by several studies (Liu & Lin, 2022; Loperena et al., 2018; Omidvar et al., 2018). Based on these findings we chose 5% RS as a non-detrimental RMS and 10% RS as detrimental RMS in our study design.

Prior research has demonstrated that exposing endothelial cells to detrimental RMS either leads to a direct increase in cell permeability or enhances endothelial permeability via pro-inflammatory mediators (Birukov et al., 2003; Birukova et al., 2006, 2012; Gawlak et al., 2014; Tian et al., 2016). Results of the present study confirm that exposure to detrimental RMS induces an increase in cell permeability in HCAECs. Compared to non-detrimental RMS, exposure to detrimental RMS led to a significant increase in endothelial permeability. In addition, immunofluorescence staining suggested lower VE-cadherin expression in HCAECs exposed to detrimental RMS, especially at cell-cell adhesion sides. Moreover, the VE-cadherin content in cell lysates of HCAECS exposed to detrimental RMS was significantly lower than in HCAECs exposed to non-detrimental RMS, suggesting a detrimental RMS triggered VE-cadherin loss.

Controversially, our western blot results are not fully in line with the results of Tian et al., who also proposed a VE-cadherin dissociation from the cell membrane but no general VE-cadherin loss in mechanically stressed endothelial cells. Even though detrimental RMS caused a downregulation of intercellular VE-cadherin expression in human pulmonary arterial endothelial cells, no noticeable difference in the VE-cadherin content in cell lysates was found compared to a static condition (Tian et al., 2016). In contrast, exposing mouse lung vascular endothelial cells to detrimental RMS led to a significant downregulation of VE-cadherin expression in cell lysates (Zhang et al., 2021). Due to the disagreement in these findings, it becomes likely that different endothelial cell types react differently to detrimental RMS. Thus, further studies should focus on the effects of detrimental RMS on VE-cadherin expression and regulation in different endothelial cell types.

Most notably, all SGLT2is employed in our study attenuated the increase in endothelial permeability and VE-cadherin loss in HCAECs subjected to detrimental RMS. To our knowledge this is the first study to report protective effects of SGLT2is in HCAECs exposed to detrimental RMS. However, SGLT2is have already been reported to exert protective effects on endothelial barrier function in endothelial cells subjected to different stress stimuli (Angé et al., 2021; Ripoll et al., 2021; Zhou et al., 2018). In diabetic cardiac microvascular endothelial cells (CMECs) incubation with EMPA preserved endothelial barrier function and integrity via AMPK mediated suppression of mitochondrial ROS production (Zhou et al., 2018). In addition, a recent study by Angé et al. also reported AMPK mediated preservation of VE-cadherin integrity and endothelial barrier protection by CANA in lipopolysaccharide (LPS) stimulated HMVECs (Angé et al., 2021). Intriguingly, AMPK activation has also been reported to be involved in lowering elevated ROS levels, among other mechanisms by reducing mitochondrial injury and NOX suppression (Marino et al., 2021; Song & Zou, 2012). It is moreover well established that increased ROS levels are a crucial promotor of endothelial barrier dysfunction and permeability (He et al., 2020; Pignatelli et al., 2018; Tseng et al., 2017; Zhou et al., 2013). In aging rat arteries increased ROS production caused an internalization and degradation of VE-cadherin and its loss from AJs, ultimately resulting in the disruption of these junctions. Blocking ROS not only reverted the degradation of VE-cadherin but also decreased the disruption of endothelial AJs (Chang et al., 2018). Therefore, we hypothesized elevated ROS levels as a potential barrier impairing mechanism in HCAECs exposed to detrimental RMS.

4.2 Role of the reduction of ROS levels on the protective effects of SGLT2is

To elucidate whether increased ROS levels are involved in the detrimental RMS induced endothelial barrier dysfunction, ROS levels in HCAECs were determined after exposure to non-detrimental and detrimental RMS. Exposing HCAECs to detrimental RMS resulted in significantly higher ROS levels compared to exposure to non-detrimental RMS. Moreover, incubation with the ROS scavenger NAC not only led to significantly lower ROS levels in HCAECs subjected to detrimental RMS, but also ameliorated the detrimental RMS induced rise in endothelial permeability. Therefore, this study suggests elevated ROS levels as a potential factor triggering permeability in HCAECs exposed to RMS. Furthermore, these results are in line with the findings of Davidovich et al., who reported that the RMS induced rise in alveolar epithelial permeability can be reduced by applying a ROS-scavenger (Davidovich et al., 2013). Even though epithelial and endothelial cells are not the same cell type and might react to RMS via different pathways, it is likely that excessive ROS levels are a general response of cells subjected to detrimental RMS.

Next, we investigated whether the reduction of ROS levels is involved in the SGLT2is mediated amelioration of endothelial barrier dysfunction in HCAECs exposed to detrimental RMS. For that reason, ROS levels of HCAECs subjected to detrimental RMS with and without addition of SGLT2is were determined. It is known that EMPA and DAPA reduce inflammation induced ROS levels in resting endothelial cells and thereby ameliorate endothelial dysfunction (Juni et al., 2021; Uthman et al., 2019). In addition, EMPA decreased mitochondrial ROS levels in CMECs stimulated with TNF-α (Juni et al., 2019). Moreover, the most recent study by Uthman et al. reported that EMPA reduced Na^+/H^+ exchanger isoform 1 activity in HUVECs and HCAECs stimulated with TNF-α and thereby diminishes oxidative stress levels (Uthman et al., 2022). Results of this study further demonstrated that all SGLT2is employed in our study significantly reduce ROS levels in HCAECs exposed to detrimental RMS. However, the ROS level reducing effect by EMPA and DAPA was stronger than the ROS level reducing effect by CANA. Interestingly, a previous in-vitro study reported that CANA exerted a dose dependent effect on ROS levels. In LPS induced macrophages incubation with high doses of the SGLT2i CANA (>20 µM) significantly attenuated ROS levels. However, incubation with 10 µM CANA was not able to attenuate ROS levels in LPS induced macrophages (Xu et al., 2018). In contrast, in our experimental setup ROS levels of HCAECs exposed to detrimental RMS were already significantly attenuated by incubation with 3µM CANA. Therefore, it is likely that different cell types as well as different models of cellular stress have an impact on the dose of CANA required to significantly reduce ROS levels.

As mentioned above, incubation with the ROS-scavenger NAC reduced the detrimental RMS induced increase in endothelial permeability. However, the combination of NAC with EMPA had no additional reducing effect on the detrimental RMS induced rise in endothelial permeability compared to EMPA alone. These results indicate that EMPA and NAC may exert their protective effects on endothelial permeability via a similar mechanism. This, in turn, further supports the hypothesis that the reduction of ROS levels is a crucial mechanism by which EMPA ameliorates endothelial barrier dysfunction in HCAECs exposed to detrimental RMS.

4.3 Study limitations

There are some limitations of this study that need to be considered.

First, experiments were conducted in an in-vitro model of HCAECs, which is not able to fully imitate the complex biophysical and biochemical interplays which occur in-vivo. Therefore, this study can only provide conclusions for the administration of SGLT2is in HCAECs exposed to RMS. The protective effects of SGLT2is on endothelial barrier dysfunction and ROS levels in HCAECs exposed to a detrimental RMS could yet be cell specific and not be applicable on other endothelial cell types. Moreover, we did not investigate the effect of RMS on vascular smooth muscle cells, fibroblast, monocytes, macrophages, and other cell types present in the vascular system. Hence, we cannot draw conclusion about how these cell types react to RMS and whether co-culture with HCAECs would have led to different results.

Second, in the present in-vitro study HCAECs were only exposed to non-detrimental and detrimental RMS. However, in-vivo endothelial cells are exposed to multiple hemodynamic forces such as RMS and shear stress (Owatverot et al., 2005; Qiu & Tarbell, 2000). It is already known that disturbances in both hemodynamic forces are associated with endothelial dysfunction and increased cardiovascular risk (Brooks et al., 2004; Chistiakov et al., 2015; Cunningham & Gotlieb, 2005; Girão-Silva et al., 2021; Thacher et al., 2010). Since the experiments of the present study only mimicked one aspect of these hemodynamic forces, it is not possible to draw conclusions of the effects of shear stress, or the combination of shear stress and RMS on endothelial dysfunction.

Third, the protective effects of EMPA, DAPA and CANA on endothelial barrier dysfunction in HCAECs were only investigated with specific drug concentrations. Namely 1µM EMPA, 1µM DAPA, and 3µM CANA. These doses were based on previous in-vitro studies, which in turn were based on maximum plasma concentrations of each drug found at clinically relevant doses

(Scheen, 2014; Uthman et al., 2018, 2020; Zhang et al., 2021). On that account, results of this study cannot conclude whether higher or lower SGLT2is dosages exert similar protective effects on endothelial barrier dysfunction.

Fourth, the effects of SGLT2is on endothelial barrier dysfunctions were determined after a relatively short time period of 26h. However, in the large cardiovascular outcome trials SGLT2is only showed their cardiovascular beneficial effects when they were given on a daily basis for a long period of time (several month/years) (Neal et al., 2017; Wiviott et al., 2019; Zinman et al., 2015). As a result, we cannot draw any conclusion about the long-term effects of SGLT2is treatment on endothelial barrier function in HCAECs exposed to detrimental RMS.

4.4 Conclusion

The results of this in-vitro study suggest that SGLT2is exert their protective effects in cultures of HCAECs exposed to a detrimental RMS, at least partly, via a reduction of ROS levels and stabilization of endothelial barrier function. Our findings could also be of relevance for a deeper understanding of the cellular mechanisms associated with CVDs.

5 Summary

One of the most challenging tasks facing modern healthcare are cardiovascular diseases (CVDs), which are the leading cause of death around the world. That is why prevention, early detection, and optimal therapy of CVDs are extremely important for the medical care of the affected patients. A key element of a healthy cardiovascular status is an intact endothelium which consists of a monolayer of endothelial cells and is in direct contact with the circulating blood. Therefore, the endothelium is permanently exposed to hemodynamic forces in the form of shear stress and repeated mechanical stress (RMS). Alterations in these forces directly affect the endothelium and can potentially activate destructive pathways. In combination with other cardiovascular risk factors, such as diabetes mellitus (DM), hypercholesterolemia, obesity, and excessive hemodynamic forces these alterations can ultimately result in CVDs.

Sodium-glucose cotransporter 2 inhibitors (SGLT2is), a recently approved class of diabetic drugs lowering blood sugar levels by inhibiting glucose reabsorption in the kidney, have shown beneficial effects beyond reducing the blood glucose level. Multiple independent clinical studies demonstrated that all SGLT2is decrease the risk of developing CVDs. However, the mechanisms behind these cardioprotective effects are still not fully elucidated.

The present study investigated the effects of the SGLT2is Empagliflozin (EMPA), Dapagliflozin (DAPA) and Canagliflozin (CANA) on human coronary artery endothelial cells (HCAECs) exposed to RMS which was applied by repeated stretching (RS) of the endothelial cell monolayer. Endothelial permeability, vascular endothelial cadherin (VE-cadherin) expression levels and ROS levels were determined after exposure to non-detrimental (5% RS) and detrimental RMS (10% RS) for 24h.

One of our key findings is, that all SGLT2is protected HCAECs against the detrimental RMS induced rise in endothelial cell permeability and loss of VE-cadherin expression. In addition, exposing HCAECs to detrimental RMS led to increased ROS levels, which were significantly reduced by incubation with all SGLT2is. Incubation with the ROS scavenger N-acetyl-l-cysteine (NAC) not only reduced ROS levels but also ameliorated endothelial permeability in HCAECs exposed to detrimental RMS, suggesting increased ROS levels as a potential factor triggering permeability in HCAECs exposed to detrimental RMS.

In summary, the present in-vitro study suggests that the protective effects of SGLT2is in the context of CVDs might be mediated, at least in part, via a stabilization of endothelial barrier function and reduction of ROS levels.

6 References

Angé, M., De Poortere, J., Ginion, A., Battault, S., Dechamps, M., Muccioli, G. G., Roumain, M., Morelle, J., Druart, S., Mathivet, T., Bertrand, L., Castanares-Zapatero, D., Horman, S., & Beauloye, C. (2021). Canagliflozin protects against sepsis capillary leak syndrome by activating endothelial α1AMPK. *Scientific Reports*, *11*(1), 13700. https://doi.org/10.1038/s41598-021-93156-1

Angelini, D. J., Hyun, S.-W., Grigoryev, D. N., Garg, P., Gong, P., Singh, I. S., Passaniti, A., Hasday, J. D., & Goldblum, S. E. (2006). TNF-α increases tyrosine phosphorylation of vascular endothelial cadherin and opens the paracellular pathway through fyn activation in human lung endothelia. *American Journal of Physiology-Lung Cellular and Molecular Physiology*, *291*(6), L1232–L1245. https://doi.org/10.1152/ajplung.00109.2006

Anker, S. D., Butler, J., Filippatos, G., Ferreira, J. P., Bocchi, E., Böhm, M., Brunner–La Rocca, H.-P., Choi, D.-J., Chopra, V., Chuquiure-Valenzuela, E., Giannetti, N., Gomez-Mesa, J. E., Janssens, S., Januzzi, J. L., Gonzalez-Juanatey, J. R., Merkely, B., Nicholls, S. J., Perrone, S. V., Piña, I. L., … Packer, M. (2021). Empagliflozin in Heart Failure with a Preserved Ejection Fraction. *New England Journal of Medicine*, *385*(16), 1451–1461. https://doi.org/10.1056/NEJMoa2107038

Beitelshees, A. L., Leslie, B. R., & Taylor, S. I. (2019). Sodium–Glucose Cotransporter 2 Inhibitors: A Case Study in Translational Research. *Diabetes*, *68*(6). https://doi.org/10.2337/dbi18-0006

Birukov, K. G. (2009). Cyclic Stretch, Reactive Oxygen Species, and Vascular Remodeling. *Antioxidants & Redox Signaling*, *11*(7). https://doi.org/10.1089/ars.2008.2390

Birukov, K. G., Jacobson, J. R., Flores, A. A., Ye, S. Q., Birukova, A. A., Verin, A. D., & Garcia, J. G. N. (2003). Magnitude-dependent regulation of pulmonary endothelial cell barrier function by cyclic stretch. *American Journal of Physiology-Lung Cellular and Molecular Physiology*, *285*(4), L785–L797. https://doi.org/10.1152/ajplung.00336.2002

Birukova, A. A., Chatchavalvanich, S., Rios, A., Kawkitinarong, K., Garcia, J. G. N., & Birukov, K. G. (2006). Differential Regulation of Pulmonary Endothelial Monolayer Integrity by Varying Degrees of Cyclic Stretch. *The American Journal of Pathology*, *168*(5), 1749–1761. https://doi.org/10.2353/ajpath.2006.050431

Birukova, A. A., Rios, A., & Birukov, K. G. (2008). Long-term cyclic stretch controls pulmonary endothelial permeability at translational and post-translational levels. *Experimental Cell Research*, *314*(19), 3466–3477. https://doi.org/10.1016/j.yexcr.2008.09.003

Birukova, A. A., Tian, Y., Meliton, A., Leff, A., Wu, T., & Birukov, K. G. (2012). Stimulation of Rho signaling by pathologic mechanical stretch is a “second hit” to Rho-independent lung injury induced by IL-6. *American Journal of Physiology-Lung Cellular and Molecular Physiology*, *302*(9), L965–L975. https://doi.org/10.1152/ajplung.00292.2011

Brooks, A. R., Lelkes, P. I., & Rubanyi, G. M. (2004). Gene Expression Profiling of Vascular Endothelial Cells Exposed to Fluid Mechanical Forces: Relevance for Focal Susceptibility to Atherosclerosis. *Endothelium*, *11*(1), 45–57. https://doi.org/10.1080/10623320490432470

Chang, F., Flavahan, S., & Flavahan, N. A. (2018). Superoxide inhibition restores endothelium-dependent dilatation in aging arteries by enhancing impaired adherens junctions. *American Journal of Physiology-Heart and Circulatory Physiology*, *314*(4), H805–H811. https://doi.org/10.1152/ajpheart.00681.2017

Chen, J., Williams, S., Ho, S., Loraine, H., Hagan, D., Whaley, J. M., & Feder, J. N. (2010). Quantitative PCR tissue expression profiling of the human SGLT2 gene and related family members. *Diabetes Therapy*, *1*(2). https://doi.org/10.1007/s13300-010-0006-4

Chien, S. (2007). Mechanotransduction and endothelial cell homeostasis: the wisdom of the cell. *American Journal of Physiology-Heart and Circulatory Physiology*, *292*(3), H1209–H1224. https://doi.org/10.1152/ajpheart.01047.2006

Chilton, R., Tikkanen, I., Cannon, C. P., Crowe, S., Woerle, H. J., Broedl, U. C., & Johansen, O. E. (2015). Effects of empagliflozin on blood pressure and markers of arterial stiffness and vascular resistance in patients with type 2 diabetes. *Diabetes, Obesity and Metabolism*, *17*(12). https://doi.org/10.1111/dom.12572

Chistiakov, D. A., Orekhov, A. N., & Bobryshev, Y. V. (2015). Endothelial Barrier and Its Abnormalities in Cardiovascular Disease. *Frontiers in Physiology*, *6*. https://doi.org/10.3389/fphys.2015.00365

Cines, D. B., Pollak, E. S., Buck, C. A., Loscalzo, J., Zimmerman, G. A., McEver, R. P., Pober, J. S., Wick, T. M., Konkle, B. A., Schwartz, B. S., Barnathan, E. S., McCrae, K. R., Hug, B. A., Schmidt, A. M., & Stern, D. M. (1998). Endothelial cells in physiology and in the pathophysiology of vascular disorders. *Blood*, *91*(10), 3527–3561.

Collins, N. T., Cummins, P. M., Colgan, O. C., Ferguson, G., Birney, Y. A., Murphy, R. P., Meade, G., & Cahill, P. A. (2006). Cyclic Strain–Mediated Regulation of Vascular Endothelial Occludin and ZO-1. *Arteriosclerosis, Thrombosis, and Vascular Biology*, *26*(1), 62–68. https://doi.org/10.1161/01.ATV.0000194097.92824.b3

Cowie, M. R., & Fisher, M. (2020). SGLT2 inhibitors: mechanisms of cardiovascular benefit beyond glycaemic control. *Nature Reviews Cardiology*, *17*(12). https://doi.org/10.1038/s41569-020-0406-8

Cunningham, K. S., & Gotlieb, A. I. (2005). The role of shear stress in the pathogenesis of atherosclerosis. *Laboratory Investigation*, *85*(1), 9–23. https://doi.org/10.1038/labinvest.3700215

Davidovich, N., DiPaolo, B. C., Lawrence, G. G., Chhour, P., Yehya, N., & Margulies, S. S. (2013). Cyclic Stretch–Induced Oxidative Stress Increases Pulmonary Alveolar Epithelial Permeability. *American Journal of Respiratory Cell and Molecular Biology*, *49*(1). https://doi.org/10.1165/rcmb.2012-0252OC

Dejana, E., Orsenigo, F., & Lampugnani, M. G. (2008). The role of adherens junctions and VE-cadherin in the control of vascular permeability. *Journal of Cell Science*, *121*(13), 2115–2122. https://doi.org/10.1242/jcs.017897

Dubrovskyi, O., Birukova, A. A., & Birukov, K. G. (2013). Measurement of local permeability at subcellular level in cell models of agonist- and ventilator-induced lung injury. *Laboratory Investigation*, *93*(2). https://doi.org/10.1038/labinvest.2012.159

Esser, S., Lampugnani, M. G., Corada, M., Dejana, E., & Risau, W. (1998). Vascular endothelial growth factor induces VE-cadherin tyrosine phosphorylation in endothelial cells. *Journal of Cell Science*, *111 (Pt 13)*, 1853–1865.

Fang, Y., Wu, D., & Birukov, K. G. (2019). Mechanosensing and Mechanoregulation of Endothelial Cell Functions. In *Comprehensive Physiology* (pp. 873–904). Wiley. https://doi.org/10.1002/cphy.c180020

Félétou, M. (2011). The Endothelium, Part I: Multiple Functions of the Endothelial Cells -- Focus on Endothelium-Derived Vasoactive Mediators. *Colloquium Series on Integrated Systems Physiology: From Molecule to Function*, *3*(4). https://doi.org/10.4199/C00031ED1V01Y201105ISP019

Fernandes, D. C., Araujo, T. L. S., Laurindo, F. R. M., & Tanaka, L. Y. (2018). Hemodynamic Forces in the Endothelium: From Mechanotransduction to Implications on Development of Atherosclerosis. In *Endothelium and Cardiovascular Diseases* (pp. 85–95). Elsevier. https://doi.org/10.1016/B978-0-12-812348-5.00007-6

Ferrannini, E., Baldi, S., Frascerra, S., Astiarraga, B., Heise, T., Bizzotto, R., Mari, A., Pieber, T. R., & Muscelli, E. (2016). Shift to Fatty Substrate Utilization in Response to Sodium–Glucose Cotransporter 2 Inhibition in Subjects Without Diabetes and Patients With Type 2 Diabetes. *Diabetes*, *65*(5). https://doi.org/10.2337/db15-1356

Ferrannini, E., Mark, M., & Mayoux, E. (2016). CV Protection in the EMPA-REG OUTCOME Trial: A “Thrifty Substrate” Hypothesis. *Diabetes Care*, *39*(7). https://doi.org/10.2337/dc16-0330

Fonseca-Correa, J. I., & Correa-Rotter, R. (2021). Sodium-Glucose Cotransporter 2 Inhibitors Mechanisms of Action: A Review. *Frontiers in Medicine*, *8*. https://doi.org/10.3389/fmed.2021.777861

Galley, H. F., & Webster, N. R. (2004). Physiology of the endothelium. *British Journal of Anaesthesia*, *93*(1), 105–113. https://doi.org/10.1093/bja/aeh163

Gawlak, G., Tian, Y., O'Donnell, J. J., Tian, X., Birukova, A. A., & Birukov, K. G. (2014). Paxillin mediates stretch-induced Rho signaling and endothelial permeability *via* assembly of paxillin-p42/44MAPK-GEF-H1 complex. *The FASEB Journal*, *28*(7), 3249–3260. https://doi.org/10.1096/fj.13-245142

Girão-Silva, T., Fonseca-Alaniz, M. H., Ribeiro-Silva, J. C., Lee, J., Patil, N. P., Dallan, L. A., Baker, A. B., Harmsen, M. C., Krieger, J. E., & Miyakawa, A. A. (2021). High stretch induces endothelial dysfunction accompanied by oxidative stress and actin remodeling in human saphenous vein endothelial cells. *Scientific Reports*, *11*(1), 13493. https://doi.org/10.1038/s41598-021-93081-3

Haybar, H., Shahrabi, S., Rezaeeyan, H., Shirzad, R., & Saki, N. (2019). Endothelial Cells: From Dysfunction Mechanism to Pharmacological Effect in Cardiovascular Disease. *Cardiovascular Toxicology*, *19*(1), 13–22. https://doi.org/10.1007/s12012-018-9493-8

He, P., Talukder, M. A. H., & Gao, F. (2020). Oxidative Stress and Microvessel Barrier Dysfunction. *Frontiers in Physiology*, *11*. https://doi.org/10.3389/fphys.2020.00472

Heerspink, H. J. L., Stefánsson, B. V., Correa-Rotter, R., Chertow, G. M., Greene, T., Hou, F.-F., Mann, J. F. E., McMurray, J. J. V., Lindberg, M., Rossing, P., Sjöström, C. D., Toto, R. D., Langkilde, A.-M., & Wheeler, D. C. (2020). Dapagliflozin in Patients with Chronic Kidney Disease. *New England Journal of Medicine*, *383*(15), 1436–1446. https://doi.org/10.1056/NEJMoa2024816

Hishikawa, K., & Lüscher, T. F. (1997). Pulsatile Stretch Stimulates Superoxide Production in Human Aortic Endothelial Cells. *Circulation*, *96*(10), 3610–3616. https://doi.org/10.1161/01.CIR.96.10.3610

Hishikawa, K., Oemar, B. S., Yang, Z., & Lüscher, T. F. (1997). Pulsatile Stretch Stimulates Superoxide Production and Activates Nuclear Factor-κB in Human Coronary Smooth Muscle. *Circulation Research*, *81*(5), 797–803. https://doi.org/10.1161/01.RES.81.5.797

Ishibashi, Y., Matsui, T., & Yamagishi, S. (2015). Tofogliflozin, A Highly Selective Inhibitor of SGLT2 Blocks Proinflammatory and Proapoptotic Effects of Glucose Overload on Proximal Tubular Cells Partly by Suppressing Oxidative Stress Generation. *Hormone and Metabolic Research*, *48*(03). https://doi.org/10.1055/s-0035-1555791

Jamaluddin, M. S., Wang, X., Wang, H., Rafael, C., Yao, Q., & Chen, C. (2009). Eotaxin Increases Monolayer Permeability of Human Coronary Artery Endothelial Cells. *Arteriosclerosis, Thrombosis, and Vascular Biology*, *29*(12), 2146–2152. https://doi.org/10.1161/ATVBAHA.109.194134

Jamaluddin, M. S., Yan, S., Lü, J., Liang, Z., Yao, Q., & Chen, C. (2013). Resistin Increases Monolayer Permeability of Human Coronary Artery Endothelial Cells. *PLoS ONE*, *8*(12), e84576. https://doi.org/10.1371/journal.pone.0084576

Joseph, P., Leong, D., McKee, M., Anand, S. S., Schwalm, J.-D., Teo, K., Mente, A., & Yusuf, S. (2017). Reducing the Global Burden of Cardiovascular Disease, Part 1. *Circulation Research*, *121*(6). https://doi.org/10.1161/CIRCRESAHA.117.308903

Juni, R. P., Al-Shama, R., Kuster, D. W. D., van der Velden, J., Hamer, H. M., Vervloet, M. G., Eringa, E. C., Koolwijk, P., & van Hinsbergh, V. W. M. (2021). Empagliflozin restores chronic kidney disease–induced impairment of endothelial regulation of cardiomyocyte relaxation and contraction. *Kidney International*, *99*(5). https://doi.org/10.1016/j.kint.2020.12.013

Juni, R. P., Kuster, D. W. D., Goebel, M., Helmes, M., Musters, R. J. P., van der Velden, J., Koolwijk, P., Paulus, W. J., & van Hinsbergh, V. W. M. (2019). Cardiac Microvascular Endothelial Enhancement of Cardiomyocyte Function Is Impaired by Inflammation and Restored by Empagliflozin. *JACC: Basic to Translational Science*, *4*(5), 575–591. https://doi.org/10.1016/j.jacbts.2019.04.003

Karg, M. V., Bosch, A., Kannenkeril, D., Striepe, K., Ott, C., Schneider, M. P., Boemke-Zelch, F., Linz, P., Nagel, A. M., Titze, J., Uder, M., & Schmieder, R. E. (2018). SGLT-2-inhibition with dapagliflozin reduces tissue sodium content: a randomised controlled trial. *Cardiovascular Diabetology*, *17*(1). https://doi.org/10.1186/s12933-017-0654-z

Kou, B., Zhang, J., & Singer, D. R. J. (2009). Effects of cyclic strain on endothelial cell apoptosis and tubulogenesis are dependent on ROS production via NAD(P)H subunit p22phox. *Microvascular Research*, *77*(2), 125–133. https://doi.org/10.1016/j.mvr.2008.08.001

Krogmann, A., Staiger, K., Haas, C., Gommer, N., Peter, A., Heni, M., Machicao, F., Häring, H.-U., & Staiger, H. (2011). Inflammatory response of human coronary artery endothelial cells to saturated long-chain fatty acids. *Microvascular Research*, *81*(1), 52–59. https://doi.org/10.1016/j.mvr.2010.11.008

Lakota, K., Hrušovar, D., Ogrič, M., Mrak-Poljšak, K., Čučnik, S., Tomšič, M., Božič, B., Žigon, P., & Sodin-Semrl, S. (2018). Analysis of Drug Effects on Primary Human Coronary Artery Endothelial Cells Activated by Serum Amyloid A. *Mediators of Inflammation*, *2018*, 1–11. https://doi.org/10.1155/2018/8237209

Lakota, K., Mrak-Poljšak, K., Rozman, B., Kveder, T., Tomšič, M., & Sodin-Semrl, S. (2007). Serum Amyloid A Activation of Inflammatory and Adhesion Molecules in Human Coronary Artery and Umbilical Vein Endothelial Cells. *European Journal of Inflammation*, *5*(2), 73–81. https://doi.org/10.1177/1721727X0700500203

Lakota, K., Mrak-Poljsak, K., Rozman, B., & Sodin-Semrl, S. (2009). Increased Responsiveness of Human Coronary Artery Endothelial Cells in Inflammation and Coagulation. *Mediators of Inflammation*, *2009*, 1–8. https://doi.org/10.1155/2009/146872

Lambers Heerspink, H. J., de Zeeuw, D., Wie, L., Leslie, B., & List, J. (2013). Dapagliflozin a glucose-regulating drug with diuretic properties in subjects with type 2 diabetes. *Diabetes, Obesity and Metabolism*, *15*(9). https://doi.org/10.1111/dom.12127

LEHOUX, S. (2006). Redox signalling in vascular responses to shear and stretch. *Cardiovascular Research*, *71*(2), 269–279. https://doi.org/10.1016/j.cardiores.2006.05.008

Lehoux, S., Esposito, B., Merval, R., Loufrani, L., & Tedgui, A. (2000). Pulsatile Stretch–Induced Extracellular Signal–Regulated Kinase 1/2 Activation in Organ Culture of Rabbit Aorta Involves Reactive Oxygen Species. *Arteriosclerosis, Thrombosis, and Vascular Biology*, *20*(11), 2366–2372. https://doi.org/10.1161/01.ATV.20.11.2366

Liu, S., & Lin, Z. (2022). Vascular Smooth Muscle Cells Mechanosensitive Regulators and Vascular Remodeling. *Journal of Vascular Research*, *59*(2), 90–113. https://doi.org/10.1159/000519845

Loperena, R., Van Beusecum, J. P., Itani, H. A., Engel, N., Laroumanie, F., Xiao, L., Elijovich, F., Laffer, C. L., Gnecco, J. S., Noonan, J., Maffia, P., Jasiewicz-Honkisz, B., Czesnikiewicz-Guzik, M., Mikolajczyk, T., Sliwa, T., Dikalov, S., Weyand, C. M., Guzik, T. J., & Harrison, D. G. (2018). Hypertension and increased endothelial mechanical stretch promote monocyte differentiation and activation: roles of STAT3, interleukin 6 and hydrogen peroxide. *Cardiovascular Research*, *114*(11), 1547–1563. https://doi.org/10.1093/cvr/cvy112

Lüllmann-Rauch, R., & Asan, E. (2019). *Taschenlehrbuch Histologie*. Georg Thieme Verlag. https://doi.org/10.1055/b-006-163361

Mancini, S. J., Boyd, D., Katwan, O. J., Strembitska, A., Almabrouk, T. A., Kennedy, S., Palmer, T. M., & Salt, I. P. (2018). Canagliflozin inhibits interleukin-1β-stimulated cytokine and chemokine secretion in vascular endothelial cells by AMP-activated protein kinase-dependent and -independent mechanisms. *Scientific Reports*, *8*(1), 5276. https://doi.org/10.1038/s41598-018-23420-4

Marchio, P., Guerra-Ojeda, S., Vila, J. M., Aldasoro, M., Victor, V. M., & Mauricio, M. D. (2019). Targeting Early Atherosclerosis: A Focus on Oxidative Stress and Inflammation. *Oxidative Medicine and Cellular Longevity*, *2019*. https://doi.org/10.1155/2019/8563845

Marino, A., Hausenloy, D. J., Andreadou, I., Horman, S., Bertrand, L., & Beauloye, C. (2021). AMP-activated protein kinase: A remarkable contributor to preserve a healthy heart against ROS injury. *Free Radical Biology and Medicine*, *166*, 238–254. https://doi.org/10.1016/j.freeradbiomed.2021.02.047

Matheus, A. S. de M., Tannus, L. R. M., Cobas, R. A., Palma, C. C. S., Negrato, C. A., & Gomes, M. de B. (2013). Impact of Diabetes on Cardiovascular Disease: An Update. *International Journal of Hypertension*, *2013*. https://doi.org/10.1155/2013/653789

Matsushita, H., Lee, K., & Tsao, P. S. (2001). Cyclic strain induces reactive oxygen species production via an endothelial NAD(P)H oxidase. *Journal of Cellular Biochemistry*, *81*(S36). https://doi.org/10.1002/jcb.1094

McMurray, J. J. V., Solomon, S. D., Inzucchi, S. E., Køber, L., Kosiborod, M. N., Martinez, F. A., Ponikowski, P., Sabatine, M. S., Anand, I. S., Bělohlávek, J., Böhm, M., Chiang, C.-E., Chopra, V. K., de Boer, R. A., Desai, A. S., Diez, M., Drozdz, J., Dukát, A., Ge, J., … Langkilde, A.-M. (2019). Dapagliflozin in Patients with Heart Failure and Reduced Ejection Fraction. *New England Journal of Medicine*, *381*(21), 1995–2008. https://doi.org/10.1056/NEJMoa1911303

Mendis, Shanthi., Puska, P., Norrving, Bo., World Health Organization., World Heart Federation., & World Stroke Organization. (2011). *Global atlas on cardiovascular disease prevention and control*. World Health Organization in collaboration with the World Heart Federation and the World Stroke Organization. https://www.who.int/cardiovascular_diseases/publications/atlas_cvd/en/

Moldobaeva, A., Jenkins, J., & Wagner, E. (2008). Effects of distension on airway inflammation and venular P-selectin expression. *American Journal of Physiology-Lung Cellular and Molecular Physiology*, *295*(5), L941–L948. https://doi.org/10.1152/ajplung.90447.2008

Neal, B., Perkovic, V., Mahaffey, K. W., de Zeeuw, D., Fulcher, G., Erondu, N., Shaw, W., Law, G., Desai, M., & Matthews, D. R. (2017). Canagliflozin and Cardiovascular and Renal Events in Type 2 Diabetes. *New England Journal of Medicine*, *377*(7), 644–657. https://doi.org/10.1056/NEJMoa1611925

Nwariaku, F. E., Liu, Z., Zhu, X., Nahari, D., Ingle, C., Wu, R. F., Gu, Y., Sarosi, G., & Terada, L. S. (2004). NADPH oxidase mediates vascular endothelial cadherin phosphorylation and endothelial dysfunction. *Blood*, *104*(10). https://doi.org/10.1182/blood-2004-05-1868

Ojima, A., Matsui, T., Nishino, Y., Nakamura, N., & Yamagishi, S. (2015). Empagliflozin, an Inhibitor of Sodium-Glucose Cotransporter 2 Exerts Anti-Inflammatory and Antifibrotic Effects on Experimental Diabetic Nephropathy Partly by Suppressing AGEs-Receptor Axis. *Hormone and Metabolic Research*, *47*(09). https://doi.org/10.1055/s-0034-1395609

Omidvar, R., Tafazzoli-Shadpour, M., Mahmoodi-Nobar, F., Azadi, S., & Khani, M.-M. (2018). Quantifying effects of cyclic stretch on cell–collagen substrate adhesiveness of vascular endothelial cells. *Proceedings of the Institution of Mechanical Engineers, Part H: Journal of Engineering in Medicine*, *232*(5), 531–541. https://doi.org/10.1177/0954411918767477

Owatverot, T. B., Oswald, S. J., Chen, Y., Wille, J. J., & Yin, F. C.-P. (2005). Effect of Combined Cyclic Stretch and Fluid Shear Stress on Endothelial Cell Morphological Responses. *Journal of Biomechanical Engineering*, *127*(3), 374–382. https://doi.org/10.1115/1.1894180

Packer, M., Anker, S. D., Butler, J., Filippatos, G., Pocock, S. J., Carson, P., Januzzi, J., Verma, S., Tsutsui, H., Brueckmann, M., Jamal, W., Kimura, K., Schnee, J., Zeller, C., Cotton, D., Bocchi, E., Böhm, M., Choi, D.-J., Chopra, V., … Zannad, F. (2020). Cardiovascular and Renal Outcomes with Empagliflozin in Heart Failure. *New England Journal of Medicine*, *383*(15), 1413–1424. https://doi.org/10.1056/NEJMoa2022190

Pastori, D., Carnevale, R., & Pignatelli, P. (2014). Is there a clinical role for oxidative stress biomarkers in atherosclerotic diseases? *Internal and Emergency Medicine*, *9*(2). https://doi.org/10.1007/s11739-013-0999-6

Piepoli, M. F., Abreu, A., Albus, C., Ambrosetti, M., Brotons, C., Catapano, A. L., Corra, U., Cosyns, B., Deaton, C., Graham, I., Hoes, A., Lochen, M.-L., Matrone, B., Redon, J., Sattar, N., Smulders, Y., & Tiberi, M. (2020). Update on cardiovascular prevention in clinical practice: A position paper of the European Association of Preventive Cardiology

of the European Society of Cardiology. *European Journal of Preventive Cardiology*, *27*(2). https://doi.org/10.1177/2047487319893035

Piepoli, M. F., Hoes, A. W., Agewall, S., Albus, C., Brotons, C., Catapano, A. L., Cooney, M.-T., Corrà, U., Cosyns, B., Deaton, C., Graham, I., Hall, M. S., Hobbs, F. D. R., Løchen, M.-L., Löllgen, H., Marques-Vidal, P., Perk, J., Prescott, E., Redon, J., … Verschuren, W. M. M. (2016). 2016 European Guidelines on cardiovascular disease prevention in clinical practice. *Atherosclerosis*, *252*. https://doi.org/10.1016/j.atherosclerosis.2016.05.037

Pignatelli, P., Menichelli, D., Pastori, D., & Violi, F. (2018). Oxidative stress and cardiovascular disease: new insights. *Kardiologia Polska*. https://doi.org/10.5603/KP.a2018.0071

Qiu, Y., & Tarbell, J. M. (2000). Interaction between Wall Shear Stress and Circumferential Strain Affects Endothelial Cell Biochemical Production. *Journal of Vascular Research*, *37*(3), 147–157. https://doi.org/10.1159/000025726

Ren, X., Ren, L., Wei, Q., Shao, H., Chen, L., & Liu, N. (2017). Advanced glycation end-products decreases expression of endothelial nitric oxide synthase through oxidative stress in human coronary artery endothelial cells. *Cardiovascular Diabetology*, *16*(1), 52. https://doi.org/10.1186/s12933-017-0531-9

Ripoll, C. V., Guo, Z., Riehl, T., Girardi, A., Kovacs, A., Oscarsson, J., Esterline, R., Kosiborod, M., & Javaheri, A. (2021). DAPAGLIFLOZIN ATTENUATES ENDOTHELIAL LEAK VIA AN APOLIPOPROTEIN M-DEPENDENT PATHWAY. *Journal of the American College of Cardiology*, *77*(18), 3403. https://doi.org/10.1016/S0735-1097(21)04757-4

Rodrigues, S. F., & Granger, D. N. (2015). Blood cells and endothelial barrier function. *Tissue Barriers*, *3*(1–2). https://doi.org/10.4161/21688370.2014.978720

Saeedi, P., Petersohn, I., Salpea, P., Malanda, B., Karuranga, S., Unwin, N., Colagiuri, S., Guariguata, L., Motala, A. A., Ogurtsova, K., Shaw, J. E., Bright, D., & Williams, R. (2019). Global and regional diabetes prevalence estimates for 2019 and projections for 2030 and 2045: Results from the International Diabetes Federation Diabetes Atlas, 9th edition. *Diabetes Research and Clinical Practice*, *157*. https://doi.org/10.1016/j.diabres.2019.107843

Scheen, A. J. (2014). Evaluating SGLT2 inhibitors for type 2 diabetes: pharmacokinetic and toxicological considerations. *Expert Opinion on Drug Metabolism & Toxicology*, *10*(5), 647–663. https://doi.org/10.1517/17425255.2014.873788

Scheen, A. J. (2019). Effect of SGLT2 Inhibitors on the Sympathetic Nervous System and Blood Pressure. *Current Cardiology Reports*, *21*(8). https://doi.org/10.1007/s11886-019-1165-1

Shasby, D. M., Ries, D. R., Shasby, S. S., & Winter, M. C. (2002). Histamine stimulates phosphorylation of adherens junction proteins and alters their link to vimentin. *American Journal of Physiology-Lung Cellular and Molecular Physiology*, *282*(6), L1330–L1338. https://doi.org/10.1152/ajplung.00329.2001

Skaria, T., Burgener, J., Bachli, E., & Schoedon, G. (2016). IL-4 Causes Hyperpermeability of Vascular Endothelial Cells through Wnt5A Signaling. *PLOS ONE*, *11*(5), e0156002. https://doi.org/10.1371/journal.pone.0156002

Song, P., & Zou, M.-H. (2012). Regulation of NAD(P)H oxidases by AMPK in cardiovascular systems. *Free Radical Biology and Medicine*, *52*(9), 1607–1619. https://doi.org/10.1016/j.freeradbiomed.2012.01.025

Sun, H.-J., Wu, Z.-Y., Nie, X.-W., & Bian, J.-S. (2020). Role of Endothelial Dysfunction in Cardiovascular Diseases: The Link Between Inflammation and Hydrogen Sulfide. *Frontiers in Pharmacology*, *10*. https://doi.org/10.3389/fphar.2019.01568

Thacher, T. N., Silacci, P., Stergiopulos, N., & da Silva, R. F. (2010). Autonomous Effects of Shear Stress and Cyclic Circumferential Stretch regarding Endothelial Dysfunction and Oxidative Stress: An ex vivo Arterial Model. *Journal of Vascular Research*, *47*(4), 336–345. https://doi.org/10.1159/000265567

Tian, Y., Gawlak, G., O'Donnell, J. J., Birukova, A. A., & Birukov, K. G. (2016). Activation of Vascular Endothelial Growth Factor (VEGF) Receptor 2 Mediates Endothelial Permeability Caused by Cyclic Stretch. *Journal of Biological Chemistry*, *291*(19), 10032–10045. https://doi.org/10.1074/jbc.M115.690487

Touyz, R. M., & Schiffrin, E. L. (2004). Reactive oxygen species in vascular biology: implications in hypertension. *Histochemistry and Cell Biology*, *122*(4). https://doi.org/10.1007/s00418-004-0696-7

Tseng, C.-Y., Wang, J.-S., & Chao, M.-W. (2017). Causation by Diesel Exhaust Particles of Endothelial Dysfunctions in Cytotoxicity, Pro-inflammation, Permeability, and Apoptosis Induced by ROS Generation. *Cardiovascular Toxicology*, *17*(4). https://doi.org/10.1007/s12012-016-9364-0

Uthman, L., Baartscheer, A., Bleijlevens, B., Schumacher, C. A., Fiolet, J. W. T., Koeman, A., Jancev, M., Hollmann, M. W., Weber, N. C., Coronel, R., & Zuurbier, C. J. (2018). Class effects of SGLT2 inhibitors in mouse cardiomyocytes and hearts: inhibition of Na+/H+ exchanger, lowering of cytosolic Na+ and vasodilation. *Diabetologia*, *61*(3). https://doi.org/10.1007/s00125-017-4509-7

Uthman, L., Homayr, A., Juni, R. P., Spin, E. L., Kerindongo, R., Boomsma, M., Hollmann, M. W., Preckel, B., Koolwijk, P., van Hinsbergh, V. W. M., Zuurbier, C. J., Albrecht, M., & Weber, N. C. (2019). Empagliflozin and Dapagliflozin Reduce ROS Generation and Restore NO Bioavailability in Tumor Necrosis Factor α-Stimulated Human Coronary Arterial Endothelial Cells. *Cellular Physiology and Biochemistry : International Journal of Experimental Cellular Physiology, Biochemistry, and Pharmacology*, *53*(5), 865–886. https://doi.org/10.33594/000000178

Uthman, L., Kuschma, M., Römer, G., Boomsma, M., Kessler, J., Hermanides, J., Hollmann, M. W., Preckel, B., Zuurbier, C. J., & Weber, N. C. (2020). Novel Anti-inflammatory Effects of Canagliflozin Involving Hexokinase II in Lipopolysaccharide-Stimulated Human Coronary Artery Endothelial Cells. *Cardiovascular Drugs and Therapy*. https://doi.org/10.1007/s10557-020-07083-w

Uthman, L., Li, X., Baartscheer, A., Schumacher, C. A., Baumgart, P., Hermanides, J., Preckel, B., Hollmann, M. W., Coronel, R., Zuurbier, C. J., & Weber, N. C. (2022). Empagliflozin reduces oxidative stress through inhibition of the novel inflammation/NHE/[Na+]c/ROS-pathway in human endothelial cells. *Biomedicine & Pharmacotherapy*, *146*, 112515. https://doi.org/10.1016/j.biopha.2021.112515

Wang, H., Naghavi, M., Allen, C., Barber, R. M., Bhutta, Z. A., Carter, A., Casey, D. C., Charlson, F. J., Chen, A. Z., Coates, M. M., Coggeshall, M., Dandona, L., Dicker, D. J., Erskine, H. E., Ferrari, A. J., Fitzmaurice, C., Foreman, K., Forouzanfar, M. H., Fraser, M. S., … Murray, C. J. L. (2016). Global, regional, and national life expectancy, all-cause mortality, and cause-specific mortality for 249 causes of death, 1980–2015: a systematic analysis for the Global Burden of Disease Study 2015. *The Lancet*, *388*(10053). https://doi.org/10.1016/S0140-6736(16)31012-1

Wang, X., Chai, H., Wang, Z., Lin, P. H., Yao, Q., & Chen, C. (2008). Serum amyloid A induces endothelial dysfunction in porcine coronary arteries and human coronary artery endothelial cells. *American Journal of Physiology-Heart and Circulatory Physiology*, *295*(6), H2399–H2408. https://doi.org/10.1152/ajpheart.00238.2008

Williams, D. M., & Evans, M. (2020). Are SGLT-2 Inhibitors the Future of Heart Failure Treatment? The EMPEROR-Preserved and EMPEROR-Reduced Trials. *Diabetes Therapy*, *11*(9). https://doi.org/10.1007/s13300-020-00889-9

Wiviott, S. D., Raz, I., Bonaca, M. P., Mosenzon, O., Kato, E. T., Cahn, A., Silverman, M. G., Zelniker, T. A., Kuder, J. F., Murphy, S. A., Bhatt, D. L., Leiter, L. A., McGuire, D. K., Wilding, J. P. H., Ruff, C. T., Gause-Nilsson, I. A. M., Fredriksson, M., Johansson, P. A., Langkilde, A.-M., & Sabatine, M. S. (2019). Dapagliflozin and Cardiovascular Outcomes in Type 2 Diabetes. *New England Journal of Medicine*, *380*(4), 347–357. https://doi.org/10.1056/NEJMoa1812389

Wright, E. M., Loo, D. D. F., & Hirayama, B. A. (2011). Biology of Human Sodium Glucose Transporters. *Physiological Reviews*, *91*(2), 733–794. https://doi.org/10.1152/physrev.00055.2009

Wu, H., Yao, Q., Lumsden, A., & Chen, C. (2004). Characterization of two populations of human coronary artery endothelial cells1. *Journal of Surgical Research*, *118*(1), 38–44. https://doi.org/10.1016/j.jss.2004.01.009

Xu, C., Wang, W., Zhong, J., Lei, F., Xu, N., Zhang, Y., & Xie, W. (2018). Canagliflozin exerts anti-inflammatory effects by inhibiting intracellular glucose metabolism and promoting autophagy in immune cells. *Biochemical Pharmacology*, *152*, 45–59. https://doi.org/10.1016/j.bcp.2018.03.013

Yan, X., Li, W., Yang, L., Dong, W., Chen, W., Mao, Y., Xu, P., Li, D., Yuan, H., & Li, Y.-H. (2018). MiR-135a Protects Vascular Endothelial Cells Against Ventilator-Induced Lung Injury by Inhibiting PHLPP2 to Activate PI3K/Akt Pathway. *Cellular Physiology and Biochemistry*, *48*(3). https://doi.org/10.1159/000492010

Yau, J. W., Teoh, H., & Verma, S. (2015). Endothelial cell control of thrombosis. *BMC Cardiovascular Disorders*, *15*(1), 130. https://doi.org/10.1186/s12872-015-0124-z

Zafarullah, M., Li, W. Q., Sylvester, J., & Ahmad, M. (2003). Molecular mechanisms of N -acetylcysteine actions. *Cellular and Molecular Life Sciences (CMLS)*, *60*(1), 6–20. https://doi.org/10.1007/s000180300001

Zhang, H., Dong, W., Li, S., Zhang, Y., Lv, Z., Yang, L., Jiang, L., Wu, T., & Wang, Y. (2021). Salidroside protects against ventilation-induced lung injury by inhibiting the expression of matrix metalloproteinase-9. *Pharmaceutical Biology*, *59*(1), 760–768. https://doi.org/10.1080/13880209.2021.1967409

Zhang, Y., Lin, X., Chu, Y., Chen, X., Du, H., Zhang, H., Xu, C., Xie, H., Ruan, Q., Lin, J., Liu, J., Zeng, J., Ma, K., & Chai, D. (2021). Dapagliflozin: a sodium–glucose cotransporter 2 inhibitor, attenuates angiotensin II-induced cardiac fibrotic remodeling by regulating TGFβ1/Smad signaling. *Cardiovascular Diabetology*, *20*(1), 121. https://doi.org/10.1186/s12933-021-01312-8

Zhou, B., Lu, Y., Hajifathalian, K., Bentham, J., Di Cesare, M., Danaei, G., Bixby, H., Cowan, M., Ali, M., Taddei, C., Lo, W., Reis-Santos, B., Stevens, G., Riley, L., Miranda, J., Bjerregaard, P., Rivera, J., Fouad, H., Ma, G., … Zuñiga Cisneros, J. (2016). Worldwide trends in diabetes since 1980: a pooled analysis of 751 population-based studies with 4·4 million participants. *The Lancet*, *387*(10027). https://doi.org/10.1016/S0140-6736(16)00618-8

Zhou, H., Wang, S., Zhu, P., Hu, S., Chen, Y., & Ren, J. (2018). Empagliflozin rescues diabetic myocardial microvascular injury via AMPK-mediated inhibition of mitochondrial fission. *Redox Biology*, *15*, 335–346. https://doi.org/10.1016/j.redox.2017.12.019

Zhou, X., Yuan, D., Wang, M., & He, P. (2013). H_2O_2 -induced endothelial NO production contributes to vascular cell apoptosis and increased permeability in rat venules. *American Journal of Physiology-Heart and Circulatory Physiology*, *304*(1), H82–H93. https://doi.org/10.1152/ajpheart.00300.2012

Zhuang, F., Bao, H., Shi, Q., Li, J., Jiang, Z., Wang, Y., & Qi, Y. (2020). Endothelial microparticles induced by cyclic stretch activate Src and modulate cell apoptosis. *The FASEB Journal*, *34*(10), 13586–13596. https://doi.org/10.1096/fj.202000581R

Zinman, B., Wanner, C., Lachin, J. M., Fitchett, D., Bluhmki, E., Hantel, S., Mattheus, M., Devins, T., Johansen, O. E., Woerle, H. J., Broedl, U. C., & Inzucchi, S. E. (2015). Empagliflozin, Cardiovascular Outcomes, and Mortality in Type 2 Diabetes. *New England Journal of Medicine*, *373*(22), 2117–2128. https://doi.org/10.1056/NEJMoa1504720

7 Appendix

7.1 List of manufacturers

AppliChem GmbH, Darmstadt, Germany; www.applichem.com
ATCC®, Manassas, VA, USA; www.atcc.org
BD Diagnostic Systems, Frankling Lakes, NJ, USA; www.bdbiosciences.com
Bio-Rad-Laboratories, Hercules, CA, USA; www.bio-rad.com
Bosch, Stuttgart, Germany; www.bosch.de
Brand, Wertheim/Grossostheim, Germany; www.brand.de
Branson, Brookfield, CT, USA; www.bransonic.com
Cell Signaling Technology, Danvers, MA, USA; www.cellsignal.com
Corning®, Corning, NY, USA; www.corning.com
Denteck, Zoetermeer, The Netherlands; www.denteck.nl
Eppendorf, Hamburg, Germany; www.eppendorf.com
Flexcell® International Cooperation, Burlington, NC, USA; www.flexcellint.com
Grant Instruments, Shepred, UK; www.grantinstruments.com
Greiner Bio One, Kremsmünster, Austria; www.greinerbioone.com
H + P Labortechnik, Oberschleißheim, Germany; www.hp-lab.com
Hanna Instruments, Woonsocket, RI, USA; www.hannainst.com
Hoshizaki, Toyoake, Japan; www.hoshizaki-europe.com
IKA, Staufen, Germany; www.ika.com
Integra, Zizers, Switzerland; www.integra-biosciences.com
ITS, Apeldoorn, The Netherlands; www.itsfoil.nl
Klinion, Oud Beijerland, The Netherlands; www.klinion.com
Leica Microsystems, Wetzlar, Germany; www.leica-microsystems.com
Leybold GmbH, Cologne, Germany; www.leybold.com
LI-COR Biosciences, Lincoln, NE, USA; www.licor.com
Liebherr, Bulle Switzerland; www.liebherr.com
MedChemExpress, Sollentuna, Sweden; www.medchemexpress.com
Merck, Darmstadt, Germany; www.merck.de
Micronic, Lelystad, The Netherlands; www.micronic.com
Molecular Devices, San José, CA, USA; www.moleculardevices.com
PAN Biotech GmbH, Aidenbach, Germany; www.pan-biotech.de
Panasonic, Kadoma, Japan; www.panasonic.com
PromoCell, Heidelberg, Germany; www.promocell.com
Sartorius, Göttingen, Germany; www.sartorius.com

Scientific Industries, Bohemia, NY, USA; www.scinetificindustries.com
Sigma-Aldrich®, Zwijndrecht, The Netherlands; www.sigmaaldrich.com
Stuart™, Stone, UK; www.stuart-equipment.com
Thermo Fisher Scientific®, Waltham, MA, USA; www.thermofisher.com
TICO Europe, Amstelveen, The Netherlands; www.ticoeurope.com
Tuttnauer, Breda, The Netherlands; www.tuttnauer.com
VWR International, Radnor, PA, USA; www.vwr.com
WLD-TEC, Arenshausen, Germany; www.wld-tec.com
Worthington Industries, Columbus, OH, USA; www.worthingtonindustries.com
Telstar, Woerden, The Netherlands; www.telstar.com

7.2 Molecular formulas

4-(2-Hydroxyethyl)-1-piperazineethanesulfonic acid (HEPES)	**$C_8H_{18}N_2O_4S$**
Calcium chloride dihydrate	**$CaCl_2 \cdot 2H_2O$**
Copper (II) sulphate	**$CuSO_4 \cdot H_2O$**
Disodium phosphate	**Na_2HPO_4**
Magnesium chloride hexahydrate	**$MgCl_2 \cdot 6H_2O$**
Mercaptoethanol	**C_2H_6OS**
Potassium chloride	**KCl**
Potassium dihydrogen phosphate	**KH_2PO_4**
Potassium sodium tartrate (KNa-tartrate)	**$KNaC_4H_4O_6 \cdot 4H_2O$**
Sodium bicarbonate	**$NaHCO_3$**
Sodium carbonate	**Na_2CO_3**
Sodium chloride	**NaCl**
Sodium dihydrogen phosphate dihydrate	**$Na_2HPO_4 \cdot 2H_2O$**
Sodium hydroxide	**NaOH**

7.3 Own publications

Li, X., **Römer, G.**, Kerindongo, R. P., Hermanides, J., Albrecht, M., Hollmann, M. W., Zuurbier, C. J., Preckel, B., & Weber, N. C. (2021). Sodium Glucose Co-Transporter 2 Inhibitors Ameliorate Endothelium Barrier Dysfunction Induced by Cyclic Stretch through Inhibition of Reactive Oxygen Species. *International Journal of Molecular Sciences*, *22*(11). https://doi.org/10.3390/ijms22116044

Uthman, L., Kuschma, M., **Römer, G.**, Boomsma, M., Kessler, J., Hermanides, J., Hollmann, M. W., Preckel, B., Zuurbier, C. J., & Weber, N. C. (2020). Novel Anti-inflammatory Effects of Canagliflozin Involving Hexokinase II in Lipopolysaccharide-Stimulated Human Coronary Artery Endothelial Cells. *Cardiovascular Drugs and Therapy*. https://doi.org/10.1007/s10557-020-07083-w

International Journal of
Molecular Sciences

MDPI

Article

Sodium Glucose Co-Transporter 2 Inhibitors Ameliorate Endothelium Barrier Dysfunction Induced by Cyclic Stretch through Inhibition of Reactive Oxygen Species

Xiaoling Li [1], Gregor Römer [1,2], Raphaela P. Kerindongo [1], Jeroen Hermanides [1], Martin Albrecht [2], Markus W. Hollmann [1], Coert J. Zuurbier [1], Benedikt Preckel [1] and Nina C. Weber [1,*]

[1] Laboratory of Experimental Intensive Care and Anesthesiology (L.E.I.C.A.), Anesthesiology, Amsterdam Cardiovascular Sciences, Amsterdam UMC, University of Amsterdam, 1105 AZ Amsterdam, The Netherlands; x.li1@amsterdamumc.nl (X.L.); g.romer@amsterdamumc.nl (G.R.); r.p.kerindongo@amsterdamumc.nl (R.P.K.); j.hermanides@amsterdamumc.nl (J.H.); m.w.hollmann@amsterdamumc.nl (M.W.H.); c.j.zuurbier@amsterdamumc.nl (C.J.Z.); b.preckel@amsterdamumc.nl (B.P.)

[2] Department of Anesthesiology and Intensive Care Medicine, Universitätsklinikum Schleswig-Holstein, Campus Kiel, 24105 Kiel, Germany; Martin.Albrecht@uksh.de

* Correspondence: n.c.hauck@amsterdamumc.nl; Tel.: +31-20-566-8215

check for updates

Citation: Li, X.; Römer, G.; Kerindongo, R.P.; Hermanides, J.; Albrecht, M.; Hollmann, M.W.; Zuurbier, C.J.; Preckel, B.; Weber, N.C. Sodium Glucose Co-Transporter 2 Inhibitors Ameliorate Endothelium Barrier Dysfunction Induced by Cyclic Stretch through Inhibition of Reactive Oxygen Species. *Int. J. Mol. Sci.* **2021**, *22*, 6044. https://doi.org/10.3390/ijms22116044

Academic Editor: Anastasios Lymperopoulos

Received: 6 May 2021
Accepted: 30 May 2021
Published: 3 June 2021

Abstract: SGLT-2i's exert direct anti-inflammatory and anti-oxidative effects on resting endothelial cells. However, endothelial cells are constantly exposed to mechanical forces such as cyclic stretch. Enhanced stretch increases the production of reactive oxygen species (ROS) and thereby impairs endothelial barrier function. We hypothesized that the SGLT-2i's empagliflozin (EMPA), dapagliflozin (DAPA) and canagliflozin (CANA) exert an anti-oxidative effect and alleviate cyclic stretch-induced endothelial permeability in human coronary artery endothelial cells (HCAECs). HCAECs were pre-incubated with one of the SGLT-2i's (1 μM EMPA, 1 μM DAPA and 3 μM CANA) for 2 h, followed by 10% stretch for 24 h. HCAECs exposed to 5% stretch were considered as control. Involvement of ROS was measured using N-acetyl-l-cysteine (NAC). The sodium-hydrogen exchanger 1 (NHE1) and NADPH oxidases (NOXs) were inhibited by cariporide, or GKT136901, respectively. Cell permeability and ROS were investigated by fluorescence intensity imaging. Cell permeability and ROS production were increased by 10% stretch; EMPA, DAPA and CANA decreased this effect significantly. Cariporide and GKT136901 inhibited stretch-induced ROS production but neither of them further reduced ROS production when combined with EMPA. SGLT-2i's improve the barrier dysfunction of HCAECs under enhanced stretch and this effect might be mediated through scavenging of ROS. Anti-oxidative effect of SGLT-2i's might be partially mediated by inhibition of NHE1 and NOXs.

Keywords: sodium glucose co-transporter 2 inhibitors (SGLT-2i's); cell permeability; reactive oxygen species (ROS); sodium-hydrogen exchanger 1 (NHE1); NADPH oxidases (NOXs)

1. Introduction

Cardiovascular diseases are the leading cause of death and disability around the world, especially in patients with diabetes [1]. Clinical trials showed that sodium glucose co-transporter 2 inhibitors (SGLT-2i's), a class of novel glucose lowering agents, improve cardiovascular outcomes in diabetic [2,3] and non-diabetic patients [4]. One contributing mechanism could be the direct endothelial protective effect of SGLT-2i's. Endothelial dysfunction plays a pivotal role in the progression of heart failure (HF). Increased ROS production within endothelial cells limits nitric oxide (NO) bioavailability for adjacent cardiac myocytes and decreases protein kinase G activity, which favours cardiac hypertrophy via hypophosphorylation of titin [5]. An in vivo experiment suggested that canagliflozin (CANA) restored endothelium-dependent relaxation of pulmonary arteries in hyperglycemic mice [6]. Recently, another study showed that empagliflozin (EMPA)

attenuated diastolic function in non-diabetic HF pigs via restoration of NO availability and PKG activity [7]. The improved diastolic function might explain the beneficial effect of EMPA on patients with HF [8,9]. Additionally, an in vitro study showed that EMPA ameliorated the inflammatory reaction of hyperglycemia-treated endothelial cells [10]. EMPA and dapagliflozin (DAPA) prevented inflammation induced reactive oxygen species (ROS) production in human endothelial cells [11,12]. Those experiments were performed in resting endothelial cells, while in situ endothelial cells are constantly exposed to mechanical forces, e.g., cyclic stretch caused by contraction and relaxation of arteries [13]. Physiological cyclic stretch plays a crucial role in preserving endothelial monolayer integrity [14], whereas, under pathological circumstances (e.g., hypertension), enhanced stretch induces ROS accumulation, inflammatory reactions, vascular stiffness and ultimately endothelial barrier dysfunction [15,16]. Using the Flexcell® Tension Systems, in vitro stretch experiments showed that 10% cyclic stretch promoted endothelium-monocyte adhesion and disrupted the integrity of the endothelial monolayer [17,18]. In contrast, 5% stretch did not induce endothelial dysfunctions and could therefore resemble a physiological condition [17].

ROS play an essential role in regulating the vascular function and might influence endothelial barrier dysfunction [19]. Increased ROS production promoted internalization and degradation of vascular endothelial (VE)-cadherin, the major component of adherent junctions (AJs) between endothelial cells, and therefore disrupted the integrity of the endothelial monolayer and increased endothelial permeability [20,21]. In alveolar epithelial cells, enhanced stretch promoted ROS production and subsequently increased cellular permeability; scavenging ROS reverted this stretch-induced barrier dysfunction, suggesting that ROS promote the permeability of dynamic cells [22].

Based on the fact that SGLT-2i's reduce ROS production in resting human endothelial cells [11,12], and that enhanced cyclic stretch increases oxidative stress and cell permeability of endothelial cells [19], we hypothesized that SGLT-2i's exert an anti-oxidative effect on stretched HCAECs and thereby ameliorate stretch-induced endothelial barrier dysfunction.

2. Results

2.1. SGLT-2i's Prevent Increased Cell Permeability and ROS Production of HCAECs Exposed to 10% Stretch

Compared with 5% stretch, 10% stretch increased cell permeability 1.61 ± 0.43 fold. 1 μM EMPA, 1 μM DAPA and 3 μM CANA significantly decreased the 10% stretch-induced cell permeability (x-fold compared to 5% stretch, EMPA: 1.20 ± 0.46, DAPA: 1.06 ± 0.37, CANA: 1.20 ± 0.39, p all <0.001 vs. 10% stretch, Figure 1a).

Additionally, 10% stretch increased ROS production 2.39 ± 0.95 fold, 1 μM EMPA, 1 μM DAPA and 3 μM CANA significantly reduced the 10% stretch-induced ROS production (x-fold compared to 5% stretch, EMPA: 1.55 ± 0.98, DAPA: 1.41 ± 0.77, CANA: 1.80 ± 0.87, p all <0.05 vs. 10% stretch, Figure 1b), suggesting a class anti-oxidative effect of SGLT-2i's.

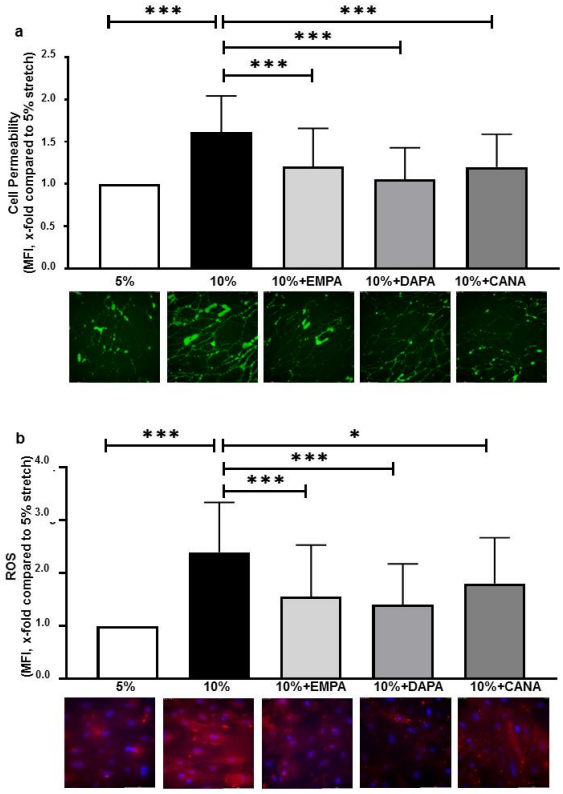

Figure 1. SGLT-2i's inhibit barrier leakage and ROS production of HCAECs exposed to 10% stretch. Cells were pre-incubated for 2 h with vehicle or one of the SGLT-2i's (1 μM EMPA, 1 μM DAPA and 3 μM CANA), and were subsequently exposed to 5% stretch plus vehicle, 10% stretch with vehicle or SGLT-2i's for 24 h. Cell permeability was measured with live cell imaging, and 6 images were made from each condition in each individual experiment (**a**) n = 5 individual experiments). ROS levels were measured at 24 h, and six images were taken from each condition in each individual experiment (**b**) n = 5 individual experiments). Representative images are shown in the lower panel and data are presented as mean ± SD. * $p < 0.05$ vs. 10% stretch, *** $p < 0.001$ vs. 10% stretch.

2.2. SGLT-2i's Revert Loss of VE-Cadherin Induced by 10% Stretch

Fluorescence staining suggested that HCAECs exposed to 10% stretch showed elongation in morphology and loss of VE-cadherin. All three SGLT-2i's restored VE-cadherin loss but did not attenuate altered morphology caused by 10% stretch (Figure 2a). Western Blot was carried out to confirm changes in VE-cadherin expression: EMPA, DAPA and CANA reverted stretch induced VE-cadherin degradation (x-fold compared to 5% stretch, EMPA: 0.90 ± 0.11 vs. 10% stretch: 0.67 ± 0.15, DAPA: 0.95 ± 0.09 vs. 10% stretch: 0.69 ± 0.07, CANA: 0.99 ± 0.12 vs. 10% stretch: 0.76 ± 0.11, p all <0.05, Figure 2b–d). None of the SGLT-2i's influenced permeability and VE-cadherin expression of HCAECs exposed to 5% stretch (Figure S1a,b).

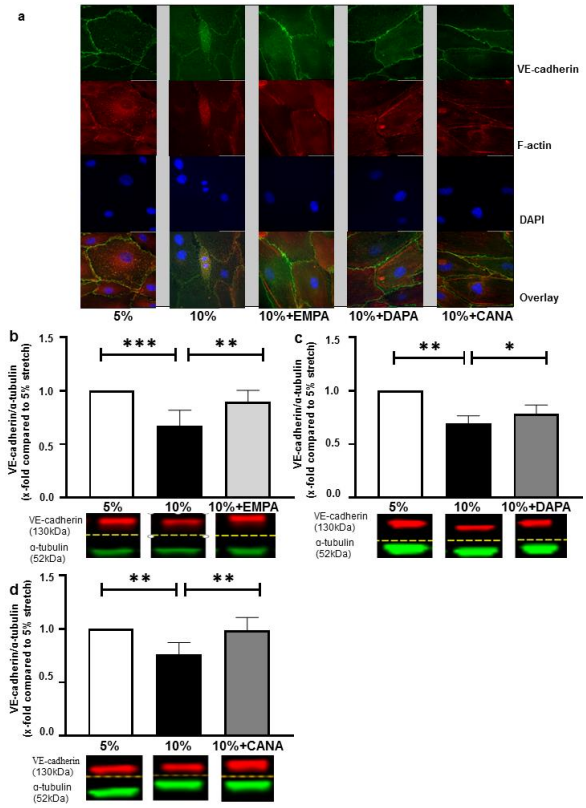

Figure 2. SGLT-2i's restore VE-cadherin loss of HCAECs exposed to 10% stretch. Cells were treated with 5% stretch plus vehicle, 10% stretch plus either vehicle or one of the SGLT-2i's (1 μM EMPA, 1 μM DAPA and 3 μM CANA). VE-cadherin and F-actin were stained after 24 h, and representative images of staining are presented (**a**) n = 3. VE-cadherin levels were quantified with western blot for EMPA treatment (**b**) n = 6, DAPA treatment (**c**) n = 6 and CANA treatment (**d**) n = 6. Representative bands of VE-cadherin and α-tubulin (internal reference) are shown in the lower panels of each bar graph (**b–d**) and data are presented as mean ± SD. * $p < 0.05$ vs. 10% stretch, ** $p < 0.01$ vs. 10% stretch, *** $p < 0.001$ vs. 10% stretch. Whole (uncropped) western blots can be found as supplemental information).

2.3. EMPA-Related Improvement of Endothelium Barrier Dysfunctions Might Be Mediated by ROS Inhibition

Previous studies showed that ROS promotes cellular permeability [23]. As part of our experiments, we also found that pyocyanin, a previously reported ROS inducer [24], increased endothelial permeability and disrupted VE-cadherin of HCAECs (Figure S3a,b).

NAC (5 mM) was applied on cells exposed to 10% stretch and it was found that NAC almost completely reverted the stretch induced ROS production (x-fold compared to 5% stretch, NAC: 1.13 ± 0.58 vs. 10% stretch: 2.48 ± 1.30, $p < 0.001$, Figure 3a). Fluorescence staining showed that 5 mM NAC also reverted stretch-induced VE-cadherin loss of HCAECs, without attenuating elongation of cells (Figure 3b), and NAC significantly decreased cell permeability (x-fold compared to 5% stretch, NAC: 1.04 ± 0.28 vs. 10% stretch: 1.48 ± 0.54, $p < 0.001$). Furthermore, compared with 1 μM EMPA, the combination

of NAC and EMPA did not further reduce the increased cell permeability of HCAECs exposed to 10% stretch (x-fold compared to 5% stretch, EMPA+NAC: 0.96 ± 0.34 vs. EMPA alone: 1.07 ± 0.36, $p > 0.05$, Figure 3c), suggesting that the protective effect of EMPA might be mediated through ROS inhibition.

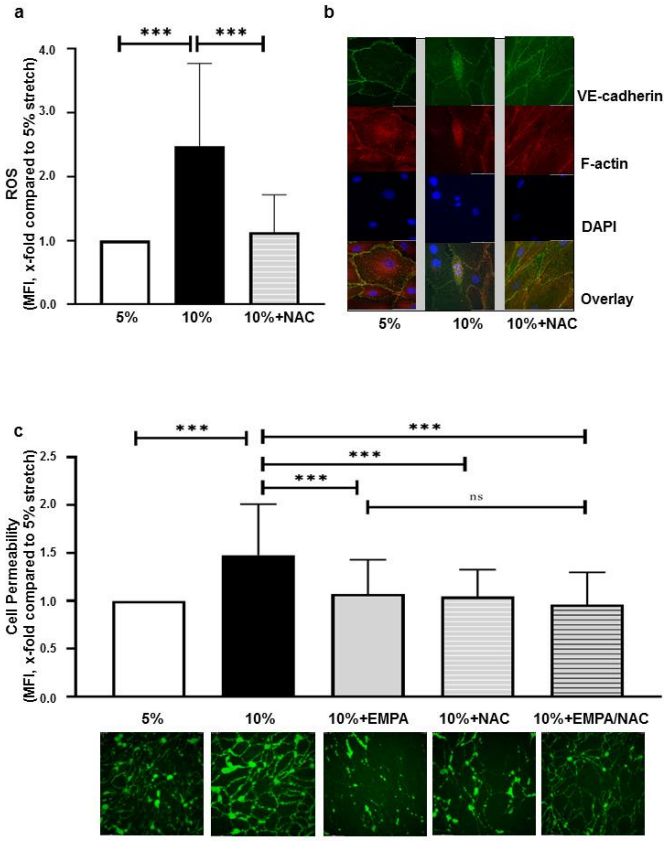

Figure 3. Alleviated stretch induced barrier dysfunction by EMPA might be mediated through ROS inhibition. ROS measurement and immunofluorescence staining were carried out in cells treated with 5% stretch plus vehicle, 10% stretch plus either vehicle or 5 mM NAC. After 24 h, 6 images per condition were taken from each individual experiment for ROS measurement (**a**) n = 5 individual experiments. Representative images of VE-cadherin and F-actin staining are presented in (**b**) (n = 3). Cell permeability was measured in cells treated with 5% stretch plus vehicle, 10% stretch plus vehicle, 1 μM EMPA, 5 mM NAC or combination of EMPA and NAC. Six images per condition were taken from each individual experiment (**c**, n = 5 individual experiments). Representative images of ROS and cell permeability are shown in the lower panel of each bar graph (**a**,**c**) and data are presented as mean ± SD. *** $p < 0.001$ vs. 10% stretch. ns: not significant.

2.4. ROS Inhibition of EMPA Might Partly Be Mediated through Inhibiting NHE1 and NOXs

Cariporide (10 μM) significantly reduced ROS production of cells undergoing 10% stretch (x-fold compared to 5% stretch, cariporide: 1.32 ± 0.89 vs. 10% stretch: 2.48 ± 1.30, $p < 0.001$). The combination of cariporide with EMPA did not further reduce ROS production (x-fold compared to 5% stretch, EMPA+cariporide: 1.47 ± 0.85 vs. EMPA, $p > 0.05$,

Figure 4a). These results correspond to the previous study showing that cariporide inhibits ROS in endothelial cells, however in that study EMPA had also an inhibitory effect on ROS largely unrelated to NHE 1 inhibition [11].

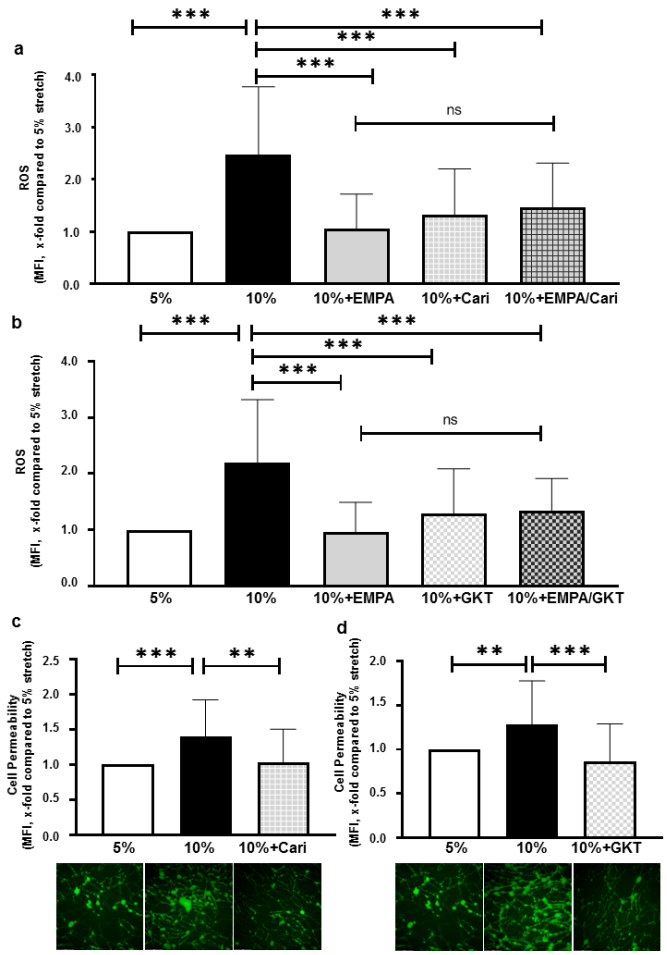

Figure 4. ROS inhibition by SGLT-2i's might be mediated through inhibition of NHE1 and NOXs. ROS levels were measured in cells treated with 5%. stretch, 10% stretch plus vehicle, 1 μM EMPA, 10 μM cariporide/1 μM GKT136901 and combination of EMPA and cariporide/GKT136901 (**a**,**b**). Six images were taken from each individual experiment (**a**) n = 5 individual experiments; (**b**) n = 5 individual experiments. Cell permeability was measured in HCAECs treated with 5% stretch plus vehicle, 10% stretch plus either vehicle, 10 μM cariporide or 1 μM GKT136901 (**c**,**d**). Six images of each condition were taken from each individual experiment (**c**, n = 5 individual experiments; (**d**) n = 5 individual experiments. Representative images are shown in the lower panels and data are presented as mean ± SD. ** $p < 0.01$ vs. 10% + Vehicle, *** $p < 0.001$ vs. 10% + Vehicle. ns: not significant.

Regarding potential targets involved in ROS production, a previous study showed that enhanced cyclic stretch activated NOXs, leading to ROS production [15]. Correspondingly,

1 µM GKT136901 (a specific inhibitor for NOX1 and NOX4) significantly decreased ROS production of cells exposed to 10% stretch (x-fold compared to 5% stretch, GKT136901: 1.30 ± 0.79 vs. 10% stretch: 2.19 ± 1.12, $p < 0.001$). A combination of GKT136901 and EMPA exerted a similar inhibitory effect, comparable to EMPA alone (x-fold compared to 5% stretch, EMPA+GKT136901: 1.34 ± 0.58 vs. EMPA alone: 0.96 ± 0.54, $p > 0.05$, Figure 4b), suggesting that the inhibition of NOXs next to, or located upstream of NHE1, mediated the inhibition of ROS by EMPA in stretched endothelial cells.

Additionally, cariporide and GKT136901 both reverted the increase in cell permeability caused by 10% stretch (Figure 4c,d), further suggesting that ROS inhibition could be the mechanism behind the anti-leakage effects of SGLT-2i's.

2.5. SGLT-2i's Do Not Inhibit Interleukin Secretions of HCAECs Exposed 10% Stretch

Compared with 5% stretch, 10% stretch increased IL-6 and IL-8 secretions of HCAECs, which were not inhibited by EMPA, DAPA or CANA (Figure 5a–f).

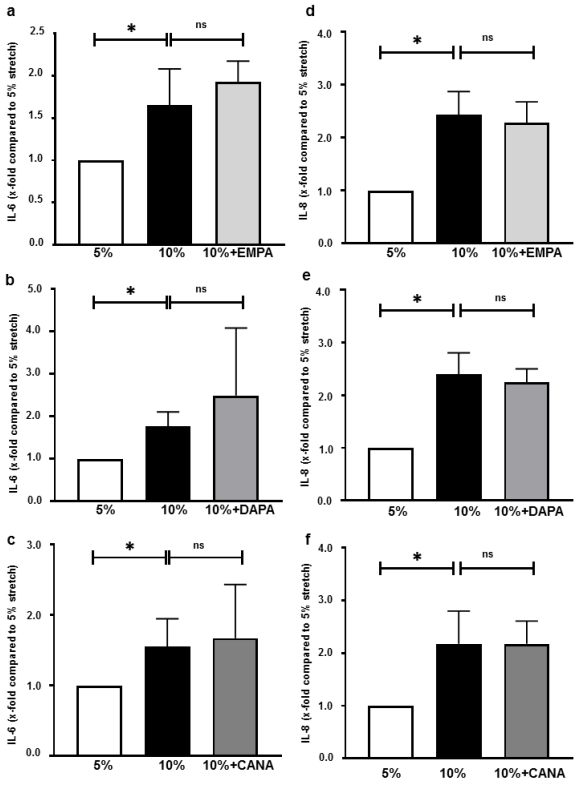

Figure 5. SGLT-2i's do not inhibit interleukin secretion of endothelial cells exposed to 10% stretch. Cells were pre-incubated for 2 h with vehicle or one of SGLT-2i's (1 µM EMPA, 1 µM DAPA and 3 µM CANA), and were subsequently exposed to 5% stretch plus vehicle, 10% stretch with vehicle or SGLT-2i's for 24 h. IL-6 and IL-8 were measured by ELISA (**a–f**) n = 6. Data are presented as mean ± SD. * $p < 0.05$ vs. 10% stretch. ns: not significant.

3. Discussion

The major findings of the present study are: (1) SGLT-2i's revert the increase in endothelial permeability and degradation of VE-cadherin caused by enhanced cyclic stretch; (2) this effect might be mediated through ROS inhibition; and (3) EMPA-related reduction in ROS production in stretched cells is likely mediated via inhibition of NHE1 and NOXs.

3.1. SGLT-2i's Improve Stretch-Induced Endothelial Barrier Dysfunction

Enhanced stretch increased cell permeability of HCAECs and caused VE-cadherin breakdown. All three SGLT-2i's, EMPA, DAPA and CANA reverted this stretch-induced cellular permeability and VE-cadherin degradation of HCAECs.

Previous studies suggested that endothelial cells exposed to enhanced stretch show increased permeability [25], which was partly mediated by polymerization of F-actin and disruption of VE-cadherin-mediated AJs [26]. Enhanced stretch also induced phosphorylation of VE-cadherin at Tyr658 via activating the vascular endothelial growth factor pathway, thus leading to the internalization and degradation of VE-cadherin [25]. Correspondingly, our data (Figure 2a–d) show that pathologically enhanced stretch increases endothelial permeability via VE-cadherin degradation, which is illustrated by compromised VE-cadherin mediated junctions in immunofluorescence staining and the decreased VE-cadherin expression in western blots.

3.2. SGLT-2i's Inhibit ROS Production under Cyclic Stretch

In vivo data suggested that enhanced stretch induced oxidative stress in arteries [13], and in line with these previous findings we demonstrated in vitro that 10% stretch increased ROS production in HCAECs (Figure 1b), with ROS being a crucial promoter for endothelial dysfunction [23,27]. Previous data proved that EMPA and DAPA inhibited inflammation induced ROS production in resting endothelial cells [11,12], thereby restoring nitric oxide bioactivity and ameliorating endothelial dysfunctions. In the present study, we report that SGLT-2i's attenuated oxidative stress in HCAECs exposed to enhanced stretch.

To look into the functional link between ROS and cell permeability, we applied pyocyanin on static cells to induce ROS production [12,24]. We observed a strong increase in endothelial permeability along with F-actin polymerization and VE-cadherin disruption in cells treated with pyocyanin (Figure S3a,b). These findings indicate the role of ROS as a potential permeability triggering factor, with probably multiple pathways contributing. For instance, enhanced ROS activate Rho signaling pathways and promote the polymerization of F-actin, thus disrupting the structure of VE-cadherin mediated AJs [28]. Furthermore, ROS directly caused Src-dependent degradation of VE-cadherin from AJs, leading to impaired endothelial barrier function [29]. The scavenging ROS in our model reverted the increased ROS levels caused by 10% stretch and concomitantly alleviated the stretch induced VE-cadherin disruption and endothelial permeability. This is consistent with a previous study showing that ROS inhibition decreased stretch induced alveolar epithelial permeability [22]. Intriguingly, we found that EMPA and NAC protected the cells to a similar extent; the combination of the two agents did not further increase this effect. Taken together, these findings suggest that ROS inhibition might be a crucial mechanism by which SGLT-2i's prevent stretch-induced endothelial permeability.

3.3. NHE1 and NOXs Might Be Partially Involved in the Anti-Oxidative Effect of EMPA

In order to elucidate the underlying mechanism of the anti-oxidative effect of SGLT2i's in our model, we focused on EMPA and specifically inhibited NHE1 and NOXs with cariporide and GKT136901, respectively. Cariporide and GKT136901 almost completely blocked the stretch induced ROS production, and neither of them further reduced ROS production when combined with EMPA, suggesting that the ROS inhibition of EMPA is partially mediated by NHE1 and NOXs.

Previous studies of our group suggested the cardiovascular protective effects of SGLT-2i's were partly mediated via NHE1 inhibition [30–32]. SGLT-2i's inhibited NHE1 activation

and sodium influx in isolated mice hearts, thus inducing coronary vasodilation. Additionally, stretch directly activated NHE1 of cardiac myocytes, in turn promoting a calcium influx and increasing heart contraction force [33]. DAPA reduced NHE1 expression in cardiomyocytes, thus lowering intracellular sodium concentration and improving myocardial function of diabetic mice [34]. Juni et al. also found that cariporide reduced ROS production of endothelial cells by 38%, however they also found that EMPA could reduce ROS even more in the presence of cariporide suggesting an effect of EMPA unrelated to NHE1 [11]. Another study showed that cariporide attenuated homocysteine induced endothelial dysfunction via reducing oxidative stress and inflammatory reactions [35]. In line with these studies we here prove that NHE1 activation is involved in stretch-induced ROS production of HCAECs and that the anti-oxidative effect of EMPA might be partly mediated via NHE1 inhibition. However, there is an ongoing discussion about the role of NHE1 activity in the cardiovascular protection of SGLT-2i's. Chung and his colleagues reported a neutral effect of EMPA on NHE1 activity with isolated rat myocytes [36], which is contrary with a more recent study conducted by Zuurbier et al. [37].

Another source of ROS in blood vessels are NOXs; previous studies showed that enhanced cyclic stretch significantly increased expression levels of NOX2 and NOX4, and apocynin (a specific NOX2 blocker) reverted this effect in endothelial cells [13,38]. In mice, EMPA reverted upregulation of NOX2 and NOX4 and attenuated ischemia-reperfusion injury in the kidneys, suggesting inhibition of NOXs might be another mechanism for ROS inhibition of EMPA [39].

Interestingly, GKT136901 and cariporide exerted similar anti-oxidative effects on stretched HCAECs in our study. Several studies revealed the potential interactions between NOXs and NHE1 in oxidative stress of endothelial cells. Activated NOXs produced hydrogen peroxide, a type of stable ROS that maintains the opening of mitochondrial ATP-dependent potassium channels (mitoKATP) and thus enhances the production of mitochondrial ROS by the electron transport chain [40,41]. Mitochondrial ROS are then released to cytosol and in turn activates NHE-1 and sodium–calcium exchange, promoting influx of calcium into the cytosol [42]. Finally, increased cytosolic calcium enhances mitochondrial calcium load and further promotes ROS production [43].

Taken together, our data support that NOXs and NHE1 might contribute to the enhanced ROS production in stretched HCAECs, but how SGLT-2i's interrupt this signaling cascade is still unclear and warrants further investigations.

3.4. SGLT-2i's Do Not Alter Interleukin Secretion of Stretched Cells

In vivo and in vitro studies have shown that pathological mechanical forces stimulate cytokine production and expression of adhesion molecules, leading to stiffness of vessels and monocyte adhesion [17,44]. Interestingly, none of the three SGLT-2i's inhibited stretch-induced interleukin secretion (Figure 5), which is in contrast to previous data showing that SGLT-2i's inhibit interleukin production of endothelial cells from humans, as well as from *ApoE*(-/-) mice [45,46]. One potential explanation might be that the stretch-induced interleukin secretion of HCAECs is much milder than that caused by lipopolysaccharide (1.5–2 fold vs. 6–7 fold) [46], making it a less optimal model to investigate the potential anti-inflammatory effects of SGLT-2i's.

3.5. Limitation and Conclusions

This study was only performed in HCAECs from non-diabetic donors and further research is required to test the effects of SGLT-2i's in diabetic cells. For the underlying mechanisms of ROS inhibition by SGLT-2i's, we indirectly demonstrated that inhibition of NHE1 and NOXs is involved, and how they interact in stretch-induced oxidative stress is yet unknown. Another drawback of this study is that we did not look into the involvement of SGLT-2 in the observed effects. However, the expression of *SGLT-2* in human ECs is highly questionable. Using western blot, we recently reported a potential signaling of *SGLT-2* in HCAECs, but as the bands persisted existing after the target gene was silenced

at mRNA level, we doubted the specificity of these bands and performed qPCR targeting SGLT2 in HCAEC showing no detectable levels of *SGLT2* [12]. In animal endothelial cells however, the presence of SGLT-2 within has been recently proven [10], but these findings might not be comparable to our data because of the different species. Moreover, investigations into other mechanisms underlying SGLT-2i's anti-oxidative effect are needed. For instance, EMPA might attenuate the overproduction of ROS in endothelial cells via ameliorating mitochondrial injury [11]. Another study suggested that the beneficial effect of EMPA on mitochondria was mediated via the activation of adenosine monophosphate-activated protein kinase AMPK [47]. However, the involvement of AMPK phosphorylation is still under discussion. In the previous studies of Uthman et al., AMPK activation was not observed in EMPA or DAPA, but only in CANA treated cells [46].

In conclusion, SGLT-2i's protect human endothelial cells against cyclic stretch-induced increased permeability and this effect is most likely mediated through ROS inhibition. Our observations provide novel insights into the possible mechanisms of the cardiovascular protection of SGLT-2i's on mechanically stimulated cells, thus helping to improve treatment of endothelial dysfunctions induced by disturbed mechanical forces.

4. Materials and Methods

4.1. Cell Culture and Cyclic Stretch Protocol

HCAECs (PCS-100-020 from ATCC, Manassas, VA, USA; C-12221 from PromoCell, Heidelberg, Germany) were used for cell culture with vascular cell growth medium (ATCC) containing supplements as previously described [46].

HCAECs were seeded onto BioFlex® 6-well plates (Flexcell International, McKeesport, PA, USA) at a density of 10,000–20,000 cells/cm^2, and all plates were pre-coated overnight with 0.25 mg/mL gelatine dissolved in 0.1 M sodium bicarbonate buffer (NaHCO3, pH = 8.3). All experiments were performed with cells at passage 7 when they reached 90–100% confluency. Cyclic stretch was applied using the FX-5000T Flexcell Tension Plus system (Flexcell International, McKeesport, PA, USA). Based on previous in vitro studies [17,18], 5% stretch was considered as the physiological model and 10% as the pathological condition. HCAECs were subjected to stretch for 24 h at a frequency of 1 Hz. Cells were starved for 18 h before experiments and pre-incubated for 2 h with vehicle or SGLT-2i's (1 µM EMPA, 1 µM DAPA and 3 µM CANA, all from MedChem, Sollentuna, Sweden). The schematic outline of this study is shown in Figure A1.

To elucidate involved mechanisms, 5 mM N-acetyl-l-cysteine (NAC, Merck Millipore, Watford, England) was applied to scavenge ROS, 1 µM GKT136901 (Calbiochem, San Diego, CA, USA) to inhibit nicotinamide adenine dinucleotide phosphate oxidases (NOXs), and 10 µM cariporide (Sigma Aldrich, St Louis, MO, USA) to inhibit sodium-hydrogen exchanger 1 (NHE1).

4.2. Cell Permeability Assay

A cell permeability assessment was performed using the method described by Dubrovskyi et al., which is based on high affinity binding between avidin and biotin [16].

EZ-Link NHS-LC-LC-Biotin (Thermo Fisher Scientific, Waltham, MA, USA) was added to 10 mg/mL of gelatin solution (dissolved in 0.1 M NaHCO3 buffer), to generate a solution of 0.57 mg/mL biotin and 9 mg/mL gelatin. The biotinylation of gelatin was performed at room temperature for 1h with constant stirring, and biotinylated gelatin was than aliquoted and stored at −20°C. For coating, gelatin aliquots were diluted in 0.1 M NaHCO3 buffer to generate a working solution with 0.25 mg/mL biotinylated gelatin and sterilized by a filter with a pore size of 0.2 µm (VWR international, Radnor, PA, USA). Three ml working solution were added to each well on the Bioflex plate. Plates were covered with aluminium foil and stored at 4 °C overnight, and unabsorbed protein was removed by washing twice with phosphate buffered saline (PBS, pH = 7.4).

After stretch, fluorescein isothiocyanate (FITC) labeled avidin (Thermo Fisher Scientific, Waltham, MA, USA) was added to medium (working concentration, 25 µg/mL)

and incubated for 3 min, after which excessive avidin was removed by PBS washing. The plastic membranes of BioFlex plates with cells were loaded on glass cover slides with mounting fluid (Thermo Fisher Scientific, Waltham, MA, USA) containing 4',6-diamidino-2-phenylindole (DAPI). Membranes were imaged with Leica DMi8 Advanced Light Microscopy (Leica Microsystems, Wetzlar, Germany) at 200× magnification, and six pictures of each condition were made from each individual experiment. The fluorescence was quantified using Image J1.8.0 and divided by the cell number to generate a mean fluorescence intensity (MFI). To reduce any bias, the quantification was carried out by two independent investigators (X.L. & G.R.) in a blinded manner.

4.3. ROS Measurement

After 24 h of cyclic stretch, CellROX ® Deep Red Reagent (Thermo Fisher Scientific, Waltham, MA, USA) was added on each well to generate a working concentration of 5 µM, and plates were covered with aluminium foil and incubated at 37 °C in a humidified incubator for 30 min. Cells were than washed once with pre-warmed PBS and fixed with 4% formalin for 15 min. The plastic membranes of BioFlex plates were loaded on glass cover slides with mounting fluid containing DAPI. Membranes were imaged with Leica DM6 Wide-Field Microscopy (Leica Microsystems, Wetzlar, Germany) at 400× magnification, and 6 pictures of each condition were taken from each individual experiment. The fluorescence was quantified using Image J1.8.0 and divided by cell number to generate a MFI. To reduce any bias, the quantification was carried out by two independent investigators (X.L. & G.R.) in a blinded manner.

4.4. Immunofluorescence Staining

After 24 h of stretch, monolayers of HCAECs were fixed with 4% formalin for 10 min. Cells were washed three times with PBS and blocked for 30 min with 1% bovine serum albumin (PAA Cell Culture Company, Cambridge, UK). VE-cadherin monoclonal antibody (1:60 dilution, Thermo Fisher Scientific, Waltham, MA, USA) was added to each well and incubated at room temperature for 1h, unbound antibody was removed by PBS washing. Afterwards, goat anti-mouse secondary antibody (1:400, Alexa Flour® 488, Thermo Fisher Scientific, Waltham, MA, USA) and Rhodamine Phalloidin (1:40, Thermo Fisher Scientific, Waltham, MA, USA) was added to each well for 30 min, followed by three times washing with PBS. Membranes were loaded on glass cover slides with mounting fluid containing DAPI and imaged with Leica DM6 Wide-Field Microscopy at 1000× magnification.

4.5. Infrared Western Blot

Whole cell lysates from two wells with the same treatments were combined. After 24 h of stretch, cells were washed with ice-cold PBS and collected in a lysis buffer, made from a homogenisation buffer (0.25 M sucrose and 0.02 M HEPES, pH = 7.4) with 0.5% Triton-100X, 1 mM dithiothreitol and HaltTM Protease and Phosphatase Inhibitor Single-Use Cocktail (diluted 1:100 Thermo Fisher Scientific, Waltham, MA, USA). The total protein concentration was determined by the Lowry method [48] and adjusted to 1000 µg/mL per blot. Membranes were incubated with primary antibodies against VE-cadherin (1:1000, CST, Danvers, MA, USA) and α-tubulin (1:20,000, Thermo Fisher Scientific, Waltham, MA, USA) overnight, followed by three times washing with PBS containing 0.1% tween 20 and incubation with the complementary secondary antibodies (1:5000, Li-Cor, Lincoln, NE, USA) for 1 h. The membranes were scanned with the Odyssey CLx operator (Li-Cor, Lincoln, NE, USA) after final washing, and quantifications of the signals of each band were carried out using Image StudioTM Software (Version 5.2, Li-Cor, Lincoln, NE, USA).

4.6. Enzyme-Linked Immunosorbent Assay (ELISA)

Two wells of supernatant from cell culture were combined and centrifuged at 4 °C for 10 min and with a centrifuge force of 150 g. Interleukin-6 (IL-6) and interleukin-8 (IL-8) in

the supernatant were measured with ELISA kits (R&D Systems, Minneapolis, MN, USA) according to manufacturer's instructions.

4.7. Lactate Dehydrogenase (LDH) Activity

To determine cell death, activity of LDH in supernatant was detected photospectrometrically at 25 °C, with pyruvate and nicotinamide adenine dinucleotide hydrogen (NADH). The formation rate of NAD+ from NADH was determined over 240 s and used for the measurement of total LDH activity. Compared with 5% stretch, 10% did not increase LDH activity of HCAECs, suggesting that apoptosis might not be involved in stretch induced permeability (Figure S2).

4.8. Sample Size and Statistical Analysis

Sample size estimation revealed that at least 5 independent experiments in each group are required to reach a power of 80%, given a physiologically relevant difference of 25% between control and intervention group and an α of 0.05 (10% standard deviation).

Statistical analyses were performed using GraphPad Prism 8.3.0 (GraphPad, San Diego, CA, USA). All data were normalized to 5% stretch and are presented as mean $\pm$ standard deviation (SD). One-way ANOVA with Bonferroni post hoc correction was carried out when comparing the difference between cells treated with SGLT-2i's and 10% stretch. $p \leq 0.05$, referred as *; ** for $p \leq 0.01$ and *** for $p \leq 0.001$, were considered statistically significant.

Supplementary Materials: The following are available online at https://www.mdpi.com/article/10.3390/ijms22116044/s1.

Author Contributions: X.L., G.R. and R.P.K. performed all experiments and analyzed the results. X.L., N.C.W. and B.P. wrote and edited the original draft. X.L., G.R., R.P.K., J.H., M.A., M.W.H., C.J.Z., B.P. and N.C.W. substantially contributed to the study design, interpretation of data, revising the article and giving final approval. All authors have read and agreed to the published version of the manuscript.

Funding: X.L. is supported by a Chinese Scholarship Council (CSC) fellowship program (NO. 2019XXXX0054). This research received no external funding.

Institutional Review Board Statement: Not applicable.

Informed Consent Statement: Not applicable.

Data Availability Statement: All data generated and analyzed during the study are included in this manuscript and its supplementary information or can be obtained from the authors upon reasonable request.

Acknowledgments: We thank Ron A. Hoebe and Derek J.B. Kleinveld for their assistance during the current study.

Conflicts of Interest: The authors declare no conflict of interest.

Appendix A

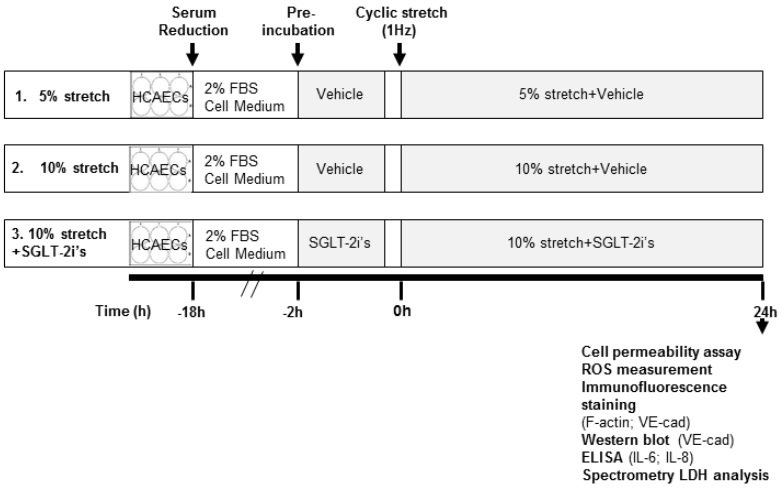

Figure A1. Study design Cells were starved for 18 h by serum reduction before a 2 h pre-incubation with either vehicle (0.06% DMSO) or one of the SGLT-2i's (1 µM EMPA, 1 µM DAPA and 3 µM CANA) under starving conditions, followed by stimulation with 10% stretch for 24 h. HCAECs exposed to 5% stretch with vehicle were considered as control. Cell permeability, ROS levels, cell morphology, VE-cadherin expression, interleukin production and LDH activity were measured after 24 h.

References

1. Timmis, A.; Townsend, N.; Gale, C.P.; Torbica, A.; Lettino, M.; Petersen, S.E.; Mossialos, E.A.; Maggioni, A.P.; Kazakiewicz, D.; May, H.T.; et al. European Society of Cardiology: Cardiovascular Disease Statistics 2019. *Eur. Heart J.* **2020**, *41*, 12–85. [CrossRef]
2. Zinman, B.; Wanner, C.; Lachin, J.M.; Fitchett, D.; Bluhmki, E.; Hantel, S.; Mattheus, M.; Devins, T.; Johansen, O.E.; Woerle, H.J.; et al. Empagliflozin, Cardiovascular Outcomes, and Mortality in Type 2 Diabetes. *N. Engl. J. Med.* **2015**, *373*, 2117–2128. [CrossRef]
3. Wiviott, S.D.; Raz, I.; Bonaca, M.P.; Mosenzon, O.; Kato, E.T.; Cahn, A.; Silverman, M.G.; Zelniker, T.A.; Kuder, J.F.; Murphy, S.A.; et al. Dapagliflozin and Cardiovascular Outcomes in Type 2 Diabetes. *N. Engl. J. Med.* **2019**, *380*, 347–357. [CrossRef]
4. Packer, M.; Anker, S.D.; Butler, J.; Filippatos, G.; Pocock, S.J.; Carson, P.; Januzzi, J.; Verma, S.; Tsutsui, H.; Brueckmann, M.; et al. Cardiovascular and Renal Outcomes with Empagliflozin in Heart Failure. *N. Engl. J. Med.* **2020**, *383*, 1413–1424. [CrossRef] [PubMed]
5. Paulus, W.J.; Tschope, C. A novel paradigm for heart failure with preserved ejection fraction: Comorbidities drive myocardial dysfunction and remodeling through coronary microvascular endothelial inflammation. *J. Am. Coll Cardiol.* **2013**, *62*, 263–271. [CrossRef] [PubMed]
6. Han, Y.; Cho, Y.E.; Ayon, R.; Guo, R.; Youssef, K.D.; Pan, M.; Dai, A.; Yuan, J.X.; Makino, A. SGLT inhibitors attenuate NO-dependent vascular relaxation in the pulmonary artery but not in the coronary artery. *Am. J. Physiol. Lung Cell Mol. Physiol.* **2015**, *309*, L1027–L1036. [CrossRef] [PubMed]
7. Santos-Gallego, C.G.; Requena-Ibanez, J.A.; San Antonio, R.; Garcia-Ropero, A.; Ishikawa, K.; Watanabe, S.; Picatoste, B.; Vargas-Delgado, A.P.; Flores-Umanzor, E.J.; Sanz, J.; et al. Empagliflozin Ameliorates Diastolic Dysfunction and Left Ventricular Fibrosis/Stiffness in Nondiabetic Heart Failure: A Multimodality Study. *JACC Cardiovasc. Imaging* **2021**, *14*, 393–407. [CrossRef] [PubMed]
8. Lee, M.M.Y.; Brooksbank, K.J.M.; Wetherall, K.; Mangion, K.; Roditi, G.; Campbell, R.T.; Berry, C.; Chong, V.; Coyle, L.; Docherty, K.F.; et al. Effect of Empagliflozin on Left Ventricular Volumes in Patients With Type 2 Diabetes, or Prediabetes, and Heart Failure With Reduced Ejection Fraction (SUGAR-DM-HF). *Circulation* **2021**, *143*, 516–525. [CrossRef]
9. Santos-Gallego, C.G.; Vargas-Delgado, A.P.; Requena-Ibanez, J.A.; Garcia-Ropero, A.; Mancini, D.; Pinney, S.; Macaluso, F.; Sartori, S.; Roque, M.; Sabatel-Perez, F.; et al. Randomized Trial of Empagliflozin in Nondiabetic Patients With Heart Failure and Reduced Ejection Fraction. *J. Am. Coll Cardiol.* **2021**, *77*, 243–255. [CrossRef]

10. Khemais-Benkhiat, S.; Belcastro, E.; Idris-Khodja, N.; Park, S.H.; Amoura, L.; Abbas, M.; Auger, C.; Kessler, L.; Mayoux, E.; Toti, F.; et al. Angiotensin II-induced redox-sensitive SGLT1 and 2 expression promotes high glucose-induced endothelial cell senescence. *J. Cell Mol. Med.* **2020**, *24*, 2109–2122. [CrossRef]
11. Juni, R.P.; Al-Shama, R.; Kuster, D.W.D.; van der Velden, J.; Hamer, H.M.; Vervloet, M.G.; Eringa, E.C.; Koolwijk, P.; van Hinsbergh, V.W.M. Empagliflozin restores chronic kidney disease-induced impairment of endothelial regulation of cardiomyocyte relaxation and contraction. *Kidney Int.* **2020**. [CrossRef]
12. Uthman, L.; Homayr, A.; Juni, R.P.; Spin, E.L.; Kerindongo, R.; Boomsma, M.; Hollmann, M.W.; Preckel, B.; Koolwijk, P.; van Hinsbergh, V.W.M.; et al. Empagliflozin and Dapagliflozin Reduce ROS Generation and Restore NO Bioavailability in Tumor Necrosis Factor alpha-Stimulated Human Coronary Arterial Endothelial Cells. *Cell Physiol. Biochem.* **2019**, *53*, 865–886. [CrossRef]
13. Oeckler, R.A.; Kaminski, P.M.; Wolin, M.S. Stretch enhances contraction of bovine coronary arteries via an NAD(P)H oxidase-mediated activation of the extracellular signal-regulated kinase mitogen-activated protein kinase cascade. *Circ. Res.* **2003**, *92*, 23–31. [CrossRef] [PubMed]
14. Fang, Y.; Wu, D.; Birukov, K.G. Mechanosensing and Mechanoregulation of Endothelial Cell Functions. *Compr. Physiol.* **2019**, *9*, 873–904. [CrossRef] [PubMed]
15. Tanaka, T.; Saito, Y.; Matsuda, K.; Kamio, K.; Abe, S.; Kubota, K.; Azuma, A.; Gemma, A. Cyclic mechanical stretch-induced oxidative stress occurs via a NOX-dependent mechanism in type II alveolar epithelial cells. *Respir. Physiol. Neurobiol.* **2017**, *242*, 108–116. [CrossRef]
16. Dubrovskyi, O.; Birukova, A.A.; Birukov, K.G. Measurement of local permeability at subcellular level in cell models of agonist- and ventilator-induced lung injury. *Lab. Investig.* **2013**, *93*, 254–263. [CrossRef] [PubMed]
17. Loperena, R.; Van Beusecum, J.P.; Itani, H.A.; Engel, N.; Laroumanie, F.; Xiao, L.; Elijovich, F.; Laffer, C.L.; Gnecco, J.S.; Noonan, J.; et al. Hypertension and increased endothelial mechanical stretch promote monocyte differentiation and activation: Roles of STAT3, interleukin 6 and hydrogen peroxide. *Cardiovasc. Res.* **2018**, *114*, 1547–1563. [CrossRef]
18. Omidvar, R.; Tafazzoli-Shadpour, M.; Mahmoodi-Nobar, F.; Azadi, S.; Khani, M.M. Quantifying effects of cyclic stretch on cell-collagen substrate adhesiveness of vascular endothelial cells. *Proc. Inst. Mech. Eng. H* **2018**, *232*, 531–541. [CrossRef] [PubMed]
19. Birukov, K.G. Cyclic stretch, reactive oxygen species, and vascular remodeling. *Antioxid Redox. Signal.* **2009**, *11*, 1651–1667. [CrossRef]
20. Andrikopoulos, P.; Kieswich, J.; Harwood, S.M.; Baba, A.; Matsuda, T.; Barbeau, O.; Jones, K.; Eccles, S.A.; Yaqoob, M.M. Endothelial Angiogenesis and Barrier Function in Response to Thrombin Require Ca2+ Influx through the Na^+/Ca^{2+} Exchanger. *J. Biol. Chem.* **2015**, *290*, 18412–18428. [CrossRef]
21. Ali, M.H.; Schlidt, S.A.; Chandel, N.S.; Hynes, K.L.; Schumacker, P.T.; Gewertz, B.L. Endothelial permeability and IL-6 production during hypoxia: Role of ROS in signal transduction. *Am. J. Physiol.* **1999**, *277*, L1057–L1065. [CrossRef]
22. Davidovich, N.; DiPaolo, B.C.; Lawrence, G.G.; Chhour, P.; Yehya, N.; Margulies, S.S. Cyclic stretch-induced oxidative stress increases pulmonary alveolar epithelial permeability. *Am. J. Respir. Cell Mol. Biol.* **2013**, *49*, 156–164. [CrossRef]
23. He, P.; Talukder, M.A.H.; Gao, F. Oxidative Stress and Microvessel Barrier Dysfunction. *Front. Physiol.* **2020**, *11*, 472. [CrossRef] [PubMed]
24. Manago, A.; Becker, K.A.; Carpinteiro, A.; Wilker, B.; Soddemann, M.; Seitz, A.P.; Edwards, M.J.; Grassme, H.; Szabo, I.; Gulbins, E. Pseudomonas aeruginosa pyocyanin induces neutrophil death via mitochondrial reactive oxygen species and mitochondrial acid sphingomyelinase. *Antioxid. Redox Signal.* **2015**, *22*, 1097–1110. [CrossRef]
25. Tian, Y.; Gawlak, G.; O'Donnell, J.J., 3rd; Birukova, A.A.; Birukov, K.G. Activation of Vascular Endothelial Growth Factor (VEGF) Receptor 2 Mediates Endothelial Permeability Caused by Cyclic Stretch. *J. Biol. Chem.* **2016**, *291*, 10032–10045. [CrossRef]
26. Van Buul, J.D.; Timmerman, I. Small Rho GTPase-mediated actin dynamics at endothelial adherens junctions. *Small GTPases* **2016**, *7*, 21–31. [CrossRef] [PubMed]
27. Tseng, C.Y.; Wang, J.S.; Chao, M.W. Causation by Diesel Exhaust Particles of Endothelial Dysfunctions in Cytotoxicity, Pro-inflammation, Permeability, and Apoptosis Induced by ROS Generation. *Cardiovasc. Toxicol.* **2017**, *17*, 384–392. [CrossRef]
28. Acevedo, A.; Gonzalez-Billault, C. Crosstalk between Rac1-mediated actin regulation and ROS production. *Free Radic. Biol. Med.* **2018**, *116*, 101–113. [CrossRef] [PubMed]
29. Chang, F.; Flavahan, S.; Flavahan, N.A. Superoxide inhibition restores endothelium-dependent dilatation in aging arteries by enhancing impaired adherens junctions. *Am. J. Physiol. Heart Circ. Physiol.* **2018**, *314*, H805–H811. [CrossRef]
30. Baartscheer, A.; Schumacher, C.A.; Wust, R.C.; Fiolet, J.W.; Stienen, G.J.; Coronel, R.; Zuurbier, C.J. Empagliflozin decreases myocardial cytoplasmic Na(+) through inhibition of the cardiac Na(+)/H(+) exchanger in rats and rabbits. *Diabetologia* **2017**, *60*, 568–573. [CrossRef]
31. Uthman, L.; Baartscheer, A.; Schumacher, C.A.; Fiolet, J.W.T.; Kuschma, M.C.; Hollmann, M.W.; Coronel, R.; Weber, N.C.; Zuurbier, C.J. Direct Cardiac Actions of Sodium Glucose Cotransporter 2 Inhibitors Target Pathogenic Mechanisms Underlying Heart Failure in Diabetic Patients. *Front Physiol.* **2018**, *9*, 1575. [CrossRef] [PubMed]
32. Uthman, L.; Baartscheer, A.; Bleijlevens, B.; Schumacher, C.A.; Fiolet, J.W.T.; Koeman, A.; Jancev, M.; Hollmann, M.W.; Weber, N.C.; Coronel, R.; et al. Class effects of SGLT2 inhibitors in mouse cardiomyocytes and hearts: Inhibition of Na(+)/H(+) exchanger, lowering of cytosolic Na(+) and vasodilation. *Diabetologia* **2018**, *61*, 722–726. [CrossRef] [PubMed]

33. Cingolani, H.E.; Perez, N.G.; Pieske, B.; von Lewinski, D.; Camilion de Hurtado, M.C. Stretch-elicited Na+/H+ exchanger activation: The autocrine/paracrine loop and its mechanical counterpart. *Cardiovasc. Res.* **2003**, *57*, 953–960. [CrossRef]
34. Arow, M.; Waldman, M.; Yadin, D.; Nudelman, V.; Shainberg, A.; Abraham, N.G.; Freimark, D.; Kornowski, R.; Aravot, D.; Hochhauser, E.; et al. Sodium-glucose cotransporter 2 inhibitor Dapagliflozin attenuates diabetic cardiomyopathy. *Cardiovasc. Diabetol.* **2020**, *19*, 7. [CrossRef]
35. Wu, S.; Gao, X.; Yang, S.; Liu, L.; Ge, B.; Yang, Q. Protective effects of cariporide on endothelial dysfunction induced by homocysteine. *Pharmacology* **2013**, *92*, 303–309. [CrossRef]
36. Chung, Y.J.; Park, K.C.; Tokar, S.; Eykyn, T.R.; Fuller, W.; Pavlovic, D.; Swietach, P.; Shattock, M.J. Off-target effects of SGLT2 blockers: Empagliflozin does not inhibit Na+/H+ exchanger-1 or lower [Na+]i in the heart. *Cardiovasc. Res.* **2020**. [CrossRef]
37. Zuurbier, C.J.; Baartscheer, A.; Schumacher, C.A.; Fiolet, J.W.T.; Coronel, R. SGLT2 inhibitor empagliflozin inhibits the cardiac Na+/H+ exchanger 1: Persistent inhibition under various experimental conditions. *Cardiovasc. Res.* **2021**. [CrossRef]
38. Liang, X.; Wang, Z.; Gao, M.; Wu, S.; Zhang, J.; Liu, Q.; Yu, Y.; Wang, J.; Liu, W. Cyclic stretch induced oxidative stress by mitochondrial and NADPH oxidase in retinal pigment epithelial cells. *BMC Ophthalmol.* **2019**, *19*, 79. [CrossRef]
39. Kuno, A.; Kimura, Y.; Mizuno, M.; Oshima, H.; Sato, T.; Moniwa, N.; Tanaka, M.; Yano, T.; Tanno, M.; Miki, T.; et al. Empagliflozin attenuates acute kidney injury after myocardial infarction in diabetic rats. *Sci. Rep.* **2020**, *10*, 7238. [CrossRef]
40. Zinkevich, N.S.; Fancher, I.S.; Gutterman, D.D.; Phillips, S.A. Roles of NADPH oxidase and mitochondria in flow-induced vasodilation of human adipose arterioles: ROS-induced ROS release in coronary artery disease. *Microcirculation* **2017**, *24*. [CrossRef]
41. Kim, Y.M.; Kim, S.J.; Tatsunami, R.; Yamamura, H.; Fukai, T.; Ushio-Fukai, M. ROS-induced ROS release orchestrated by Nox4, Nox2, and mitochondria in VEGF signaling and angiogenesis. *Am. J. Physiol. Cell Physiol.* **2017**, *312*, C749–C764. [CrossRef]
42. Aredia, F.; Czaplinski, S.; Fulda, S.; Scovassi, A.I. Molecular features of the cytotoxicity of an NHE inhibitor: Evidence of mitochondrial alterations, ROS overproduction and DNA damage. *BMC Cancer* **2016**, *16*, 851. [CrossRef]
43. Javadov, S. The calcium-ROS-pH triangle and mitochondrial permeability transition: Challenges to mimic cardiac ischemia-reperfusion. *Front Physiol.* **2015**, *6*, 83. [CrossRef] [PubMed]
44. Iwaki, M.; Ito, S.; Morioka, M.; Iwata, S.; Numaguchi, Y.; Ishii, M.; Kondo, M.; Kume, H.; Naruse, K.; Sokabe, M.; et al. Mechanical stretch enhances IL-8 production in pulmonary microvascular endothelial cells. *Biochem. Biophys. Res. Commun.* **2009**, *389*, 531–536. [CrossRef] [PubMed]
45. Han, J.H.; Oh, T.J.; Lee, G.; Maeng, H.J.; Lee, D.H.; Kim, K.M.; Choi, S.H.; Jang, H.C.; Lee, H.S.; Park, K.S.; et al. The beneficial effects of empagliflozin, an SGLT2 inhibitor, on atherosclerosis in ApoE (-/-) mice fed a western diet. *Diabetologia* **2017**, *60*, 364–376. [CrossRef] [PubMed]
46. Uthman, L.; Kuschma, M.; Romer, G.; Boomsma, M.; Kessler, J.; Hermanides, J.; Hollmann, M.W.; Preckel, B.; Zuurbier, C.J.; Weber, N.C. Novel Anti-inflammatory Effects of Canagliflozin Involving Hexokinase II in Lipopolysaccharide-Stimulated Human Coronary Artery Endothelial Cells. *Cardiovasc. Drugs* **2020**. [CrossRef]
47. Zhou, H.; Wang, S.; Zhu, P.; Hu, S.; Chen, Y.; Ren, J. Empagliflozin rescues diabetic myocardial microvascular injury via AMPK-mediated inhibition of mitochondrial fission. *Redox. Biol.* **2018**, *15*, 335–346. [CrossRef] [PubMed]
48. Olson, B. Assays for Determination of Protein Concentration. *Curr. Protoc. Pharm.* **2016**, *73*, A.3A.1–A.3A.32. [CrossRef] [PubMed]

Cardiovascular Drugs and Therapy (2021) 35:1083–1094
https://doi.org/10.1007/s10557-020-07083-w

ORIGINAL ARTICLE

Novel Anti-inflammatory Effects of Canagliflozin Involving Hexokinase II in Lipopolysaccharide-Stimulated Human Coronary Artery Endothelial Cells

Laween Uthman[1] · Marius Kuschma[1,2] · Gregor Römer[1] · Marleen Boomsma[1] · Jens Kessler[2] · Jeroen Hermanides[1] · Markus W. Hollmann[1] · Benedikt Preckel[1] · Coert J. Zuurbier[1] · Nina C. Weber[1]

Accepted: 16 September 2020 / Published online: 13 October 2020

Abstract

Purpose Vascular inflammation and disturbed metabolism are observed in heart failure and type 2 diabetes mellitus. Glycolytic enzyme hexokinase II (HKII) is upregulated by inflammation. We hypothesized that SGLT2 inhibitors Canagliflozin (Cana), Empagliflozin (Empa) or Dapagliflozin (Dapa) reduces inflammation via HKII in endothelial cells, and that HKII-dependent inflammation is determined by ERK1/2, NF-κB. and/or AMPK activity in lipopolysaccharide (LPS)-stimulated human coronary artery endothelial cells (HCAECs).

Methods HCAECs were pre-incubated with 3 μM or 10 μM Cana, 1 μM, 3 μM or 10 μM Empa or 0.5 μM, 3 μM or 10 μM Dapa (16 h) and subjected to 3 h LPS (1 μg/mL). HKII was silenced via siRNA transfection. Interleukin-6 (IL-6) release was measured by ELISA. Protein levels of HK I and II, ERK1/2, AMPK and NF-κB were detected using infra-red western blot.

Results LPS increased IL-6 release and ERK1/2 phosphorylation; Cana prevented these pro-inflammatory responses (IL-6: pg/ml, control 46 ± 2, LPS 280 ± 154 $p < 0.01$ vs. control, LPS + Cana 96 ± 40, $p < 0.05$ vs. LPS). Cana reduced HKII expression (HKII/GAPDH, control 0.91 ± 0.16, Cana 0.71 ± 0.13 $p < 0.05$ vs. control, LPS 1.02 ± 0.25, LPS + Cana 0.82 ± 0.24 $p < 0.05$ vs. LPS). Empa and Dapa were without effect on IL-6 release and HKII expression in the model used. Knockdown of HKII by 37% resulted caused partial loss of Cana-mediated IL-6 reduction (pg/ml, control 35 ± 5, LPS 188 ± 115 $p < 0.05$ vs. control, LPS + Cana 124 ± 75) and ERK1/2 activation by LPS. In LPS-stimulated HCAECs, Cana, but not Empa or Dapa, activated AMPK. AMPK activator A769662 reduced IL-6 release.

Conclusion Cana conveys anti-inflammatory actions in LPS-treated HCAECs through 1) reductions in HKII and ERK1/2 phosphorylation and 2) AMPK activation. These data suggest a novel anti-inflammatory mechanism of Cana through HKII.

Keywords Canagliflozin · Hexokinase 2 · Endothelial cells · Inflammation

Introduction

Chronic vascular inflammation is a common early signature in patients with type 2 diabetes mellitus (T2DM) and is strongly associated with an increased risk of cardiovascular disease [1–3]. The metabolic profile of T2DM consists of hyperglycemia, which instigates a shift toward disturbed glucose utilization leading to accumulation of glycolytic intermediates and reactive oxygen species in endothelial cells [4]. Hexokinase (HKII) is an early glycolytic enzyme that facilitates glucose conversion to glucose-6-phosphate (G6P) leading to increased metabolic flux through glycolysis. However, increased expression and activity of HKII and upregulated glycolysis are observed in inflammatory conditions [5–8]. Blocking HKII ameliorates inflammatory signaling in activated isolated

Electronic supplementary material The online version of this article (https://doi.org/10.1007/s10557-020-07083-w) contains supplementary material, which is available to authorized users.

✉ Nina C. Weber
N.C.Hauck@amsterdamumc.nl

[1] Department of Anaesthesiology, Laboratory of Experimental Intensive Care and Anesthesiology (L.E.I.C.A.), Amsterdam Cardiovascular Sciences, Amsterdam UMC, University of Amsterdam, Meibergdreef 9, Amsterdam 1105, AZ, the Netherlands

[2] Department of Anesthesiology, University Hospital Heidelberg, University of Heidelberg, Heidelberg, Germany

human cells and in small animal models of inflammation [5, 6, 8–11]. Targeting enhanced glycolysis via HKII inhibition may hence alleviate the inflammation that is involved in the vascular pathology of T2DM.

The kidney-targeted sodium-glucose cotransporter 2 (SGLT2) inhibitors Canagliflozin (Cana), Empagliflozin (Empa), and Dapagliflozin (Dapa) exhibited pronounced beneficial effects on cardiovascular outcome in patients with and without T2DM, including reductions in heart failure events, hospital admissions, and chronic kidney disease [12–15]. Recent data suggest that direct, SGLT2 unrelated, cardiovascular actions of SGLT2 inhibitors account, at least in part, for the reported cardiovascular benefits [16–21]. Interestingly, several of these studies suggest an anti-inflammatory mechanism underlying the positive clinical outcomes of SGLT2 inhibitors [18, 22, 23]. Others report that glucose uptake is hindered by SGLT2 inhibitors in a variety of cell types, including endothelial cells [24–26].

At the site of the endothelium, inflammation is best characterized by the release of pro-inflammatory cytokines and enhanced expression of adhesion molecules. Both facilitate leukocyte recruitment and translocation through the vascular wall leading to endothelial dysfunction [27]. The presence of leukocytes also promotes fibrosis and enables atherosclerotic plaque formation in the coronary circulation. In cell and animal models of diabetes as well as in patients with T2DM, elevated levels of circulating and endothelial inflammatory markers, such as interleukin 6 (IL-6) and vascular cell adhesion molecule 1, as well as markers of endothelial dysfunction are generally observed [28–32].

Diabetes mellitus associates with changes in the gut microbiome, increasing the leakiness of LPS through the gut wall, thereby further inducing tissue inflammation [33]. LPS can bind to the toll-like receptor 4 (TLR4) that is expressed on endothelial cells. TLR4 binding simultaneously activates nuclear factor-κB (NF-κB) and the mitogen-activated protein kinases (MAPK), including extracellular regulated kinases 1 and 2 (ERK1/2) [34]. In macrophages, activation of TLR4 by LPS shifts the cell metabolism to a glycolytic phenotype, with elevated glucose consumption, lactate production, and increased HKII expression and activity [7]. Furthermore, a central regulator of cellular metabolic pathways and an anti-inflammatory signaling protein is the adenosine monophosphate (AMP)-activated kinase (AMPK) [35, 36]. Previous studies have reported that SGLT2 inhibitors can activate AMPK, and that AMPK activation may contribute to the anti-inflammatory mechanism of these drugs [18, 19, 37]. Collectively, these findings suggest a strong association between cell metabolism and inflammation. Targeting metabolic intermediates of glycolysis to attenuate inflammation may be a key strategy to reduce early vascular abnormalities occurring in diabetes-associated cardiovascular disorders.

An anti-inflammatory action of SGLT2 inhibitors has not been previously linked to changes in endothelial glycolytic enzymes, such as HKII. Therefore, in this present study, we hypothesized that (1) SGLT2 inhibitors Cana, Empa, and Dapa reduce LPS-stimulated inflammation in human cardiac endothelial cells; (2) HKII is involved in the possible anti-inflammatory effects of the SGLT2 inhibitors; and (3) ERK1/2, NF-κB, and AMPK activity have a role in the HKII-dependent anti-inflammatory actions of SGLT2 inhibitors.

Methods

Cell Culture and Experimental Procedure

HCAECs were purchased from Promocell (Heidelberg, Germany) and grown in vascular basal cell medium with supplements (ATCC, Manassas, VA, USA), containing 5-ng/ml vascular endothelial growth factor, 5-ng/ml epidermal growth factor, 5-ng/ml fibroblastic growth factor, 15-ng/ml insulin-like growth factor 1, 10-mM L-glutamine, 0.75-U/ml heparin sulfate, 1-μg/ml hydrocortisone, 50-μg/ml ascorbic acid, 1% amphotericin B, 1% penicillin-streptomycin, and 10% FBS. Cells were grown at 37 °C in a Heracell™ 150i CO_2 incubator (Thermo Fisher Scientific, Waltham, MA, USA). All experiments were performed with cells from passage 5 to 8 when they reached 80–90% confluency. At the start of each experiment, cells were pre-incubated overnight (16 h) with vehicle or different compounds, including SGLT2 inhibitors at concentrations 3- and 10-μM Cana, 1-, 3- and 10-μM Empa, 0.5-, 3- and 10-μM Dapa (all three from MedChem, Sollentuna, Sweden), 1-μM TAK-242 to inhibit LPS-induced TLR4 signaling, 50-μM PD-98059 to inhibit ERK phosphorylation (Cambridge Bioscience, Cambridge, UK), 100-μM A7869662 to activate AMPK, or a combination of two compounds, in serum-reduced (2% FBS) media. The next day, HCAECs were subjected to 1-μg/mL LPS (Sigma Aldrich, Saint Louis, MO, USA) with vehicle or intervention for 3 h.

Transfection with Small Interfering RNA (siRNA) for HKII

Knockdown of HKII in HCAECs was performed as previously described [38, 39]. In short, cells in 6-wells plates with confluency between 50 and 80% were transfected with 20-nM siRNA for HKII (Art# 4390824, ID# S6560, lot# ASO2DUJU, Thermo Fisher Scientifics) or negative control (AM4611, Ambion by Thermo Fischer Scientifics) for 24 h using Lipofectamine RNAiMax (Invitrogen by Thermo Fischer Scientifics, Waltham, MA, USA) and in antibiotic- and antimycotic-free medium. Cells were passaged 24 h after the start of transfection at a ratio of 1:2. Thereafter, the cells were cultured in antibiotic- and antimycotic-free medium for 48 h before the media was collected for IL-6 levels

determination and cells were lysed for western blotting. At end experiment, a confluency of 80–90% was reached by the cells.

Western Blot

Whole cell lysates were collected directly at the end of the experiment. Briefly, cells were rinsed with ice-cold PBS and collected in lysis buffer, made from RIPA buffer (150-mM NaCl, 50-mM TrisHCl, 1% Nonidet P40, 0.25% sodium deoxycholate, and 0.1% SDS), supplemented with 1-mM phenylmethylsulfonyl fluoride, 2-mM Na_3VO_4, 1-mM dithiothreitol, 1-mM sodium pyrophosphate, 50-μM sodium fluoride, and a protease inhibitor mixture (17-μM leupeptin, 1-μM aprotinin, and 12-μM pepstatin (all three from Sigma Aldrich)). After centrifugation at 14000 g, 4 °C for 10 min, the supernatant was collected and stored at − 80 °C until use. Samples were sonicated on ice in repeated short cycles (5 s, energy mode, 20 Joules, 70% amplitude, repeated for 4 times) using the Low Power Ultrasonic Systems 2000 Lpt/LPe with microtip (Branson, Danbury, CT, USA).

Western blotting was performed as described previously [40]. Sample protein contents, determined with the Lowry method, were adjusted to the same concentration for each blot. After overnight incubation with primary antibodies against phospho-AMPK, AMPK, HKI, HKII, phospho-ERK, ERK, and GLUT1 (1:1000, all from CST, Danvers, MA, USA) and household protein GAPDH (CST, 1:5000), membranes were washed with phosphate-buffered saline (PBS) containing 0.1% tween (Sigma) and incubated with the complementary secondary antibody (IRdye, 1:5000, Li-Cor, Lincoln, NE, USA) for 1 h at room temperature before they were washed again. The membranes were scanned with the Odyssey CLx operator (Li-Cor) at auto-scan setting for dynamic range, 169-μm resolution and medium quality, and quantification of the bands was performed with Image Studio™ Software (Version 5.2, Li-Cor). For quantification of the band signals, the signal from each band was normalized to the signal from the largest band on the membrane according to the manufacturer's instructions, to reduce the chances of technical variation. Whole membrane scans used for the results sections are provided in the ESM (Electronic Supplementary Materials).

Enzyme-Linked Immunosorbent Assay (ELISA)

The supernatant from each well was collected and spun at 250 g, 4 °C for 10 min. Levels of IL-6 were determined using ELISA (R&D Systems, Minneapolis, MN, USA) according to manufacturer's instructions.

Hexokinase Activity

HK activity was measured photospectrometrically in cell extracts at 25 °C with glucose-6-phosphate dehydrogenase, glucose, adenosine triphosphate, and nicotinamide adenine dinucleotide (NAD^+), in the presence of rotenone to inhibit mitochondrial respiration [41]. The rate of NADH formation from NAD^+ was determined over 180 s and used for the measure of total HK activity. HK activity was corrected for total protein concentration in each sample.

Sample Size Calculation and Statistical Analyses

Four experiments were needed to detect a physiologically relevant difference of 25% between control and intervention, given a standard deviation of 10%, a power of 80%, and an α of 0.05. Data are presented as mean ± standard deviation (SD). The distribution of the data was tested using the Shapiro-Wilk test. Normal distributed data were tested by one-way ANOVA with Bonferroni post hoc testing or by a Student's t test. Non-normally distributed data were tested with Kruskal-Wallis and Mann-Whitney U test with Bonferroni correction. In each experiment, we attempted to avoid experimental bias by single-well use by pooling two wells with cells. The number of experiments mentioned in the figures refers to the number of technical replicates with cells from two donors (PCS-100-020 from ATCC, LOT# 59885589 and C-12221 from PromoCell, LOT# 425Z0191.1). Graphs were created in Graphpad Prism 8 and statistical analysis was performed using IBM SPSS Statistics 25. The cut-off values for statistical significance were indicated in the figures by *, **, and *** for $p < 0.05$, $p < 0.01$, and $p < 0.001$, respectively.

Results

Cana, but not Empa or Dapa, Attenuates IL-6 Release in LPS-Induced HCAECs

Exposing HCAECs to 1-μg/mL LPS for 3 h significantly increased IL-6 release. Cana (10 μM) almost completely blocked LPS-induced IL-6 release (Fig. 1a), whereas Empa (1 μM, Fig. 1b) or Dapa (0.5 μM, Fig. 1c) did not significantly alter IL-6 levels in the cell media. In addition, HCAECs treated with 10-μM Empa or Dapa exhibited no change in LPS-induced IL-6 release (ESM Fig. 1a–b). At a concentration of 3 μM, however, none of the SGLT2 inhibitors were able to lower LPS-induced IL-6 release (ESM Fig. 1c–e). No changes in IL-6 release were observed in healthy HCAECs exposed to an SGLT2 inhibitor (Fig. 1a–c). TAK-242 was able to nullify LPS-induced IL-6 release, confirming the involvement of TLR4 in IL-6 production by LPS (Fig. 1d).

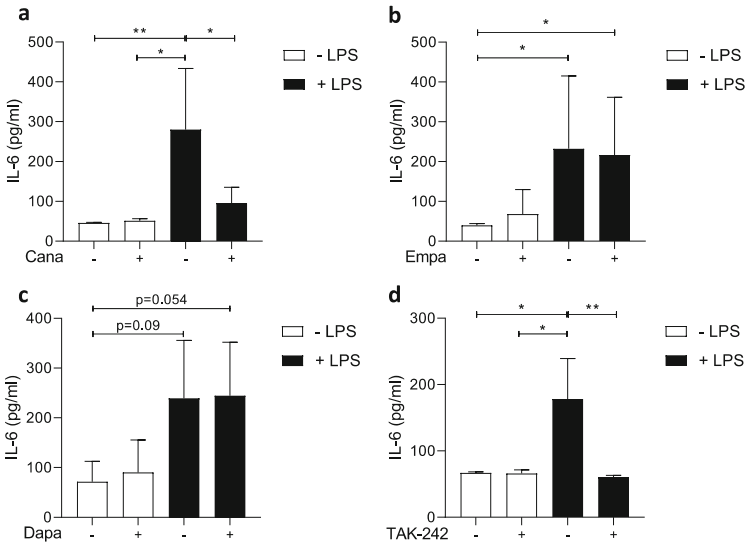

Fig. 1 Cana, but not Empa or Dapa, attenuates IL-6 release in LPS-induced HCAECs. Cells were pre-incubated for 16 h with vehicle or an SGLT2 inhibitor and subsequently stimulated by 1-μg/mL LPS for 3 h with vehicle or an SGLT2 inhibitor. IL-6 release into the cell media was determined for Cana- (**a**, $n = 4$, 10 μM), Empa- (**b**, $n = 6$, 1 μM), and Dapa- (**c**, $n = 6$, 0.5 μM) treated HCAECs. TAK-242 (**d**, $n = 3$, 100 μM) served as a positive control to validate the inhibition of LPS-induced IL-6 release in our model. Data are presented as mean ± SD. $^{*}p < 0.05$, $^{**}p < 0.01$, tested by one-way ANOVA with Bonferroni correction

Cana Reduces IL-6 Release by Lowering HKII Expression

Increased glycolysis, and in particular elevated HKII expression, is a signature of an activated inflammatory condition [5–11]. Incubating HCAECs for 19 h with 10-μM Cana resulted in a reduced expression of HKII in non-stimulated and LPS-stimulated HCAECs (Fig. 2a). In contrast, administration of 1-μM Empa or 0.5-μM Dapa did not affect HKII expression in non-stimulated HCAECs (ESM Fig. 2). Furthermore, the expression of HKI and the total HK activity were unaffected by Cana in non-stimulated HCAECs (Fig. 2b+c).

Using siRNA transfection, knockdown of HKII by 37 ± 9% was achieved (Fig. 3a), without affecting HKI expression (Fig. 3b). Incubation with LPS caused augmented IL-6 release in siRNA HKII-treated HCAECs; however, this time Cana was unable to significantly reduce LPS-induced IL-6 release (Fig. 3c), indicating the involvement of HKII in the attenuating effect of Cana on cytokine release.

Inhibition of LPS-Induced ERK Phosphorylation by Cana Is Mediated by HKII

To further explore downstream effects of Cana on LPS-induced IL-6 generation, we investigated whether Cana affected changes in the phosphorylation of ERK1/2 and NF-κB. First, LPS caused augmented ERK1/2 phosphorylation and Cana reduced LPS-induced ERK1/2 phosphorylation (Fig. 4a). While NF-κB phosphorylation was also increased with LPS, Cana did not affect NF-κB phosphorylation (Fig. 4b).

To examine the possible involvement of HKII in LPS-induced ERK1/2 phosphorylation, we investigated LPS effects on ERK1/2 in cells treated with siRNA for HKII. Reducing HKII completely mitigated LPS activation of ERK1/2 (Fig. 4c). As a consequence, Cana was without effect on LPS-induced ERK1/2 phosphorylation. These data indicate that decreasing HKII is upstream of ERK1/2 phosphorylation by Cana. Conversely, using PD-98059 to inhibit ERK1/2 phosphorylation in HCAECs, we also observed reduced HKII expression in HCAECs (Fig. 4d), indicating HKII reductions also occur downstream of ERK1/2 phosphorylation. These data suggest that reducing HKII expression blocks LPS-induced ERK1/2 phosphorylation, and that reduced ERK1/2 activity leads to lower HKII levels, irrespective of LPS treatment. ERK 1/2 phosphorylation and HKII reductions are intrinsically intertwined.

Cana Induces AMPK Phosphorylation in Healthy and LPS-Stimulated HCAECs

Previous studies have suggested the activation of AMPK as a contributing factor to SGLT2 inhibitor's anti-inflammatory actions in various cell types [18, 19, 25], offering the possibility that Cana's reducing effect on IL-6 production can also be mediated through AMPK activation. However, it is still unknown whether HKII is involved in AMPK effects on inflammation. Therefore, we investigated whether Cana

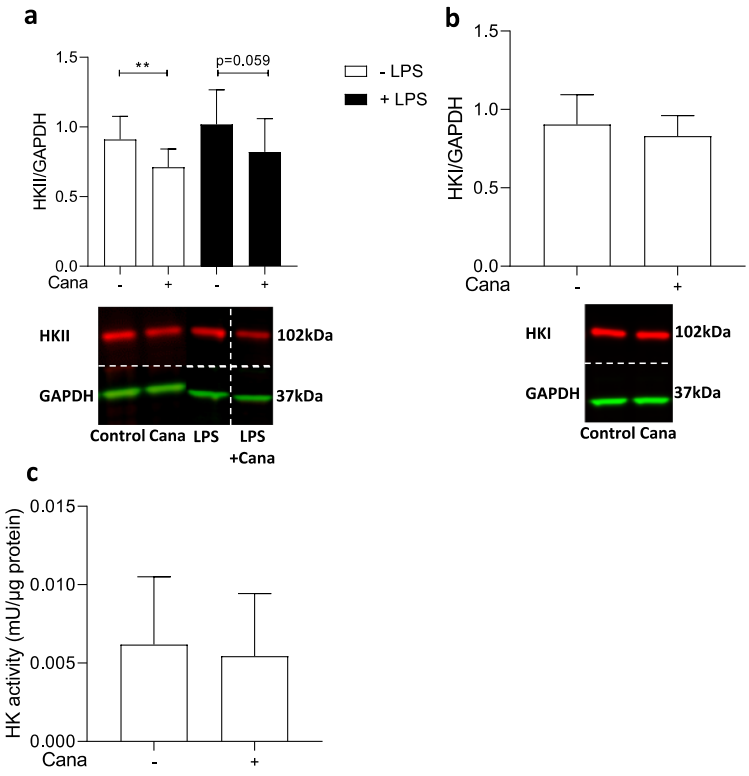

Fig. 2 Cana reduces HKII, but not HKI, expression. Cells were exposed to vehicle or Cana (10 μM) for 16 h and subsequently subjected to 3 h LPS (**a**, $n = 12$). HKII and HKI levels (**b**, in non-stimulated, $n = 7$) were determined using infrared western blot. Representative bands are shown below each figure. Whole membrane scans are shown in the ESM. Total HK activity was detected photospectrometrically in whole cell lysate (**c**, $n = 7$–8). Data are presented as mean ± SD. *$p < 0.05$, tested by independent sample t test

activated AMPK, if AMPK activation resulted in reduction of IL-6 release, and if AMPK activation was dependent on HKII. First, we show that Cana phosphorylated AMPK at Thr172 in LPS-induced HCAECs (Fig. 5a). Second, activation of AMPK by A769662 (ESM Fig. 3a) leads to inhibition of LPS-induced IL-6 release (Fig. 5b). Furthermore, Cana administration resulted in increased AMPK phosphorylation in HKII knockdown HCAECs exposed to LPS (Fig. 5c), indicating that HKII is not involved in activation of AMPK by Cana. Empa and Dapa did not enhance AMPK phosphorylation in either non-stimulated or LPS-stimulated HCAECs (ESM Fig. 3b and c).

Discussion

The main findings of the present study are that the SGLT2 inhibitor Canagliflozin alleviates the release of the pro-inflammatory cytokine IL-6, lowers HKII expression, inhibits ERK1/2 phosphorylation, and activates AMPK in LPS-stimulated and/or non-stimulated HCAECs. The other two SGLT2 inhibitors Empa and Dapa did not show a significant reduction in IL-6 release, HKII expression, and AMPK activity in the model used. Reduced HKII expression seems to be associated with Cana's anti-inflammatory effect by mediating LPS-induced IL-6 release and ERK1/2 phosphorylation, but not AMPK activation. These data suggest that under normoglycemic and inflammatory conditions, Cana exerts an anti-inflammatory activity by lowering HKII. A graphic summary of our findings is provided in Fig. 6.

Anti-inflammatory Actions of Cana

We observed that the SGLT2 inhibitor Cana, but not Empa or Dapa, directly reduces the release of the pro-inflammatory cytokine IL-6 by LPS-activated endothelial cells. Our data correspond well with previous studies, showing that Cana reduces IL-6 release in IL-1β-stimulated human endothelial cells and in LPS-stimulated macrophages [18, 42]. However, the effect of Cana on IL-6 release reduction was absent at a

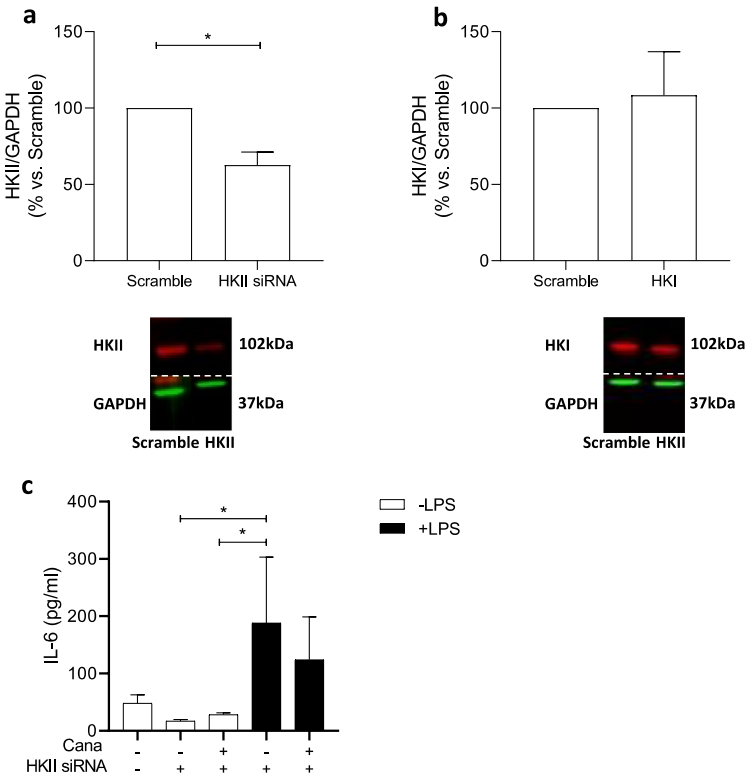

Fig. 3 Knockdown of HKII caused partial loss of Cana-mediated IL-6 reduction HCAECs were transfected by siRNA for HKII or Scramble and pre-treated at t = 72 h post-transfection with vehicle or 10-μM Cana for 16 h and subsequently exposed to 0- or 1-μg/mL LPS with vehicle/Cana. Knockdown of HKII (**a**, n = 4) was achieved without change in HKI expression (**b**, n = 4). Representative bands are shown below each figure. Whole membrane scans are shown in the ESM. IL-6 release by Scramble vs. HKII knockdown cells in the presence of Cana/vehicle, with or without LPS (**c**). Data are presented as mean ± SD. *$p < 0.05$, tested by t test (**a**–**b**) and one-way ANOVA with Bonferroni correction (**c**)

lower concentration of 3 μM, suggesting that Cana may only be effective in attenuating IL-6 release at the higher concentrations. While we observed no direct cell effect of Empa or Dapa on LPS-induced IL-6 release, attenuated markers of endothelial dysfunction, i.e., ROS and nitric oxide, have been reported in activated endothelial cells exposed to Empa or Dapa, but without change in the expression of adhesion molecules [22, 23]. In the present study, we cannot rule out that Empa and Dapa do affect LPS-induced IL-6 release due to the higher variations observed in the experiments using Empa or Dapa. An explanation for the divergence between the effects of Cana vs. Empa or Dapa on LPS-induced cytokine release could be the different concentrations used. Cana was used at 10 μM, whereas Empa and Dapa were used at 1 μM and 0.5 μM, respectively, which are considered clinically relevant concentrations. However, using Empa or Dapa at 10 μM did also not cause reduced LPS-induced IL-6 release. Notably, the half maximal inhibitory concentration (IC50) of Cana for SGLT1 is estimated to be 710 nM, while Empa and Dapa have an IC50 for SGLT1 of 8300 nM and 1400 nM, respectively [43]. Thus in this context, SGLT1 and perhaps also other SGLT isoforms might be inhibited by Cana with the concentrations used in the present study.

One hypothesis for the direct cellular effects of SGLT2 inhibitors is the off-target inhibition of the Na^+/H^+ exchanger 1 (NHE1). NHE1 activity is enhanced in endothelial cells exposed to LPS [44]. Inhibition of NHE1 by a variety of different NHE inhibitors reduced LPS-induced apoptosis, cytokine production, and NF-κB activation [44, 45]. Cardiac NHE1 inhibition by SGLT2 inhibitors was reported as a class effect, showing similar inhibitory potentials for NHE1 by Cana, Empa, and Dapa [16]. Accordingly, NHE1 might have been activated by LPS stimulation, and Cana might have inhibited NHE1. Yet, since we observed different outcomes of Cana, Empa, and Dapa on LPS-induced cytokine release, NHE1 inhibition could not account for the anti-inflammatory effects of Cana in our model.

LPS induces inflammation after binding to TLR4 and activating downstream signaling events. These events lead to NF-κB activation and its translocation to the cell nucleus to stimulate production of pro-inflammatory molecules [27, 34,

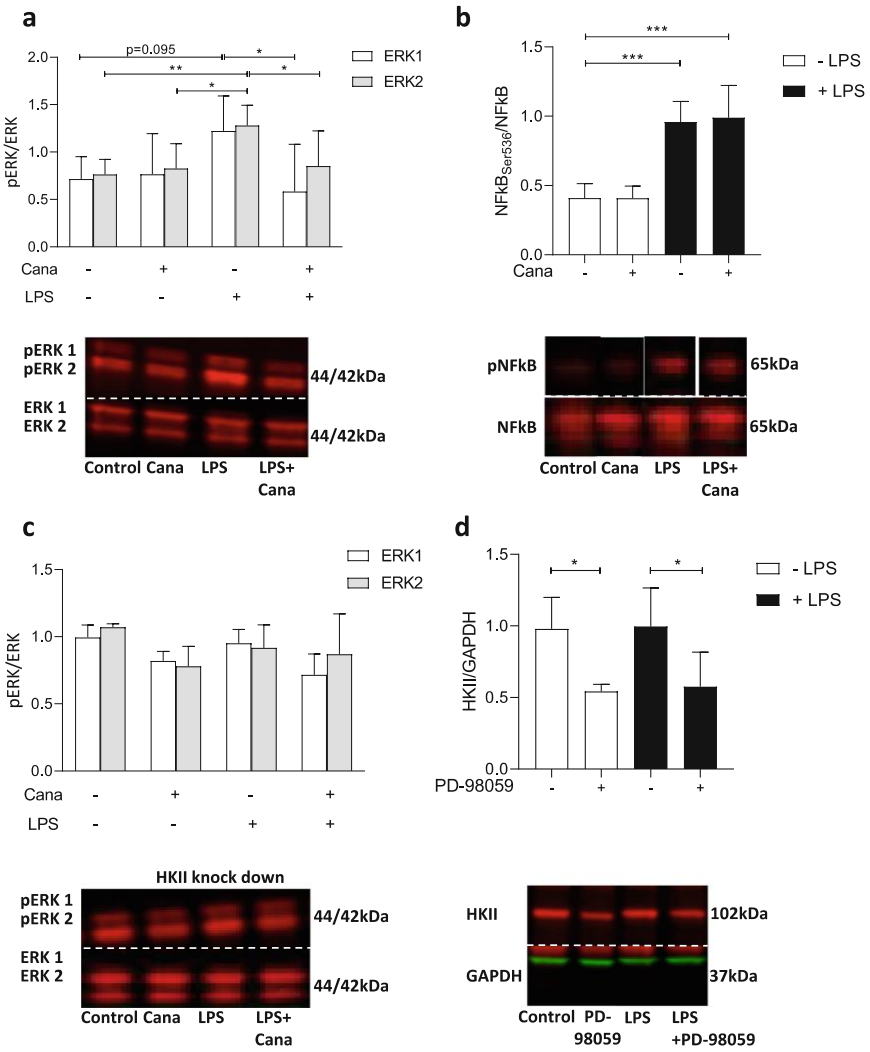

Fig. 4 Cana inhibits LPS-induced ERK phosphorylation but does not affect NF-κB. ERK1/2 phosphorylation (**a**, $n = 8$) and NF-κB phosphorylation (**b**, $n = 7$) were measured in LPS stimulated and non-stimulated HCAECs. ERK1/2 phosphorylation was also determined in HKII knock-down HCAECs exposed to Cana and/or LPS (**c**, $n = 4$). HKII expression was measured in cells subjected to PD-98059 (**d**, $n = 5$). Representative bands are shown below each figure. Whole membrane scans are shown in the ESM. Data are presented as mean ± SD. $^{*}p < 0.05$, $^{**}p < 0.01$, $^{***}p < 0.001$, tested by one-way ANOVA with Bonferroni correction

45]. Concomitantly, MAPK that are involved in inflammatory processes, including ERK1 and ERK2, become activated [34]. In the present study, Cana inhibited LPS-induced ERK1/2 phosphorylation in HCAECs. Yet, since Cana does not affect NF-κB activation, which is observed in the present study as well as by other investigators [18], Cana may not act on the classical LPS-pathway upstream of both ERK1/2 and NF-κB. It is reported that Cana inhibits cell proliferation at clinically relevant concentrations, including the concentration used in the present study (10 μM) [18, 24, 46]. Cana's anti-proliferative effect could be explained by a reduction in ERK1/2 activity, since ERK1/2 not only exerts pro-

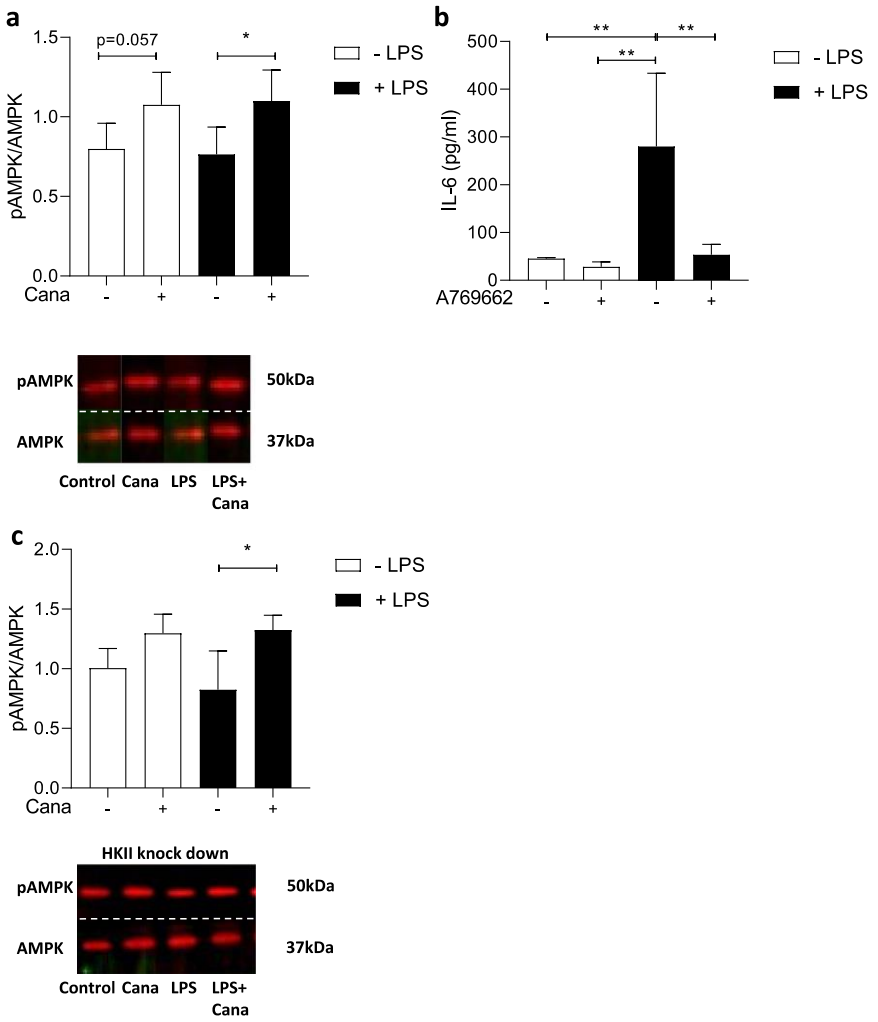

Fig. 5 Cana induces AMPK phosphorylation, independent of HKII, in LPS-stimulated HCAECs. Cells were pre-incubated for 16 h with vehicle or Cana (10 μM) and subsequently stimulated by 1-μg/mL LPS for 3 h with vehicle or Cana. Phosphorylation of AMPK at site threonine 172 by Cana was determined in normal HCAECs (**a**, $n = 7$). Activation of AMPK by A769662 inhibits LPS-induced IL-6 release (**c**, $n = 5$). In HKII knock-down HCAECs, Cana still phosphorylated AMPK (**c**, $n = 4$). Representative bands are shown below each figure. Whole membrane scans are shown in the ESM. Data are presented as mean ± SD. *$p < 0.05$, tested by one-way ANOVA with Bonferroni correction

apoptotic and pro-inflammatory actions but also plays a role in proliferation and survival pathways [47]. In summary, reduction of ERK1/2 activity by Cana is observed during LPS stimulation, which may to some degree be related to the anti-inflammatory actions of Cana, although more research is needed to understand the role of ERK1/2 in the functional effects of Cana.

Hexokinase as Target to Reduce Inflammation

Enhanced glycolysis is a central phenomenon in inflammation induced by LPS. A recent study showed that inflammation was associated with enhanced endothelial glycolysis and accumulation of glycolytic intermediates in human aortic endothelial cells [48]. HKII is one of several rate-limiting enzymes

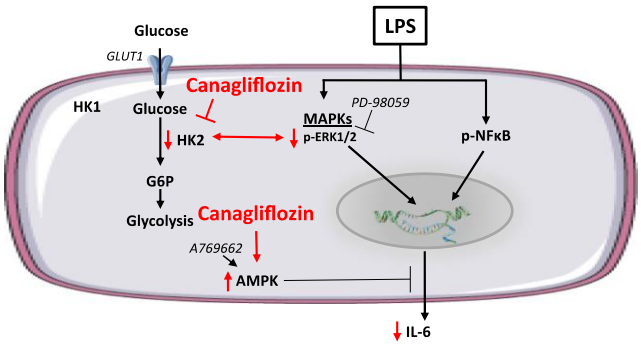

Fig. 6 Summary of Cana effects in LPS-stimulated HCAECs. Cana reduces IL-6 release, at least in part, by lowering HKII and blocking ERK1/2 activation. Cana also activates AMPK, and AMPK activation is associated with reduced LPS-induced IL-6 release in HCAECs. Effects of Cana are indicated by red marks

of glycolysis. HKII has been previously reported to be upregulated during inflammatory processes. In primary astrocytes exposed to hypoxia, HKII expression and activity were increased [49]. LPS strongly induced HKII gene expression after 24 h in human monocyte-dendritic cells [7]. In the present study, knockdown of HKII caused partial loss of Cana-mediated IL-6 reduction in HCAECs. Targeting hexokinase and therefore inhibiting glycolytic overload was previously proposed as a treatment strategy against inflammatory responses [8, 9]. We observed that Cana was able to reduce HKII expression in healthy HCAECs and LPS-stimulated HCAECs. We did not see an upregulation of HKII expression by LPS in our model, but this is likely due to the short time period that the HCAECs were exposed to LPS (3 h) as compared with previous studies showing enhanced HKII after 12 h or 24 h of LPS stimulation [6, 7]. To investigate whether reduction of HKII expression was associated with the anti-inflammatory effects of Cana, Cana effects were studied in partial HKII knockdown cells. While IL-6 release was still induced by LPS, Cana was unable to attenuate IL-6 release under reduced HKII conditions. This may imply that reduced LPS-induced IL-6 release by Cana is, at least partly, mediated by HKII. Furthermore, silencing HKII abrogated LPS-induced ERK1/2 phosphorylation, suggesting that HKII plays an important role in the induction of ERK1/2 activation during inflammation (or vice versa). Our data propose that Cana's effect on reduced ERK1/2 phosphorylation and IL-6 release during inflammation is, at least partly, related to Cana's effect on reduced HKII expression.

AMPK Activation by Cana

Activation of AMPK by SGLT2 inhibitors have been previously reported [19, 25, 42]. We observed that Cana activated AMPK phosphorylation in LPS-stimulated HCAECs. Furthermore, AMPK activation by A769669 resulted in reduced LPS-induced IL-6 release. Cana was shown to reduce inflammation in IL-1β stimulated human endothelial cells [18], an effect that was at least partially associated with AMPK activation. The same authors reported that activation of AMPK by Cana was associated with inhibition of mitochondrial complex 1 inhibition in human kidney cells, mouse hepatocytes, and fibroblasts [25]. In LPS-stimulated immune cells, Cana at concentrations between 10 and 40 μM exhibited anti-inflammatory effects, reduced glucose metabolism, and promotes AMPK activation [42]. Cana's inhibition of glucose metabolism is in line with our observation that HKII is reduced by Cana. Cana was still able to induce AMPK phosphorylation in HKII knockdown HCAECs stimulated with LPS, suggesting that Cana's effect on AMPK is not mediated by HKII. HK expression and AMPK activity have been reported to be negatively related with each other in inflammatory conditions and may both be effective targets to alleviate inflammation-induced endothelial dysfunction [8, 9, 35]. Our data show that Cana activates AMPK and that AMPK activation reduces LPS-induced cytokine release. Furthermore, reduced HKII expression by Cana is not responsible for the increased AMPK phosphorylation; thus, it is likely that Cana increased AMPK activity through a different pathway or that Cana activates AMPK prior to Cana's HKII lowering effect.

Empa and Dapa have primarily been related to direct AMPK activation in cardiac cells [19, 37, 50]. In our experiments, only Cana, not Empa and Dapa, induced AMPK phosphorylation in human cardiac endothelial cells (supplementary data), which is also reported in another endothelial cell study [18]. Activation of AMPK by SGLT2 inhibitors may possibly depend on the cell type and species origin (human cardiac endothelial cells vs. mouse cardiac fibroblasts and cardiomyocytes).

Finally, Cana has been found to activate autophagy in non-endothelial cell types [42]. The effects of Cana on autophagy in endothelial cells have not been studied. Our observations that Cana inhibits ERK1/2 and activates AMPK suggest that Cana increases autophagy in endothelial cells.

Limitations and Conclusion

This study was only performed in non-diabetic HCAECs to understand the anti-inflammatory actions of SGLT2 inhibitors. We performed experiments in HCAECs that originate from two donors; therefore, the generalization of the results might be problematic and more experiments from different cell batches, types, and donors are needed to further validate our results. Nonetheless, the use of a single donor in human cell studies seems to be commonplace (e.g., in Hela cells [51], A549 cells [52], and HCAECs [53–56]). The effects of LPS on cellular stress were only investigated at a single time point in the present study. In our experiments, we assessed HKII expression in the cell lysate. The cellular location of HKII is crucial for its detrimental or protective function and its effects on cell metabolism [57]. Future studies should investigate the effect of Cana on the cellular localization of HKII, i.e., whether Cana affects mitochondrial bound HKII as well as cytosolic HKII.

In conclusion, Canagliflozin's direct anti-inflammatory actions in human cardiac endothelial cells are associated with reduced hexokinase 2 expression.

Acknowledgments We appreciate Ruud Geelen for his support in the data acquisition during this project.

Funding This study was supported by a grant from the European Foundation for the Study of Diabetes/Novo Nordisk Program (2018) and the IARS/SCA midcareer grant.

Compliance with Ethical Standards

Conflict of Interest The authors declare that they have no conflict of interests

Ethical Approval This article does not contain any studies with human participants or animals performed by any of the authors.

References

1. Van Greevenbroek MMJ, Schalkwijk CG, Stehouwer CDA. Obesity-associated low-grade inflammation in type 2 diabetes mellitus: causes and consequences. Neth J Med. 2013;71:174–87.
2. Paulus WJ, Tschöpe C. A novel paradigm for heart failure with preserved ejection fraction: comorbidities drive myocardial dysfunction and remodeling through coronary microvascular endothelial inflammation. J Am Coll Cardiol. 2013;62:263–71.
3. Hameed I, Masoodi SR, Mir SA, Nabi M, Ghazanfar K, Ganai BA. Type 2 diabetes mellitus: from a metabolic disorder to an inflammatory condition. World J Diabetes. 2015;6:598–612.
4. Treps L, Conradi LC, Harjes U, Carmeliet P. Manipulating angiogenesis by targeting endothelial metabolism: hitting the engine rather than the drivers—a new perspective? Pharmacol Rev. 2016;68:872–87.
5. Everts B, Amiel E, Huang SCC, Smith AM, Chang CH, Lam WY, et al. TLR-driven early glycolytic reprogramming via the kinases TBK1-IKKε supports the anabolic demands of dendritic cell activation. Nat Immunol. 2014;15:323–32.
6. Bustamante MF, Oliveira PG, Garcia-Carbonell R, Croft AP, Smith JM, Serrano RL, et al. Hexokinase 2 as a novel selective metabolic target for rheumatoid arthritis. Ann Rheum Dis. 2018;77:1636–43.
7. Perrin-Cocon L, Aublin-Gex A, Diaz O, Ramière C, Peri F, André P, et al. Toll-like receptor 4–induced glycolytic burst in human monocyte-derived dendritic cells results from p38-dependent stabilization of HIF-1α and increased hexokinase II expression. J Immunol. 2018;201:1510–21.
8. Seki SM, Gaultier A. Exploring non-metabolic functions of glycolytic enzymes in immunity. Front Immunol. 2017;8:1549.
9. Palsson-Mcdermott EM, O'Neill LAJ. The Warburg effect then and now: from cancer to inflammatory diseases. BioEssays. 2013;35:965–73.
10. Zheng Z, Ma H, Zhang X, Tu F, Wang X, Ha T, et al. Enhanced glycolytic metabolism contributes to cardiac dysfunction in polymicrobial sepsis. J Infect Dis. 2017;215:1396–406.
11. Tannahill G, Curtis A, Adamik J, Palsson-McDermott E, McGettrick A, Goel G, et al. Succinate is a danger signal that induces IL-1β via HIF-1α. Nature. 2013;496:238–42.
12. Zinman B, Wanner C, Lachin JM, Fitchett D, Bluhmki E, Hantel S, et al. Empagliflozin, cardiovascular outcomes, and mortality in type 2 diabetes. N Engl J Med. 2015;373:2117–28.
13. Neal B, Perkovic V, Mahaffey KW, de Zeeuw D, Fulcher G, Erondu N, et al. Canagliflozin and cardiovascular and renal events in Type 2 Diabetes. N Engl J Med. 2017;377:644–57.
14. Wiviott SD, Raz I, Bonaca MP, Mosenzon O, Kato ET, Cahn A, et al. Dapagliflozin and cardiovascular outcomes in type 2 diabetes. N Engl J Med. 2019;380:347–57.
15. McMurray JJV, Solomon SD, Inzucchi SE, Kober L, Kosiborod MN, Martinez FA, et al. Dapagliflozin in patients with heart failure and reduced ejection fraction. N Engl J Med. 2019;381:1995–2008.
16. Uthman L, Baartscheer A, Bleijlevens B, Schumacher CA, Fiolet JWT, Koeman A, et al. Class effects of SGLT2 inhibitors in mouse cardiomyocytes and hearts: inhibition of Na+/H+ exchanger, lowering of cytosolic Na+ and vasodilation. Diabetologia. 2018;61:722–6.
17. Uthman L, Nederlof R, Eerbeek O, Baartscheer A, Schumacher C, Buchholtz N, et al. Delayed ischaemic contracture onset by empagliflozin associates with NHE1 inhibition and is dependent on insulin in isolated mouse hearts. Cardiovasc Res. 2019;115:1533–45.
18. Mancini SJ, Boyd D, Katwan OJ, Strembitska A, Almabrouk TA, Kennedy S, et al. Canagliflozin inhibits interleukin-1β-stimulated cytokine and chemokine secretion in vascular endothelial cells by AMP-activated protein kinase-dependent and -independent mechanisms. Sci Rep. 2018;8:5276.
19. Ye Y, Bajaj M, Yang HC, Perez-Polo JR, Birnbaum Y. SGLT-2 Inhibition with dapagliflozin reduces the activation of the Nlrp3/ASC inflammasome and attenuates the development of diabetic cardiomyopathy in mice with Type 2 diabetes. Further Augmentation of the Effects with Saxagliptin, a DPP4 Inhibitor. Cardiovasc Drugs Ther. 2017;31:119–32.
20. Andreadou I, Efentakis P, Balafas E, Togliatto G, Davos CH, Varela A, et al. Empagliflozin limits myocardial infarction in vivo

and cell death in vitro: Role of STAT3, mitochondria, and redox aspects. Front Physiol. 2017;8:1077.
21. Uthman L, Baartscheer A, Schumacher CA, Fiolet JWT, Kuschma MC, Hollmann MW, et al. Direct cardiac actions of sodium glucose cotransporter 2 inhibitors target pathogenic mechanisms underlying heart failure in diabetic patients. Front Physiol. 2018;9:1575.
22. Uthman L, Homayr A, Juni RP, Spin EL, Kerindongo R, Boomsma M, et al. Empagliflozin and dapagliflozin reduce ROS generation and restore no bioavailability in tumor necrosis factor α-stimulated human coronary arterial endothelial cells. Cell Physiol Biochem. 2019;53:865–86.
23. Gaspari T, Spizzo I, Liu H, Hu Y, Simpson RW, Widdop RE, et al. Dapagliflozin attenuates human vascular endothelial cell activation and induces vasorelaxation: a potential mechanism for inhibition of atherogenesis. Diab Vasc Dis Res. 2017;15:64–73.
24. Kaji K, Nishimura N, Seki K, Sato S, Saikawa S, Nakanishi K, et al. Sodium glucose cotransporter 2 inhibitor canagliflozin attenuates liver cancer cell growth and angiogenic activity by inhibiting glucose uptake. Int J Cancer. 2018;142:1712–22.
25. Hawley SA, Ford RJ, Smith BK, Gowans GJ, Mancini SJ, Pitt RD, et al. The Na+/glucose cotransporter inhibitor canagliflozin activates AMPK by inhibiting mitochondrial function and increasing cellular AMP levels. Diabetes. 2016;65:2784–94.
26. El-daly M, Krishna V, Venu P, Mihara K, Kang S, Fedak PWM, et al. Hyperglycaemic impairment of PAR2-mediated vasodilation: prevention by inhibition of aortic endothelial sodium-glucose-co-Transporter-2 and minimizing oxidative stress. Vasc Pharmacol. 2018;109:56–71.
27. Zeuke S, Ulmer AJ, Kusumoto S, Katus HA, Heine H. TLR4-mediated inflammatory activation of human coronary artery endothelial cells by LPS. Cardiovasc Res. 2002;56:126–34.
28. Lee DM, Battson ML, Jarrell DK, Hou S, Ecton KE, Weir TL, et al. SGLT2 inhibition via dapagliflozin improves generalized vascular dysfunction and alters the gut microbiota in type 2 diabetic mice. Cardiovasc Diabetol BioMed Central. 2018;17:62.
29. Haubner F, Lehle K, Münzel D, Schmid C, Birnbaum DE, Preuner JG. Hyperglycemia increases the levels of vascular cellular adhesion molecule-1 and monocyte-chemoattractant-protein-1 in the diabetic endothelial cell. Biochem Biophys Res Commun. 2007;360:560–5.
30. Oelze M, Kröller-Schön S, Welschof P, Jansen T, Hausding M, Mikhed Y, et al. The sodium-glucose co-transporter 2 inhibitor empagliflozin improves diabetes-induced vascular dysfunction in the streptozotocin diabetes rat model by interfering with oxidative stress and glucotoxicity. PLoS One. 2014;9:e112394.
31. Odegaard AO, Jacobs DR, Sanchez OA, Goff DC, Reiner AP, Gross MD. Oxidative stress, inflammation, endothelial dysfunction and incidence of type 2 diabetes. Cardiovasc Diabetol. 2016;15:1–12.
32. Zhang X, Ma L, Peng F, Wu Y, Chen Y, Yu L, et al. The endothelial dysfunction in patients with type 2 diabetes mellitus is associated with IL-6 gene promoter polymorphism in Chinese population. Endocrine. 2011;40:124–9.
33. Cani PD, Bibiloni R, Knauf C, Waget A, Neyrinck AM, Delzenne NM, et al. Changes in gut microbiota control metabolic endotoxemia-induced inflammation in high-fat diet–induced obesity and diabetes in mice. Diabetes. 2008;57:1470–81.
34. Dauphinee SM, Karsan A. Lipopolysaccharide signaling in endothelial cells. Lab Investig. 2006;86:9–22.
35. Cordero MD, Williams MR, Ryffel B. AMP-activated protein kinase regulation of the NLRP3 inflammasome during aging. Trends Endocrinol Metab. 2018;29:8–17.
36. He C, Li H, Viollet B, Zou MH, Xie Z. AMPK suppresses vascular inflammation in vivo by inhibiting signal transducer and activator of transcription-1. Diabetes. 2015;64:4285–97.
37. Lu Q, Liu J, Li X, Sun X, Zhang J, Ren D, et al. Empagliflozin attenuates ischemia and reperfusion injury through LKB1/AMPK signaling pathway: empagliflozin and cardiac ischemic insult. Mol Cell Endocrinol. 2020;501:110642.
38. Smit KF, Konkel M, Kerindongo R, Landau MA, Zuurbier CJ, Hollmann MW, et al. Helium alters the cytoskeleton and decreases permeability in endothelial cells cultured in vitro through a pathway involving Caveolin-1. Sci Rep. 2018;8:4768.
39. Chen Z, Oliveira SDS, Zimnicka AM, Jiang Y, Sharma T, Chen S, et al. Reciprocal regulation of eNOS and caveolin-1 functions in endothelial cells. Mol Biol Cell. 2018;29:1190–202.
40. Smit KF, Brevoord D, De Hert S, de Mol BA, Kerindongo RP, van Dieren S, et al. Effect of helium pre- or postconditioning on signal transduction kinases in patients undergoing coronary artery bypass graft surgery. J Transl Med. 2016;14:294.
41. Nederlof R, Van Den Elshout MAM, Koeman A, Uthman L, Koning I, Eerbeek O, et al. Cyclophilin D ablation is associated with increased end-ischemic mitochondrial hexokinase activity. Sci Rep. 2017;7:12749.
42. Xu C, Wang W, Zhong J, Lei F, Xu N, Zhang Y, et al. Canagliflozin exerts anti-inflammatory effects by inhibiting intracellular glucose metabolism and promoting autophagy in immune cells. Biochem Pharmacol. 2018;152:45–59.
43. Grempler R, Thomas L, Eckhardt M, Himmelsbach F, Sauer A, Sharp DE, et al. Empagliflozin, a novel selective sodium glucose cotransporter-2 (SGLT-2) inhibitor: characterisation and comparison with other SGLT-2 inhibitors. Diabetes Obes Metab. 2012;14:83–90.
44. Cui GM, Zhao YX, Zhang NN, Liu ZS, Sun WC, Peng QS. Amiloride attenuates lipopolysaccharide-accelerated atherosclerosis via inhibition of NHE1-dependent endothelial cell apoptosis. Acta Pharmacol Sin. 2013;34:231–8.
45. Németh ZH, Deitch EA, Lu Q, Szabó C, Haskó G. NHE blockade inhibits chemokine production and NF-κB activation in immunostimulated endothelial cells. Am J Phys Cell Phys. 2002;283:396–403.
46. Behnammanesh G, Durante GL, Khanna YP, Peyton KJ, Durante W. Canagliflozin inhibits vascular smooth muscle cell proliferation and migration: role of heme oxygenase-1. Redox Biol. 2020. https://doi.org/10.1016/j.redox.2020.101527.
47. Xu Z, Sun J, Tong Q, Lin Q, Qian L, Park Y, et al. The role of ERK1/2 in the development of diabetic cardiomyopathy. Int J Mol Sci. 2016;17:i2001.
48. Schnitzler JG, Hoogeveen RM, Ali L, Prange KH, Waissi F, van Weeghel M, et al. Atherogenic lipoprotein(a) increases vascular glycolysis, thereby facilitating inflammation and leukocyte extravasation. Circ Res. 2020. https://doi.org/10.1161/CIRCRESAHA.119.316206.
49. Mergenthaler P, Kahl A, Kamitz A, van Laak V, Stohlmann K, Thomsen S, et al. Mitochondrial hexokinase II (HKII) and phosphoprotein enriched in astrocytes (PEA15) form a molecular switch governing cellular fate depending on the metabolic state. Proc Natl Acad Sci. 2012;109:1518–23.
50. Ye Y, Jia X, Bajaj M, Birnbaum Y. Dapagliflozin attenuates Na+/H+ exchanger-1 in cardiofibroblasts via AMPK activation. Cardiovasc Drugs Ther. 2018;32:553–8.
51. Schrerer WF, Syverton JT, Gey GO. Studies on the propagation in vitro of poliomyelitis viruses. J Exp. Med. 1953;97:695–710.
52. Rees P, Wills JW, Brown MR, Barnes CM, Summers HD. The origin of heterogeneous nanoparticle uptake by cells. Nat Commun. 2019;10:1–8.
53. Chen L, Qin L, Liu X, Meng X. CTRP3 Alleviates Ox-LDL–induced inflammatory response and endothelial dysfunction in mouse aortic endothelial cells by activating the PI3K/Akt/eNOS pathway. Inflammation. 2019;42:1350–9.

54. Shyu KG, Wang BW, Pan CM, Fang WJ, Lin CM. Hyperbaric oxygen boosts long noncoding RNA MALAT1 exosome secretion to suppress microRNA-92a expression in therapeutic angiogenesis. Int J Cardiol. 2019;274:271–8.
55. Morton J et al. Strikingly different atheroprotective effects of apolipoprotein A-I in early- versus late-stage atherosclerosis. JACC Basic to Transl Sci. 2018;3:187–99.
56. Garczorz W et al. Exenatide exhibits anti-inflammatory properties and modulates endothelial response to tumor necrosis factor α-mediated activation. Cardiovasc Ther. 2018;36:1–8.
57. Nederlof R, Denis S, Lauzier B. Rosiers C Des, Laakso M, Hagen J, et al. Acute detachment of hexokinase II from mitochondria modestly increases oxygen consumption of the intact mouse heart. Metabolism. 2017;72:66–74.

8 Acknowledgements

I am extremely grateful to have had the opportunity to perform my experiments in the Laboratory for Experimental Intensive Care and Anesthesiology (L.E.I.C.A.), Department of Anesthesiology, Academisch Medisch Centrum (AMC) at the University of Amsterdam in Amsterdam. Even though the COVID-19 crisis paralyzed whole Europe in 2020, I have been incredibly fortunate to keep on working and living in the Netherlands, making unforgettable memories and experiences for my lifetime.

To Dr. Nina-Hauck Weber, head of Laboratory at L.E.I.C.A, who integrated me in her research group and put a lot of trust in my work right from the start. Who was always there for guiding, supervising, and supporting my experimental process even when, if not particularly, things did not work the way we expected.

To Prof. Dr. Martin Albrecht, who gave me the opportunity to conduct my experiments abroad but more importantly excellently guided the journey of my thesis before going abroad, during my whole stay in Amsterdam and the following writing process.

To Xiaoling Li, who I was working with on the same research project and supported my scientific work process throughout my whole stay in Amsterdam.

To Derek J.B. Kleinveld, who assisted the whole research project and with whom I had a lot of interesting and memorable conversations about scientific research and clinical medicine.

To all my fellow PhD students, medical students, and technicians at the L.E.I.C.A., for their support throughout my whole stay in Amsterdam, and in particular t o Raphaela P. Kerindongo, who patiently introduced me to the world of performing all kinds of different experimental techniques.

To my friends, who gave emotional support, visited me in Amsterdam and made my time there unforgettable.

To my family for always providing their unconditional support, for giving me the opportunity to pursue whatever goal I might have, in whatever country it may possibly be. Without their support and commitment, I would not be where I am now